Novel Functionalized Polyolefin Flocculant for Treatment of Oil Sands Tailings

by

Zahra Rostami Najafabadi

A thesis submitted in partial fulfillment of the requirements for the degree of

Doctor of Philosophy

in

Chemical Engineering

Department of Chemical and Materials Engineering

University of Alberta

Abstract

Bitumen is most commonly extracted from oil sands using the Clark hot water extraction process that produce slurry residues, called tailings. Sand particles in tailings quickly settle and produce mature fine tailings (MFT), which are stored in large tailing ponds. Currently, tailing ponds cover about 257 km^2 of Alberta's oil sands region, and only a small fraction of this large area has been reclaimed.

Paste technology, which involves the use of polymeric flocculants, is commonly used to treat oil sands tailings. However, existing commercial flocculants—polyacrylamide (PAM) or partially hydrolyzed anionic polyacrylamide (HPAM)—still suffer from limitations such as shear sensitivity, poor dispersion in tailings, inability to flocculate fine clay particles effectively, and retention of large amounts of water in the sediments.

Many investigations such as, modification of acrylamide polymers by addition of hydrophobic groups, and synthesizing partially hydrophobic flocculants with novel chemistries have been done to improve MFT dewatering. Most of these studies highlighted how hydrophobic modifications could enhance MFT dewatering, but the relation between flocculant microstructure and its flocculation and dewatering performance is still missing.

This thesis addresses some of these challenges by synthesizing a family of novel partially hydrophobic flocculants composed of hydrolyzed poly(methyl acrylate) side chains of different molecular weights and densities grafted via reverse ATRP onto two ethylene-propylene-diene (EPDM) backbones of different molecular weights. We investigated how graft molecular weight

and density, as well as backbone length, affected the flocculation and dewatering of oil sands mature fine tailings (MFT) through a statistical approach.

This research was broken down into three main investigations:

1- Synthesis of ethylene/propylene/diene terpolymers grafted with hydrolyzed poly(methyl acrylate) (EPDM-*g*-HPMA).

   EPDM terpolymers were grafted with PMA by reverse ATRP. Two EPDM samples with the same 5-ethylidene-2-norbornene, ethylene, and propylene fractions, but different weight average molecular weights, were used as backbones. The PMA graft molecular weights and densities were controlled by varying the concentration and conversion of methyl acrylate, as well as the concentration of initiator. The grafted copolymers were characterized by Fourier-transform infrared spectroscopy, proton nuclear magnetic resonance, and gel permeation chromatography to measure the graft densities and molecular weights of the grafted copolymer. Copolymers with graft molecular weights varying from 12 to 179 kDa and grafting densities from 11 to 53 % were made following this procedure.

2- Assessing the characteristics of the novel partially hydrophobic flocculant (EPDM-*g*-HPMA) on the flocculation and dewatering of mature fine tailings.

   In this study, the impact of the side chains molecular weight and density of EPDM-*g*-HPMA on the flocculation and dewatering of oil sands mature fine tailings were assessed using a central composite experimental design by measurements of initial settling rate, capillary suction time, supernatant turbidity, and sediment solids content. Flocculants with high

molecular weight grafts and low grafting densities reduced initial settling rates, decreased supernatant turbidities, and increased the sediments solids content. The capillary suction time, however, depended mostly on the charge density and on the hydrophobicity of the grafted copolymer. The effect of the EPDM backbone molecular weight was also investigated. Shorter backbones resulted in flocculants that dispersed more easily in water and consequently, settled the sediments faster, decreased the supernatant turbidity and increased the solids content in the sediments.

3- Evaluation of floc structure and its effect on dewatering and rheology of the flocculated MFT. In this study, a combination of confocal microscopy and rheology was used to investigate the effect of EPDM-*g*-HPMA graft density on its dispersion in water, sediment solids content and long-term dewatering of oil sands tailings. Microscopy observations and rheology measurements showed that increasing graft density from 30 % to 50 % makes the flocculant easier to disperse in the medium and consequently, leads the flocculant with higher graft density to produce sediments with higher solids contents, increase the rate of initial dewatering, and also enhance the viscoelastic response of the flocculated sediments right after sedimentation. However, the long-term rheological properties of the flocculated sediments were similar for all flocculants. Tri-dimensional microscopic details of the spatial distribution of water within the flocculated sludge showed that increasing the graft density in EPDM-*g*-HPMA causes trapping more water within the individual flocs and consequently, decreases the post-flocculation dewatering rate.

Preface

Chapter 3 of this thesis has been published in *Z. Rostami Najafabadi and J.B.P. Soares, "Ethylene/Propylene/Diene Terpolymers Grafted with Poly(methyl acrylate) by Reverse Atom Transfer Radical Polymerization" Macromol. Chem. Phys, vol. 222, article no. 2100189, 2021.* I synthesised the grafted copolymer, analyzed the product using a combination of analytical and mathematical modelling methods, and wrote the manuscripts.

Chapter 4 of this thesis has been published as *Z. Rostami Najafabadi and J.B.P. Soares, "Flocculation and Dewatering of Oil Sands Tailings with a Novel Functionalized Polyolefin Flocculant" Separation and Purification Technology, vol. 274, article no. 119018, 2021.* I was responsible for the design of experiments, performance of the flocculation experiments, data analysis, as well as for the manuscript composition.

Chapter 5 of this thesis are published as *G. Kalyanaraman, Z. Rostami Najafabadi, J.B.P. Soares, and M. Trifkovic "Flocculation Efficiency and Spatial Distribution of Water in Oil Sands Tailings Flocculated with a Partially Hydrophobic Graft Copolymer" Appl. Mat. Interf, vol. 13, pp.43726-43733, 2021.* I was responsible for synthesis of the grafted copolymer, flocculation methodology, and writing the small part of the article. Ms. Gayathri Kalyanaraman was responsible for flocculated sediments quantification methodology, performance of the experiments, data analysis, as well as writing the article, and Professor Milana Trifcovik contributed to the manuscript composition and edits.

The paper presented in Appendix A has been published in *Z. Rostami Najafabadi and J.B.P. Soares, "Flocculation and Dewatering of Oil Sands Tailings with a Novel Functionalized Polyolefin Flocculant" Separation and Purification Technology, vol. 274, article no. 119018, 2021.* I was responsible for the design of experiments, data analysis, and manuscript composition.

In all the aforementioned papers, Professor João B. P. Soares contributed to the manuscript composition and edits.

Acknowledgement

I would like to express my genuine acknowledgment and gratitude to my supervisor, Professor João B. P. Soares. I truly appreciate for his continuous and inspiring guidance and support in my research, for his encouragement, massive knowledge, patience and understanding whenever I had tough times even in my personal life, and his fantastic attitude. It has been a great pleasure for me to be part of his great research group.

I also would like to thank Prof. Milana Trifcovik, University of Calgary, and her research group for amazing and productive collaboration, which provided a valuable learning experience during this research.

I am grateful to my peers and colleagues who have helped me in accomplishing this thesis. My thanks goes to Mr. Mohammed Ghuzi for his help on the synthesis of some of the polymers and performance of some of the flocculation tests, Dr. Linda Botha for her valuable discussions on the quantitative NMR technique, Mr. Alvaro Omana and Mr. Bruno Luppi (Department of Chemistry, University of Alberta, Edmonton, Alberta, Canada) for their sincere help with the molecular weight analysis of the copolymers studied in this work, and Dr. Vahid Vajihinejad for his valuable discussions on the use of central composite experimental designs.

My deepest thanks goes to my parents for their love, support, and being a great encouragement in my life.

I am forever indebted to my husband, Farhad, without him, I never would have been able to raise three kids and doing Ph.D. program at the same time. I am grateful to him from the bottom of my heart for his endless love and kindness, energy, and support that he gave me during this amazing chapter of my life.

Table of Contents

1 Introduction 1

1.1 Motivation 1

1.2 Research Objective 3

1.3 Thesis Outline 4

2 Background and Literature Review 8

2.1 MFT Composition 8

2.2 Polymeric Flocculants 11

2.3 Functionalization of Polyethylene 13

2.3.1 Functionalization of Polyethylene by Direct Polymerization 13

2.3.2 Functionalization of Polyolefins by Grafting 17

3 Ethylene/Propylene/Diene Terpolymers Grafted with Poly(methyl acrylate) by Reverse Atom Transfer Radical Polymerization 26

3.1 Introduction 26

3.2 Experimental 30

3.2.1 Materials 30

3.2.2 Synthesis of EPDM-*g*-PMA 30

3.2.3 Purification of EPDM-*g*-PMA 31

3.2.4 Characterization of EPDM-*g*-PMA 31

3.3 Results and Discussion 32

3.3.1 Polymer Synthesis 32

3.3.2 Composition Characterization of EPDM-*g*-PMA 38

3.3.3 Molecular Weight Characterization of EPDM-*g*-PMA 44

3.4 Conclusions 47

4 Flocculation and Dewatering of Oil Sands Tailings with a Novel Functionalized Polyolefin Flocculant 53

4.1 Introduction 53

4.2 Experimental Details 57

4.2.1 Materials 57

4.2.2 Experimental Design 57

4.2.3 Synthesis of EPDM-*g*-PMA 58

4.2.4 EPDM-*g*-PMA Base Hydrolysis 58

4.2.5 Settling and Flocculation Tests 59

4.2.6 Filter Press Operation 60

4.3 Results and Discussion 61

4.3.1 MFT Sample Composition 61

4.3.2 Effect of Graft Molecular Weight and Density of EPDM-*g*-HPMA on Flocculation 62

4.3.3 Effect of Backbone Length of EPDM-*g*-HPMA on Flocculation 77

4.4 Conclusions 89

5 Flocculation Efficiency and Spatial Distribution of Water in Oil Sands Tailings Flocculated with a Partially Hydrophobic Graft Copolymer 95

5.1 Introduction 96

5.2 Materials and Methods 97

5.2.1 Materials 97

5.2.2 Flocculation Methodology 98

5.2.3 Microstructure Imaging of the Flocculant and the Flocculated Sediment by Confocal Microscopy 98

5.2.4 Shear Rheology 99

5.3 Results and Discussion 100

5.3.1 Flocculant Characterization 100
5.3.2 Characterization of the Polymer-Treated MFT 101
5.3.3 Rheological Characterization of the Flocculated MFT Sediments 105
5.4 Conclusion 106
6 Conclusion and Future Work 112
6.1 Conclusion 112
6.2 Future Work 114
Bibliography 116
1 Supplementary Information for Chapter 4 128

List of Tables

Table 3-1 Polymerization conditions for EPDM-*g*-PMA synthesis and their properties. 34
Table 3-2 Masses of different fractions of the EPDM-*g*-PMA samples. 36
Table 4-1 MFT sample composition. 61
Table 4-2 ISR for 5 wt. % MFT treated with EPDM-*g*-HPMA. 62
Table 4-3 ANOVA table for ISR. 63
Table 4-4 CST of the sediments for 5, 10 and 20 wt. % MFT treated with EPDM-*g*-HPMAs. 68
Table 4-5 Supernatant turbidity for 5, 10 and 20 wt. % MFT treated with EPDM-*g*-HPMAs. 71
Table 4-6 Sediment solids content for 5, 10 and 20 wt. % MFT treated with EPDM-*g*-HPMAs. 74
Table 4-7 EPDM-*g*-HPMAs properties. 78
Table 4-8 Turbidity of anionic EPDM-*g*-HPMAs suspension in water. 80
Table 5-1 The mass balance of the solids, bitumen and water in the MFT samples flocculated and aged for 120 days obtained from confocal imaging and Dean Stark, along with the volume fraction calculation based on the average densities for solids, water and bitumen. ..104

Table A 1 ANOVA table for CST for 5 wt.% MFT. 128
Table A 2 ANOVA table for CST for 10 wt.% MFT. 129
Table A 3 ANOVA table for CST for 20 wt.% MFT. 130
Table A 4 ANOVA table for turbidity for 5 wt.% MFT. 131
Table A 5 ANOVA table for turbidity for 10 wt.% MFT. 132
Table A 6 ANOVA table for turbidity for 20 wt.% MFT. 133
Table A 7 ANOVA table for solid content for 5 wt.% MFT. 134
Table A 8 ANOVA table for solid content for 10 wt.% MFT. 135
Table A 9 ANOVA table for solid content for 20 wt.% MFT. 136

List of Figures

Figure 1-1 Scheme for oil sands processing using the Clark hot water extraction process [3]. 2

Figure 2-1 schematics of tetrahedral and octahedral sheets in clays. a) Single tetrahedron, b) Isomeric view of the tetrahedral sheet, c) single octahedron, d) isomeric view of the octahedral sheet [6, 7].....9

Figure 2-2 Layer structure of clays. a) 1:1 structure of kaolinite, b) 2:1 structure of illite [9]. 10

Figure 2-3 Copolymerization of ethylene with vinyl acrylate comonomer by Pd-diimine catalyst [23].....15

Figure 2-4 CST comparison of HB*f*PE with 35, 40, and 50 mol % and anionic PAM on 20 wt. % MFT after 24 hours [17] (dashed line show the CST value for a blank run, when no flocculant was added to the MFT). 16

Figure 2-5 Comparison of flocculation performance of HB*f*PE with different functional contents and HPAM at 1000 ppm [17]. 16

Figure 2-6 ATRP mechanism. k_{act}: activation rate constant, k_{deact}: deactivation rate constant, k_p: propagation rate constant, k_t: termination rate constant, P_nX: dormant species, Mt^n/L: activator, $P_n^{\bullet}$: polymer radical, $X\text{-}Mt^{n+1}/L$: deactivator, $P_n\text{-}P_m$: dead chain [35]. 18

Figure 2-7 Synthesis of graft copolymer by ATRP via grafting from and grafting through processes [30].....19

Figure 2-8 Reverse ATRP mechanism. I-I: initiator, $I^{\bullet}$: primary radical, M: monomer, k_i: initiation rate constant, k_{act}: activation rate constant, k_{deact}: deactivation rate constant, k_p: propagation rate constant, k_t: termination rate constant, $I\text{-}P_nX$: dormant species, Mt^n/L: activator, $I\text{-}P_n^{\bullet}$: polymer radical, $X\text{-}Mt^{n+1}/L$: deactivator, $P_n\text{-}P_m$: dead chain [41].....21

Figure 3-1 Copolymerization of ethylene and methyl acrylate with a Pd-diimine catalyst [7]. 27

Figure 3-2 Reverse ATRP mechanism. I-I: initiator, $I^{\bullet}$: primary radical, M: monomer, k_i: initiation rate constant, k_{act}: activation rate constant, k_{deact}: deactivation rate constant, k_p:

propagation rate constant, k_t: termination rate constant, I-P_nX: dormant species, Mt^n/L: activator, I-$P_n^{\bullet}$: polymer radical, X-Mt^{n+1}/L: deactivator, P_n-P_m: dead chain [25].....29
Figure 3-3 Graft copolymerization of methyl acrylate on EPDM by reverse ATRP. 33
Figure 3-4 Product purification process steps. 35
Figure 3-5 ln([*MA*]$_0$/[*MA*]) versus polymerization time. Polymerization conditions: T = 90 °C, initial [*AIBN*]$_0$/[*CuBr2*]$_0$/[*PMDETA*]$_0$ ratio = 1/1.5/3. a) [*MA*]$_0$ = 5.0 M, and [*AIBN*]$_0$ = 0.00526 M, b) [*MA*]$_0$ = 7.6 M, and [*AIBN*]$_0$ = 0.0030, and c) [*MA*]$_0$ = 9.6 M, and [*AIBN*]$_0$ = 0.00121. 38
Figure 3-6 FTIR spectra of EPDM, PMA and EPDM-*g*-PMA. 39
Figure 3-7 ^{1}H NMR spectra of EPDM and EPDM-*g*-PMA with different graft molecular weights and densities. Polymers are labeled as EPDM-*g*-PMA-M_b-M_g-ρ_g-M_{MA} where M_b is the average molecular weight of the backbone in kDa, M_g is the average molecular weight of the PMA grafts in kDa, ρ_g is the percentual graft density, and M_{MA} is mol% of MA incorporated in the grafted copolymer. The asterix (*) indicates residual solvent signals for methanol, acetone, hexane, toluene, and isobutanol. 41
Figure 3-8 Close-up view of ^{1}H NMR spectrum of the EPDM and EPDM-*g*-PMAs with different graft molecular weights and densities: a) resonance of the unsaturated (=CH–) protons, and b) resonance of the terminal group (CHBr-$COOCH_3$) protons. 42
Figure 3-9 Measured ρ_g (%) by ^{1}H NMR versus estimated ρ_g (%) calculated by mass balance. 44
Figure 3-10 EPDM (M_b = 210 kDa) molecular weight distribution. 45
Figure 3-11 Estimated versus measured average molecular weights of EPDM-*g*-PMA samples: a) M_w, and b) M_n. 47
Figure 4-1 ISR model plots: a) normal plot, b) scatterplot of the standardized residuals as a function of the standardized predicted values, c) residuals versus run number, d) predicted versus observed values.....63
Figure 4-2 Surface response plot for ISR as a function of graft molecular weight and density. 64
Figure 4-3 ISR for 5 wt. % MFT treated with EPDM-g-HPMA of different graft molecular weights and densities versus mass percentage of HPMA in EPDM-*g*-HPMA.....66

Figure 4-4 Flocculation of 5 wt. % MFT using EPDM-*g*-HPMA with different graft molecular weights: a) EPDM-*g*-HPMA-210-49-14 (M_g = 49 kDa), b) EPDM-*g*-HPMA-210-147-16 (M_g = 147 kDa).....66
Figure 4-5 Flocculation of MFT with EPDM-*g*-HPMA-210-147-16: a) 10 wt.% MFT, b) 20 wt.% MFT. 67
Figure 4-6 Surface response of log(CST) for diluted MFT treated with EPDM-*g*-HPMA of different graft molecular weights and densities: a) 5 wt. % MFT, b) 10 wt. % MFT, c) 20 wt. % MFT. 69
Figure 4-7 log(CST) for diluted MFT treated with EPDM-*g*-HPMA of different graft molecular weights and densities versus mass percentage of HPMA in EPDM-*g*-HPMA: a) 5 wt. % MFT, b) 10 wt. % MFT, c) 20 wt. % MFT, d) MFT samples of all concentrations. 70
Figure 4-8 Surface response of log(T) for diluted MFT treated with EPDM-g-HPMAs with different graft molecular weights and densities: a) 5 wt. % MFT, b) 10 wt. % MFT, c) 20 wt. % MFT. 72
Figure 4-9 Supernatant turbidity for diluted MFT treated with EPDM-*g*-HPMA of different graft molecular weights and densities versus mass percentage of HPMA in EPDM-*g*-HPMA: a) 5 wt. % MFT, b) 10 wt. % MFT, c) 20 wt. % MFTs.....73
Figure 4-10 Surface response of sediment solids content for diluted MFT treated with EPDM-*g*-HPMA of different graft molecular weights and densities: a) 5 wt. % MFT, b) 10 wt. % MFT, and c) 20 wt. % MFT. 76
Figure 4-11 Solids content for diluted MFT treated with EPDM-*g*-HPMA of different graft molecular weights and densities versus mass percentage of HPMA in EPDM-*g*-HPMA: a) 5 wt. % MFT, b) 10 wt. % MFT, c) 20 wt. % MFT. 77
Figure 4-12 Settling rates for 5 wt. % MFT treated with HPAM and EPDM-*g*-HPMA with two different backbones (M_b = 115 and 210 kDa) at graft molecular weights (M_g): a) M_g = 100 kDa, b) M_g = 150 kDa, c) M_g = 180 kDa. 79
Figure 4-13 Flocculation of 5 wt. % MFT using EPDM-*g*-HPMA with the same graft molecular weight and density, but different backbone length: a) EPDM-*g*-HPMA-210-177-16, M_b = 210 kDa, b) EPDM-*g*-HPMA-115-179-13, M_b = 115 kDa. 80
Figure 4-14 Cappilary suction times for diluted MFT treated with HPAM and EPDM-*g*-HPMA flocculants: a) 5 wt. % MFT, b) 10 wt. % MFT,) 20 wt. % MFT. 82

Figure 4-15 Supernatent turbidity of diluted MFT treated with HPAM and EPDM-*g*-HPMA flocculants: a) 5 wt. % MFT, b) 10 wt. % MFT,) 20 wt. % MFT.....84
Figure 4-16 Sediment solids content for diluted MFT treated with HPAM and EPDM-*g*-HPMA flocculants: a) 5 wt. % MFT, b) 10 wt. % MFT,) 20 wt. % MFT.....86
Figure 4-17 Sediment solids contents for undiluted MFT treated with 2000 ppm of HPAM, and different dosages of EPDM-*g*-HPMA-115-179-13. 87
Figure 4-18 Filter cakes for flocculation of undiluted MFT with: a) 2000 ppm HPAM, b) 4000 ppm EPDM-*g*-HPMA-115-179-13, c) 8000 ppm EPDM-*g*-HPMA-115-179-13, and d) 10000 ppm EPDM-*g*-HPMA-115-179-13.....88
Figure 5-1 Schematic of the Protocol used to obtain the 3D image of the flocculated MFT sediments by confocal laser scanning microscope. a) Raw image of the sediments, b) Raw clay channel, c) Raw bitumen channel, d) Binary image of the clay channel by contrast enhancement, reconstruction and thresholding, e) Binary image of the bitumen channel by contrast enhancement, reconstruction and thresholding, f) Noise reduction, contrast enhancement, smoothening and thresholding of the raw clay channel once again to obtain an actual 3D representation of the flocculated sediments, g) Noise reduction, contrast enhancement, smoothening and thresholding of the raw bitumen channel once again to obtain an actual 3D representation of the flocculated sediments, h) Reconstruction using the stack of images to attain the 3D structure of the flocculated MFT sediments.....99
Figure 5-2 Microstructure and viscosity of different EPDM-*g*-HPMA in DI water, obtained by confocal laser scanning microscope and stress-controlled rheometer respectively. a) EPDM-*g*-HPMA 30 (Avg. size = ~35.08 μm), b) EPDM-*g*-HPMA 40 (Avg. size = ~10.29 μm), c) EPDM-*g*-HPMA 50 (Avg. size = ~4.79 μm).....100
Figure 5-3 Microstructure of flocculated MFT treated with 2000 ppm of flocculant after 1 day and 120 days obtained from confocal laser scanning microscope. a) 3D structures of sediments (red: solids, white: water, and green: bitumen), b) volume fraction evolution, c) 3D fractal dimension evolution. 101
Figure 5-4 Volume fraction of solids, bitumen and water in sediments flocculated with different EPDM-*g*-HPMA after 120 days. a) Volume fractions estimated from the 3D image data and measured by Dean-Stark analysis. b) Volume fraction of *inter-floc* and *intra-floc* water calculated based on 3D image quantification results and Dean-Stark analysis. c) Schematic of

typical polymer-flocculated MFT sediments showing intra-floc water, which is outside the resolution of confocal microscopy. 103
Figure 5-5 Shear sweep results for the flocculated MFT sediments flocculated with different EPDM-*g*-HPMA at 2000 ppm over 120 days. (a), (b), (c), (d) corresponds to stress sweep results from rheology after day 1, day 7, day 14 and day 120 respectively. (e) LVE storage modulus for flocculated MFT sediments at different aging times. 105

Figure A 1 CST model plots for 5 wt.% MFT: a) normal plot, b) scatterplot of the standardized residuals as a function of the standardized predicted values, c) residuals versus run number, d) predicted versus observed values. 129
Figure A 2 CST model plots for 10 wt.% MFT: a) normal plot, b) scatterplot of the standardized residuals as a function of the standardized predicted values, c) residuals versus run number, d) predicted versus observed values. 130
Figure A 3 CST model plots for 20 wt.% MFT: a) normal plot, b) scatterplot of the standardized residuals as a function of the standardized predicted values, c) residuals versus run number, d) predicted versus observed values. 131
Figure A 4 Turbidity model plots for 5 wt.% MFT: a) normal plot, b) scatterplot of the standardized residuals as a function of the standardized predicted values, c) residuals versus run number, d) predicted versus observed values. 132
Figure A 5 Turbidity model plots for 10 wt.% MFT: a) normal plot, b) scatterplot of the standardized residuals as a function of the standardized predicted values, c) residuals versus run number, d) predicted versus observed values. 133
Figure A 6 Turbidity model plots for 20 wt.% MFT: a) normal plot, b) scatterplot of the standardized residuals as a function of the standardized predicted values, c) residuals versus run number, d) predicted versus observed values. 134
Figure A 7 Solid content model plots for 5 wt.% MFT: a) normal plot, b) scatterplot of the standardized residuals as a function of the standardized predicted values, c) residuals versus run number, d) predicted versus observed values. 135
Figure A 8 Solid content model plots for 10 wt.% MFT: a) normal plot, b) scatterplot of the standardized residuals as a function of the standardized predicted values, c) residuals versus run number, d) predicted versus observed values. 136

Figure A 9 Solid content model plots for 20 wt.% MFT: a) normal plot, b) scatterplot of the standardized residuals as a function of the standardized predicted values, c) residuals versus run number, d) predicted versus observed values. 137

Chapter 1

1 Introduction

1.1 Motivation

Natural bitumen deposits are reported in many countries including Canada, Venezuela, the United States, and Russia [1]. In terms of proven global crude oil reserves, Alberta ranks third, after Saudi Arabia and Venezuela. In 2017, Alberta's total proven oil reserves were 165 billion barrels [2]. Bitumen is extracted from oil sands using the Clark hot water extraction (CHWE) process. This process includes mining the oil sands ore, crushing it, and mixing it with warm water and caustic at 75-80 °C to make a slurry. The formed slurry is transferred to a primary separation vessel (PSV) to liberate and aerate bitumen aggregates from the slurry. The bitumen froth, recovered from the PSV, is transferred to the froth treatment stage to recover more bitumen, and the slurry residues, called tailings, are transported to tailing ponds for solid-liquid separation [3]. Figure 1-1 shows the general process flowsheet for oil sands processing.

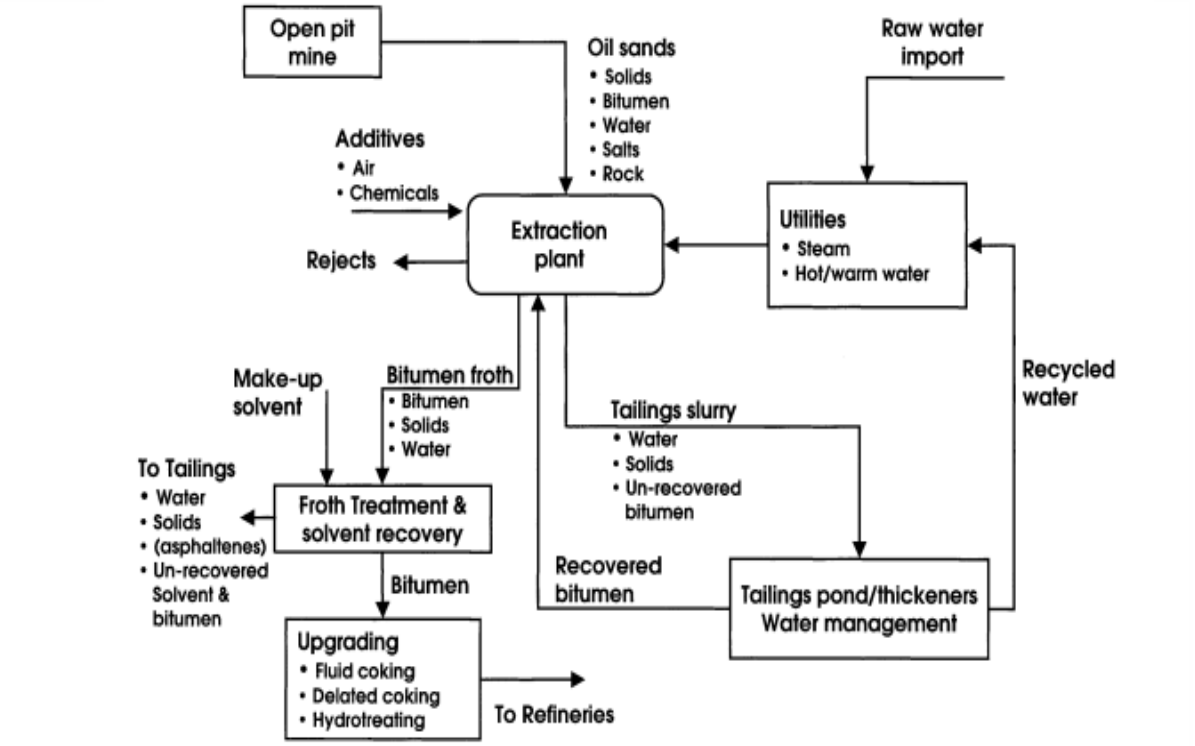

Figure 1-1: Scheme for oil sands processing using the Clark hot water extraction process [3].

Oil sands tailings are aqueous suspensions of coarse sands (particles greater than 44 μm), fine solids and clays (particles less than 44 μm), and 1-5 wt. % residual bitumen, with pH varying from 8 to 9 [4]. In the pond, the coarse particles settle rapidly, but the fine solids remain suspended above the sediments. After three to five years of settling, the concentration of suspended fine solids reaches 30 to 40% by weight, which is known as mature fine tailings (MFT). It may take centuries to consolidate untreated MFT [5].

Tailings ponds and their operating structures covered about 257 km^2 of Alberta's oil sands region in 2016 [6]. Unfortunately, only a small fraction of this large area has been reclaimed thus far. Therefore, it is essential to find more effective ways to separate the suspended solids from the water trapped in tailing ponds.

Different chemical and mechanical methods have been developed to treat oil sands tailing: 1) consolidated tailings, 2) paste technology, 3) filtered tailings, 4) thin lift dewatering, 5) centrifuge

fluid fine tailing, 6) rim ditching, and 7) wet landscape reclamation. Unfortunately, none of these methods can dewater tailings above the 75 wt. % solids required for land reclamation [5, 7].

Paste technology, which involves the use of polymeric flocculants, is commonly used to treat different types of mining waste. For oil sands tailings, paste technology is often combined with other treatments, such as coagulation and centrifugation. To date, most studies have used commercially available polyacrylamide (PAM) or partially hydrolyzed anionic polyacrylamide (HPAM) [8] flocculants. Despite promoting fast settling and initial water release rates, both PAM and HPAM suffer from limitations such as shear sensitivity, poor dispersion in tailings, inability to flocculate fine clay particles effectively, and retention of large amounts of water in the sediments [9].

To address these challenges, many investigations have done to develop polymer flocculants with novel chemistries as alternatives to polyacrylamide flocculants. For example, natural polymers [10], inorganic–organic hybrid PAM flocculants [11-13], stimuli-responsive polymers [14-17], cationic copolymer flocculants [18, 19] or partially hydrophobic polymers [20-22].

Recently, new hyperbranched polyethylenes containing polar functional groups, such as acrylic acid, were synthesized and used to densify oil sands tailings [20, 21]. The authors showed that in the presence of cations in the process water, the polar functional groups in the hyperbranched functionalized polyethylene adsorbed onto the surface of the clay particles, causing them to flocculate. Because of their hydrophobic polyethylene cores, more water was expelled from the sediments. Compared to a commercial HPAM, the hyperbranched functionalized polyethylene flocculant had better flocculation and dewatering performance. However, its low molecular weights of only up to 7000 g/mol and its insufficient polar group density, limited its flocculation behaviour [20, 21]. We need to address this limitation by graft polar polymer chains to the polyolefin backbone to produce functionalized polyolefin copolymers with higher molecular weights and higher polar functional groups for treating oil sands tailings.

1.2 Research Objective

The specific objectives of this thesis were:

I. Synthesis of a family of novel hybrid flocculants by reverse ATRP combining a hydrophobic ethylene/propylene/diene copolymer backbone and hydrolyzed poly(methyl acrylate) grafts (EPDM-*g*-HPMA)
II. Systematic investigation of how graft molecular weight and density, as well as backbone length, affect the flocculation and dewatering of oil sands tailing using a statistical approach.
III. Study the effect of the polymer grafting density on the post flocculation long-term consolidation.

1.3 Thesis Outline

This thesis consist of 6 chapters. **Chapter 1** (the current chapter) introduced the challenges associated with the treatment of oil sands tailings, motivations behind this work, and the objectives of this thesis.

Chapter 2 discusses the fundamentals related to the MFT composition and colloidal suspensions. This chapter also reviews the flocculants used for dewatering of MFT. Further, it reviews the literature on the functionalization of polyethylene by a variety of methods, which was the starting point for us to make functional polyolefin graft copolymer flocculants to treat oil sands tailings.

Chapter 3 explains the synthesis of ethylene-propylene-diene terpolymers (EPDM) grafted with poly(methyl acrylate) side chains with controlled graft molecular weights and densities by reverse atom transfer radical polymerization (ATRP). Further, it shows that this process could be conducted successfully by comparing mathematical modelling estimates with polymer characterization results. The results obtained in this chapter are published as *Z. Rostami Najafabadi and J.B.P. Soares, "Ethylene/Propylene/Diene Terpolymers Grafted with Poly(methyl acrylate) by Reverse Atom Transfer Radical Polymerization" Macromol. Chem. Phys, vol. 222, article no. 2100189, 2021.*

Chapter 4 introduces ethylene-propylene-diene grafted with hydrolysed poly(methyl acrylate) (EPDM-*g*-HPMA) as a novel partially hydrophobic flocculants for treatment of oil sands tailings. In this chapter, we investigated how graft molecular weight and density, as well as backbone

length, affect the flocculation and dewatering of oil sands tailing using a statistical approach. The results presented in this chapter are published as *Z. Rostami Najafabadi and J.B.P. Soares, "Flocculation and Dewatering of Oil Sands Tailings with a Novel Functionalized Polyolefin Flocculant" Separation and Purification Technology, vol. 274, article no. 119018, 2021.*

Chapter 5 describes the results obtained from a collaborative research with Professor Milana Trifcovik's group at University of Calgary, Alberta, Canada. In this chapter, it was investigated how the graft density of EPDM-*g*-HPMA affect its dispersion in water and flocculation efficiency in terms of sediment solids content and long-term dewatering of oil sands tailings. The results presented in this chapter are published as *G. Kalyanaraman, Z. Rostami Najafabadi, J.B.P. Soares, and M. Trifkovic "Flocculation Efficiency and Spatial Distribution of Water in Oil Sands Tailings Flocculated with a Partially Hydrophobic Graft Copolymer" Appl. Mat. Interf, vol. 13, pp.43726-43733, 2021.*

Chapter 6 provides a summary of the investigations carried out in this thesis and recommendations for future work.

Appendix A contains statistical analyses in flocculation and dewatering design of experiments. This appendix has been published in *Z. Rostami Najafabadi and J.B.P. Soares, "Flocculation and Dewatering of Oil Sands Tailings with a Novel Functionalized Polyolefin Flocculant" Separation and Purification Technology, vol. 274, article no. 119018, 2021.*

References

[1] L. Gross, T.L. Joly and C. Westman, Extracting home in the oil sands: settler colonialism and environmental change in subarctic Canada, Milton: Routledge, 2020.

[2] Anonymous "Government, Alberta Energy (2014), Oil sands Alberta, http://www.energy.alberta.ca/oilsands/791.asp".

[3] J. Masliyah, Z. Zhou, Z. Xu, J. Czarnecki and H. Hamza, "Understanding water-based bitumen extraction from athabasca oil sands", Can.J.Chem.Eng., vol. 82, pp. 628-654, 2004.

[4] L. Botha and J.B.P. Soares, "The Influence of Tailings Composition on Flocculation", Can.J.Chem.Eng., vol. 93, pp. 1514-1523, 2015.

[5] K.L. Kasperski and R.J. Mikula, "Waste streams of mined oil sands: Characteristics and remediation", Elements, vol. 7, pp. 387-392, 2011.

[6] Alberta Energy Regulator, "State of Fluid Tailings Management for Mineable Oil Sands", Alberta Energy Regulator, 2019.

[7] J.H. Masliyah, Z. Xu, J.A. Czarnecki and M. Dabros, Handbook on theory and practice of bitumen recovery from Athabasca Oil Sands, Cochrane, Alberta: Kingsley Knowledge Pub., 2013.

[8] H. Li, J. Long, Z. Xu and J.H. Masliyah, "Synergetic role of polymer flocculant in low-temperature bitumen extraction and tailings treatment", Energy Fuels, vol. 19, pp. 936-943, 2005.

[9] D.R.L. Vedoy and J.B.P. Soares, "Water-soluble polymers for oil sands tailing treatment: A Review", Can.J.Chem.Eng., vol. 93, pp. 888-904, 2015.

[10] L. Pennetta De Oliveira, S.P. Gumfekar, F. Lopes Motta and J.B.P. Soares, "Dewatering of Oil Sands Tailings with Novel Chitosan-Based Flocculants", Energy Fuels, vol. 32, pp. 5271-5278, 2018.

[11] X.W. Wang, X. Feng, Z. Xu and J.H. Masliyah, "Polymer aids for settling and filtration of oil sands tailings", Can.J.Chem.Eng., vol. 88, pp. 403-410, 2010.

[12] H. Li, J. Long, Z. Xu and J.H. Masliyah, "Novel polymer aids for low-grade oil sand ore processing", Can.J.Chem.Eng., vol. 86, pp. 168-176, 2008.

[13] S. Wang, L. Alagha and Z. Xu, "Adsorption of organic–inorganic hybrid polymers on kaolin from aqueous solutions", Colloids Surf.Physicochem.Eng.Aspects, vol. 453, pp. 13-20, 2014.

[14] J. Long, H. Li, Z. Xu and J.H. Masliyah, "Improving oil sands processability using a temperature-sensitive polymer", Energy Fuels, vol. 25, pp. 701-707, 2011.

[15] H. Li, J. Zhou, R. Chow, A. Adegoroye and A.S. Najafi, "Enhancing treatment and geotechnical stability of oil sands fine tailings using thermo-sensitive poly(n-isopropyl acrylamide)", Can.J.Chem.Eng., vol. 93, pp. 1780-1786, 2015.

[16] Y. Wang, Y. Kotsuchibashi, Y. Liu and R. Narain, "Temperature-responsive hyperbranched amine-based polymers for solid-liquid separation", Langmuir, vol. 30, pp. 2360-2368, 2014.

[17] D. Zhang, T. Thundat and R. Narain, "Flocculation and dewatering of mature fine tailings using temperature-responsive cationic polymers", Langmuir, vol. 33, pp. 5900-5909, 2017.

[18] C. Wang, C. Han, Z. Lin, J. Masliyah, Q. Liu and Z. Xu, "Role of Preconditioning Cationic Zetag Flocculant in Enhancing Mature Fine Tailings Flocculation", Energy Fuels, vol. 30, pp. 5223-5231, 2016.

[19] A. Alamgir, D. Harbottle, J. Masliyah and Z. Xu, "Al-PAM assisted filtration system for abatement of mature fine tailings", Chem.Eng.Sci., vol. 80, pp. 91-99, 2012.

[20] L. Botha, S. Davey, B. Nguyen, A.K. Swarnakar, E. Rivard and J.B.P. Soares, "Flocculation of oil sands tailings by hyperbranched functionalized polyethylenes (HBfPE)", Minerals Eng, vol. 108, pp. 71-82, 2017.

[21] L. Botha, D. Vedoy and J. Soares, "Novel hyperbranched functionalized polyethylenes for the treatment of oil sands tailings", in 19th International Seminar on Paste and Thickened Tailings, 2016.

[22] L.G. Reis, R.S. Oliveira, T.N. Palhares, L.S. Spinelli, E.F. Lucas, D.R.L. Vedoy, E. Asare and J.B.P. Soares, "Using acrylamide/propylene oxide copolymers to dewater and densify mature fine tailings", Minerals Eng, vol. 95, pp. 29-39, 2016.

Chapter 2

2 Background and Literature Review

2.1 MFT Composition

Oil sands tailings are waste streams of the oil sands extraction process. In terms of mineral size, tailings are divided into coarse sand particles with particle size of greater than 44 μm, and silt and fine clay particles with particle size of less than 44 μm. After tailings are transported to tailing ponds for solid-liquid separation, the coarse particles settle rapidly, and fresh tailings release a portion of their water. This water goes to the surface and recycle to the extraction process. The remaining slurry, containing about 15% solids, called fluid fine tailings (FFT). The FFT loses more water throughout the consolidation process during few years of settling and make a thick slurry called mature fine tailings (MFT) [1, 2].

MFT are gel-like suspensions containing less water and finer clay particles than fresh tailings, which consolidate more slowly. Further, the compositions and particle size fractions of clays in oil sands ores and tailings differ from their produced MFT. Kaolinite is the dominant clay type in typical oil sand ores and tailings for an average particle size distribution; however, clays like kaolinite-smectite and illite-smectite with finer particles (in the range of < 2 μm and < 0.2 μm) are concentrated in MFT [3, 4].

Understanding the surface properties of clays is important as they affect the MFT dewatering. The most abundant clay minerals in MFT are kaolinite and illite, with small amounts of montmorillonite and smectite. General features of clays are small particle size with high specific surface area, swelling capacity, cation exchange capacity, layer charge, layered crystal structure and anisotropic dimensions. In general, the layered clays are made of tetrahedral and octahedral sheets. A tetrahedral sheet (T) consists a formation of four oxygen atoms around a cation, which

makes a tetrahedron. These tetrahedrons share their oxygen atoms of all three corners with three adjacent tetrahedrons and arrange the two-dimensional pattern of tetrahedral sheets (Figure 2-1). The main cation in the tetrahedral sheet is Si^{4+}, which can also be substituted with $Al^{3+}$and Fe^{3+} [5, 6]. The other main structural element of clays would be the octahedral sheets (M). The octahedral units are octahedrons, which consist two planes of close-packed oxygen and hydroxyl ions, with a cation in the octahedral spaces between the two planes. The octahedrons share their edges with adjacent octahedrons to form a two-dimensional pattern of octahedral sheets (Figure 2-1).

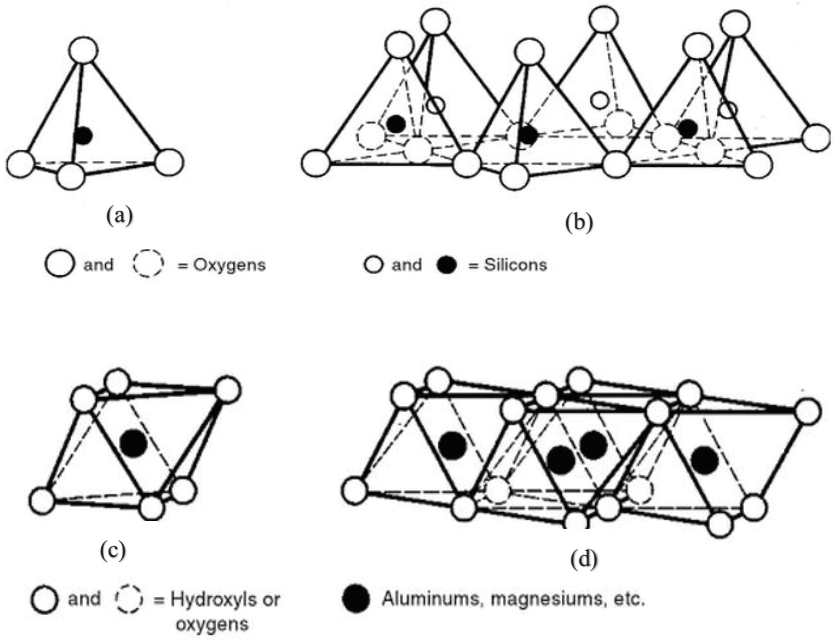

Figure 2-1: schematics of tetrahedral and octahedral sheets in clays. a) Single tetrahedron, b) Isomeric view of the tetrahedral sheet, c) single octahedron, d) isomeric view of the octahedral sheet [6, 7].

Clay minerals are made up of octahedral and tetrahedral sheets joined together in layers. Two main arrangements of octahedral and tetrahedral layers in clay minerals are the 1:1 (TM) and the 2:1 (TMT), which result different types of clays. Kaolinite is an example of 1:1 layer structures, whereas illite has 2:1 structures, as shown in Figure 2-2 [8, 9].

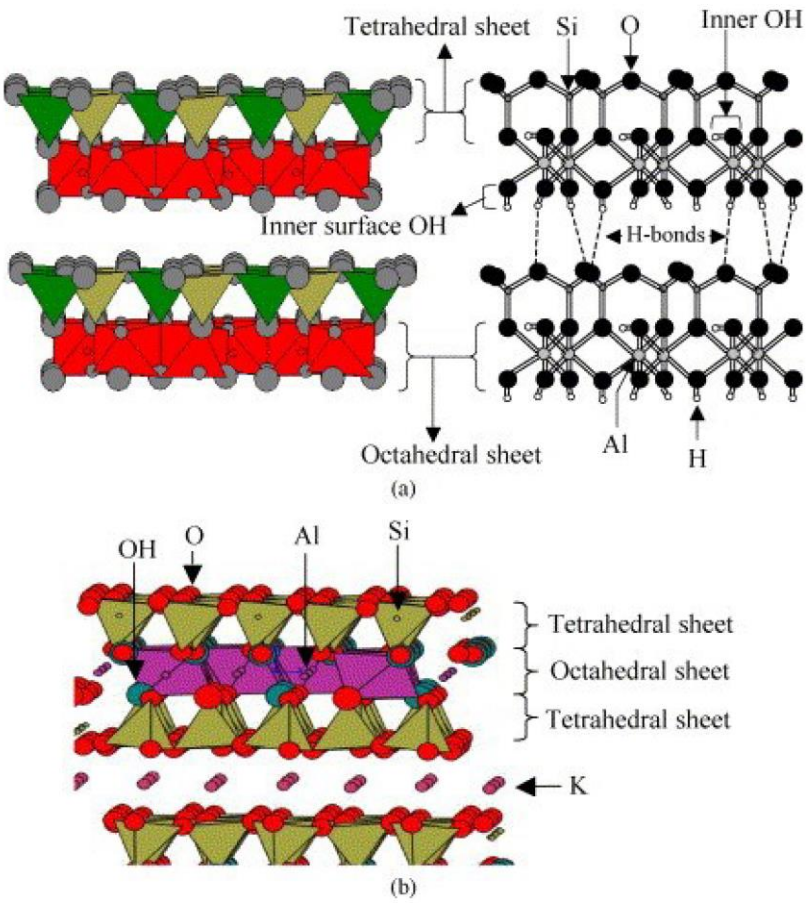

Figure 2-2: Layer structure of clays. a) 1:1 structure of kaolinite, b) 2:1 structure of illite [9].

A key characteristic of clay minerals is that they carry charges. The clay charges can be categorized in two types of structural (permanent) and surface (PH dependent) charges. Ion substitutions and imperfections are the source of structural charge. Ionic substitutions of higher valance cations like Si^{+4} in tetrahedral and Al^{+3} in octahedral sheets by lower valance cations including Al^{+3} in tetrahedral and Mg^{+2} or Fe^{+2} in octahedral structures respectively, creates the permanent negative charges in clay minerals. Clay surfaces also carry permanent negative charges due to ion substitution that are pH-insensitive; however, the edges are pH dependent and become negatively charged at higher pH. Hydrogen also can be replaced by cations along the edges when it is exposed to hydroxyls [8]. Surface charges may also be produced through the dissociation of surface groups. As shown in Equation 2-1, negative charges accumulate on clay surfaces due to the reaction between the silica and water to form silicic acid. This silicic acid also transforms to silicic anion

on the surface of clays, and H^+ ions that diffuse into the solution. This process is pH sensitive; at high pH, the equilibrium shifts to the right and generates more negative charges on the clay surfaces.

$$(SiO_2)_S + H_2O \leftrightarrow (H_2SiO_3)_S \leftrightarrow (HSiO_3^-)_S + H^+ \quad (2\text{-}1)$$

A different cation exchange also takes place in the interlayers of some clays. The replacement of interlayer cations with larger cations cause a swelling in the clay structure. Some interlayers of clay structure are not accessible, like kaolinite and illite, which makes them non-swelling clays. However, if the interlayers are accessible and cation exchange one happens with larger cations, such clay structures will expand, which makes them categorized as swelling clays. The presence of a small fraction of swelling clays, like smectite clays, causes significant expansion in MFT that forms a gel-like slurry.

2.2 Polymeric Flocculants

Paste technology, which involves the use of polymeric flocculants, is commonly used to treat different types of mining waste. To date, most studies have used commercially available polyacrylamide (PAM) or partially hydrolyzed anionic polyacrylamide (HPAM) [10] flocculants to treat oil sands tailings. Despite promoting fast settling and initial water release rates, both PAM and HPAM suffer from limitations such as shear sensitivity, poor dispersion in tailings, inability to flocculate fine clay particles effectively, and retention of large amounts of water in the sediments [11].

Many investigations have been done to develop polymer flocculants with novel chemistries as alternatives to polyacrylamide to address the MFT dewatering issue; however, the major outcomes included an increase in settling rate and improvement of supernatant turbidity. But, the flocs formed using such flocculants still hold a significant amount of water that cannot be further recovered.

Hydrophobically-modified polymers are potential candidates to enhance dewatering of MFT and obtain compact sediments. Lu et al. synthesized the random copolymers based on N-isopropylacrylamide (NIPAAm) containing 2-aminoethyl methacrylamide hydrochloride (AEMA) and 5-methacrylamido-1,2-benzoboroxole (MAAmBo), P($AEMA_{51}$-*st*-$MAAmBo_{76}$-*st*-$NIPAM_{381}$), for the flocculation and dewatering of the fine particle suspensions. They have shown, the lower critical solution temperatures (LCSTs) of P($AEMA_{51}$-*st*-$MAAmBo_{76}$-*st*-$NIPAM_{381}$) decreases because of the hydrophobic nature of the benzoboroxole moieties, resulting in strong hydrophobic interaction at temperatures higher than the LCSTs. They have also shown the polymer caused fast settling rate of the particles due to the strong adhesion of benzoboroxole residues to the kaolin hydroxyl groups, the electrical double layer force, and the hydrophobic force. The viscosity of this flocculant is also low, which makes the mixing of flocculant with suspension more efficient and facilitates the adsorption of polymer chains onto clay particles [12].

Similarly, activated sludge was flocculated by another hydrophobically modify PADB flocculant containing acrylamide (AM) and acryloyloxyethyl trimethyl ammonium chloride (DAC). Results showed that the structure of the polymer used in this study had an obvious correlation with dewaterability. PADB with porous structure had better dewatering efficiency, which produced smaller and likely drier, flocs. The reduction in flocs size improved the compaction of sediments and recovery of clear water, at the cost of settling rate of the suspension [13].

Other modified PAMs, such as temperature-sensitive poly-N-isopropylacrylamide (PNIPAM), have been evaluated because their higher hydrophobicity repels water trapped in the sediments. PNIPAM is hydrophilic below its lower critical solution temperature (LCST) of 32 °C, but turns hydrophobic above its LCST, enabling PNIPAM to repel water trapped in the sediments [14]. PNIPAM was shown to flocculate finer particles, consolidate sediments, and generate supernatants with lower turbidity than HPAM [15]. However, heating large volumes of MFT/PNIPAM suspensions above the LCST of 32 ºC is necessary for optimal performance, making this flocculant less attractive from an economic perspective.

Other investigations have shown that polyacrylamide-graft-poly(propylene oxide) (PAM-*g*-PPO) flocculates and dewaters MFT more effectively than commercial HPAM, likely due to the presence of the hydrophobic PPO grafts. PAM-*g*-PPO is also less shear sensitive and easier to mix with MFT because of its lower molecular weight. Despite of these advantages, high dosages (up to

10,000 ppm) were needed for optimal performance, which might restrict large scale applications [16].

Botha et al. [17, 18] synthesized hyperbranched polyethylene containing polar functional groups, and used it to treat oil sands tailings. The authors showed that in the presence of cations in the process water, the polar functional groups in the hyperbranched functionalized polyethylene adsorbed onto the surface of the clay particles, causing them to flocculate. Because of the hydrophobic polyethylene core, less water was retained in the sediments. The hyperbranched functionalized polyethylene improved flocculation and dewatering performance with respect to a commercial HPAM, but was limited by its low molecular weights of only up to 7000 g/mol and its insufficient polar group density [17, 18]. Therefore, one is stands as one of the motivation of this work is the optimization of this class of flocculants to achieve higher molecular weights and higher polar functional groups by grafting polar polymer chains to the polyethylene backbone.

2.3 Functionalization of Polyethylene

This section reviews the literature on the functionalization of polyethylene by a variety of methods, which used as the starting point to make functional polyethylene graft copolymer flocculants to treat oil sands tailings.

2.3.1 Functionalization of Polyethylene by Direct Polymerization

Polyethylene is one of the most useful commodity polymers today because of its versatility and wide range of applications. Most commercial polyethylenes are made of only carbon and hydrogen atoms, and therefore are highly hydrophobic and incompatible with polar polymers and additives. Naturally, they are not soluble or even dispersible in water. Copolymers of ethylene and polar comonomers, however, are very interesting materials because they combine the advantages of functional comonomers to the versatility and low cost of polyethylene [19].

Functional polyethylene may be made by the direct copolymerization of ethylene and polar monomers. This approach, however, is limited by low catalyst activities and insufficient degrees of functionalization, since most ethylene polymerization catalysts are poisoned by polar monomers

[19]. Brookhart et al. developed late transition metal catalysts, such as Ni-diimine and Pd-diimine catalyts, that are less oxophilic than early transition metal catalysts (Ziegler–Natta and metallocene catalysts, traditionally used to make commodity polyethylene resins) and can be used to copolymerize ethylene and polar comonomers such as acrylates, ethers, and hydroxyls. Pd-diimine catalysts can make polyethylene with branched topologies in a single polymerization step via the chain walking polymerization mechanism. In this method, the functionalization of unreactive carbon–hydrogen bonds occurs by movement of the catalyst around on the substrate to find preferable bond-forming sites [20-22]. A number of studies on the unique properties of hyperbranched functional polyethylenes (HB*f*PE) have been published, and reviews on the synthesis and application of these polymers are available [23, 24].

Hyperbranched functional polyethylenes have been used as high performance UV-curable cross linkers, inorganic nanofillers, and potential vehicles for drug delivery [23, 24]. Prior to the investigation of Botha et al. [17], however, functional polyethylenes had never been used as flocculants in any type of application. Botha et al. used a Pd-diimine catalyst to synthesize hyperbranched functional polyethylenes (HB*f*PE) using methyl acrylate as comonomer (Figure 2-3). Triisobutyl aluminium (TIBAL) was used to protect the polar functionality and reduce catalyst poisoning. Copolymers molecular weights up to 7,000 g/mol and methyl acrylate incorporation of 12 mol % to 50 mol % were obtained. The degree of branching was controlled by changing ethylene pressure, and comonomer content was controlled by varying concentration of methyl acrylate and TIBAL. The copolymer was hydrolyzed in a post polymerization step to obtain anionic functional groups enabling dispersal of the polymer in water, as shown in Equation 2-2 [17].

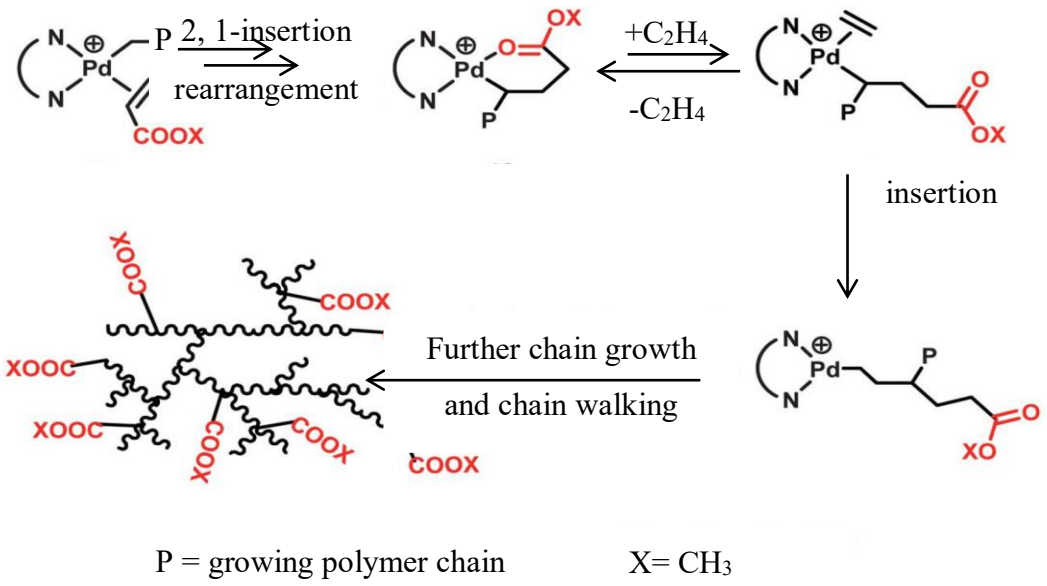

Figure 2-3: Copolymerization of ethylene with vinyl acrylate comonomer by Pd-diimine catalyst [23].

$$R\text{-}COOCH_3 \xrightarrow[H_2O]{K^+ OH^-} R\text{-}COOH + CH_3OH \qquad (2\text{-}2)$$

The authors used these copolymers to flocculate diluted MFT (20 wt. % solids), obtaining better flocculation and dewatering performance with respect to a commercial HPAM, especially for the copolymers with higher functional group contents. The HP*f*PE produced supernatants with lower turbidity, and sediments with lower capillary suction time (CST) than those obtained with the reference HPAM. Figure 2-4 shows how varying the dosage of HB*f*PEs and HPAM affected the CST of a 20 wt. % MFT suspension [17]. The HB*f*PE with 35, 40, and 50 mol % MA obtained lower CST for all dosages up to 4000 ppm, compared to HPAM. HB*f*PE with 35 mol % MA (lower functional group content) had the highest CST values in the HB*f*PE series, but they were still better than HPAM for all dosage.

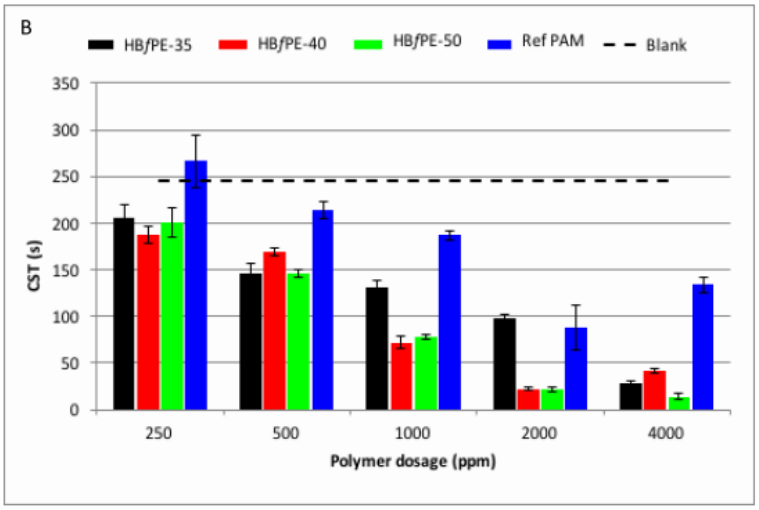

Figure 2-4**:** CST comparison of HB*f*PE with 35, 40, and 50 mol % and anionic PAM on 20 wt. % MFT after 24 hours [17] (dashed line show the CST value for a blank run, when no flocculant was added to the MFT).

Moreover, HB*f*PE promoted faster settling rates than HPAM with 1,000 ppm dosage, as shown in Figure 2-5 [17].

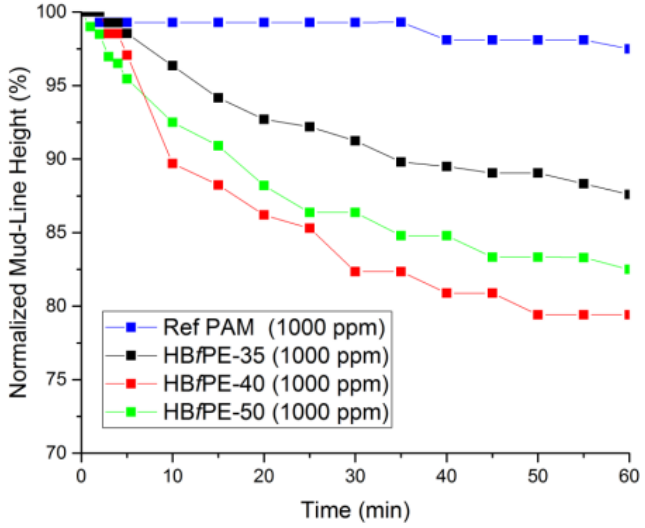

Figure 2-5: Comparison of flocculation performance of HB*f*PE with different functional contents and HPAM at 1000 ppm [17].

These results from a new class of flocculants for the treatment of mature fine tailing are promising, but HB*f*PE have much lower molecular weight (< 10,000 g/mol) [17] than other PAM flocculants usually used in industry (~ 17 million g/mol) [10]. Therefore, the next optimization step for this class of flocculants is to achieve higher molecular weights and higher polar functional groups by grafting polar polymer chains to the polyethylene backbone.

2.3.2 Functionalization of Polyolefins by Grafting

2.3.2.1 Hydroboration

Functionalized polyolefin copolymers with graft structures can be produced with a high degree of functionalization and high molecular weight via hydroboration. A number of studies, reviews, and books are available on the synthesis and application of functionalized polyolefin copolymers with graft structures [19, 25-27]. The hydroboration of high molecular weight rubbers like ethylene/propylene/diene (EPDM) terpolymers may be a convenient alternative to make functional polyolefin copolymers with higher molecular weights. This is a two-step process where a high molecular weight EPDM (made in a previous polymerization step) containing pendant double bonds reacts with borane groups to form reactive intermediates. The borane groups attached to the EPDM backbone can be easily oxidized at ambient temperature to form polymeric radicals that can further react with other monomers, especially polar vinyl monomers [25]. The decomposition of boron peroxides gives an alkoxy radical, which is very reactive, and a borinate radical, which is not very active and reversibly bonds to the growing chain end by weak interactions. Then, by dissociation from this resting state, the chain can grow further, and it minimizes chain transfer and termination reactions. This procedure, however, faces some challenges such as long polymerization times, sensitivity of borane to air, and oxygen control difficulties during the oxidation step, since excess amounts of oxygen during the oxidation step poisons free-radical polymerization and also over-oxidates the boranes to boronates and borates, which are poor free radical initiators [19, 27]. Graft copolymerization by controlled free radical polymerization can overcome these difficulties.

2.3.2.2 Reverse Atom Transfer Radical Polymerization

In 1995, atom transfer radical polymerization (ATRP) was discovered by Matyjaszeweski's [28] and Sawamoto's [29] groups independently. The technical literature on this method has been growing very fast, and many studies have been done on the synthesis of polymers by ATRP using a large variety of monomers [30-34]. ATRP is a controlled radical polymerization (CRP) technique that can make polymers with predetermined molecular weights, and narrow molecular weight distributions, as chain transfer and termination is suppressed, or at least significantly reduced, during ATRP. Figure 2-6 shows the general mechanism of ATRP. This process occurs in the presence of an initiator/dormant macromolecular species that has an easily transferable halide atom (RX /P_nX) and a catalyst. The catalyst (or activator) is a metal in lower oxidation state (Mt^n) with a suitable ligand (L). Polymerization starts when the halide atom transfers from the initiator to the catalyst to form a free radical ($P_n^{\bullet}$) and a metal halide at higher oxidation state ($X\text{-}Mt^{n+1}$) (deactivator). Fairly soon, an equilibrium is established for this reversible process that is mostly shifted towards the side with low radical concentration and, as a result, the likelihood of chain termination and transfer taking place are minimized [35].

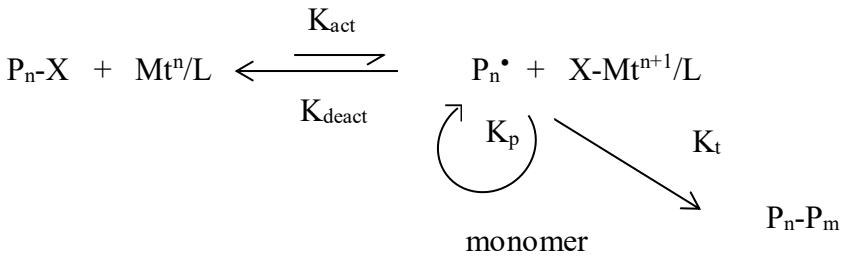

Figure 2-6: ATRP mechanism. k_{act}: activation rate constant, k_{deact}: deactivation rate constant, k_p: propagation rate constant, k_t: termination rate constant, P_nX: dormant species, Mt^n/L: activator, $P_n^{\bullet}$: polymer radical, $X\text{-}Mt^{n+1}/L$: deactivator, $P_n\text{-}P_m$: dead chain [35].

ATRP is a powerful technique that can be carried out in a wide range of polymerization temperatures, and it is not very sensitive to the presence of oxygen. It can make polymers with well-defined compositions such as block copolymers, polymers with controlled molecular topology (combs, stars, etc.), and functional polymers [30-33]. In addition, in an ideal ATRP

process, the initiation step is so fast that all chains are initiated at nearly the same time and grow at the same rate; in other words, at any instance of the polymerization (assuming that chain transfer and termination events happen at negligible frequencies), we have a population of polymeric radicals possessing polydispersity of one. As a consequence, polymer molecular weight changes linearly with monomer conversion [33].

Various di-block, tri-block, and multiblock copolymers have been synthesized by ATRP using the macroinitiator method. In this method, the first monomer type (A) is polymerized with an initiator having an end carbon halide to make macroinitiators (carbon halide at a polymer chain end). In a subsequent step, the macroinitiators are allowed to initiate the polymerization of a second monomer type (B) to produce AB block copolymers, which can be also used as macroinitiators to initiate the polymerization of a third monomer type to produce tri-block copolymers. Bifunctional initiators can also be used to prepare ABA triblock copolymers [30-34].

Star polymers may also be prepared via ATRP using multifunctional initiators with more than two reactive carbon-halogen bonds. The number of arms is defined by the functionality of the initiator, and the arm length is determined by the molar ratio of monomer to initiator [31].

Graft copolymers are also easily made by ATRP via the two main approaches illustrated in Figure 2-7: Grafting from makes graft copolymers from macroinitiators with pendant functionalities, and grafting through synthesizes graft copolymers by polymerization of macromonomers [30].

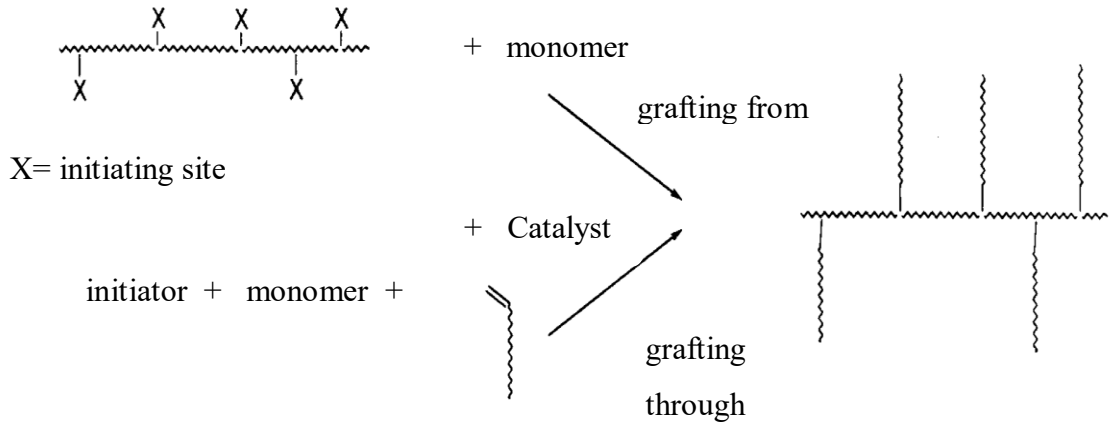

Figure 2-7: Synthesis of graft copolymer by ATRP via grafting from and grafting through processes [30].

One of the big advantages of ATRP is being tolerant to many monomer functionalities such as hydroxyl, amino, esters, since ATRP is a free radical process [31, 32]. This powerful method can be used to graft polar polymer chains to polyolefin backbones to broad their applications. A number of studies, and reviews on the synthesis and applications of functional polyolefin copolymers with graft structures are available [30-32, 36-39]. The synthesis of functional polyolefin graft copolymers by ATRP is a two-step process: in the first step, a halide group must be attached onto the pololefin backbone, and in the second step grafts are grown from the halide groups [40].

Reverse ATRP, on the other hand, requires only one step to create graft copolymers. Figure 2-8 illustrates some features of the reverse ATRP mechanism. In this process, a thermal initiator like azobisisobutyronitrile (AIBN) is decomposed by heat to generate free radicals. The combination of a thermal initiator, a metal halide such as $CuCl_2$ or $CuBr_2$ in their higher oxidation states, and a ligand to bind the catalyst initiates the polymerization as the radical initiator reacts with the transition metal, forming metal species in lower oxidation states and dormant species. The formed transition metal in lower oxidation state promotes the ATRP process [41].

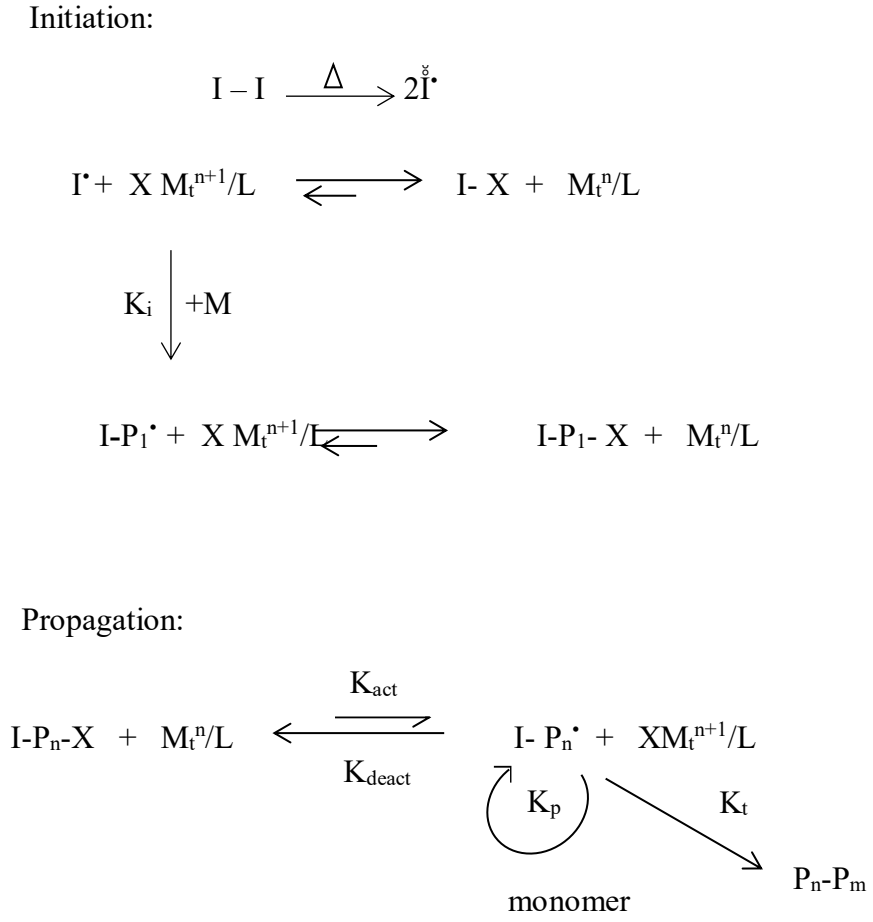

Figure 2-8: Reverse ATRP mechanism. I-I: initiator, I•: primary radical, M: monomer, k_i: initiation rate constant, k_{act}: activation rate constant, k_{deact}: deactivation rate constant, k_p: propagation rate constant, k_t: termination rate constant, $I\text{-}P_nX$: dormant species, Mt^n/L: activator, $I\text{-}P_n^{\bullet}$: polymer radical, $X\text{-}Mt^{n+1}/L$: deactivator, $P_n\text{-}P_m$: dead chain [41].

Reverse ATRP has been used to synthesize functional polyolefin graft copolymers for different applications [42-44]. Grafting polar polymer chains onto polyolefin backbone can improve the interaction of the grafted chains with wide range of materials, making them suitable for many applications such as drug delivery, biomaterials, and coating. They can also be used as compatibilizers for polymer blends [36, 37]. The major advantage of this approach for this thesis was its capability of making functional polyolefin graft copolymers with predetermined grafts molecular weights and narrow molecular weight distributions, under negligible chain transfer and termination reactions. Reverse ATRP was the starting point for us to make series of functional polyolefin graft copolymers with distinct graft molecular weights and density as flocculants to treat oil sands tailings.

References

[1] L. Botha and J.B.P. Soares, "The Influence of Tailings Composition on Flocculation", Can.J.Chem.Eng., vol. 93, pp. 1514-1523, 2015.

[2] K.L. Kasperski and R.J. Mikula, "Waste streams of mined oil sands: Characteristics and remediation", Elements, vol. 7, pp. 387-392, 2011.

[3] O.E. Omotoso and R.J. Mikula, "High surface areas caused by smectitic interstratification of kaolinite and illite in Athabasca oil sands", Appl.Clay.Sci., vol. 25, pp. 37-47, 2004.

[4] H.A.W. Kaminsky, T.H. Etsell, D.G. Ivey and O. Omotoso, "Distribution of clay minerals in the process streams produced by the extraction of bitumen from athabasca oil sands", Can.J.Chem.Eng., vol. 87, pp. 85-93, 2009.

[5] D.M. Moore and R.C. Reynolds, X-ray diffraction and the identification and analysis of clay minerals, Oxford University Press, 1997.

[6] F. Bergaya, B.K.G. Theng and G. Lagaly, Handbook of clay science. [electronic resource], Elsevier, 2006.

[7] D.M. Clementz, "Interaction of petroleum heavy ends with montmorillonite", Clays Clay Miner., vol. 24, pp. 312-319, 1976.

[8] J.H. Masliyah, Z. Xu, J.A. Czarnecki and M. Dabros, Handbook on theory and practice of bitumen recovery from Athabasca Oil Sands, Cochrane, Alberta: Kingsley Knowledge Pub., 2013.

[9] K.L. Konan, C. Peyratout, J.P. Bonnet, A. Smith, A. Jacquet, P. Magnoux and P. Ayrault, "Surface properties of kaolin and illite suspensions in concentrated calcium hydroxide medium" J.Colloid Interface Sci., vol. 307, pp. 101-108, 2007.

[10] H. Li, J. Long, Z. Xu and J.H. Masliyah, "Synergetic role of polymer flocculant in low-temperature bitumen extraction and tailings treatment", Energy Fuels, vol. 19, pp. 936-943, 2005.

[11] D.R.L. Vedoy and J.B.P. Soares, "Water-soluble polymers for oil sands tailing treatment: A Review", Can.J.Chem.Eng., vol. 93, pp. 888-904, 2015.

[12] H. Lu, Y. Wang, L. Li, Y. Kotsuchibashi, R. Narain and H. Zeng, "Temperature- and pH-Responsive Benzoboroxole-Based Polymers for Flocculation and Enhanced Dewatering of Fine Particle Suspensions", ACS Appl.Mater.Interfaces, vol. 7, pp. 27176-27187, 2015.

[13] H. Zheng, Y. Sun, J. Guo, F. Li, W. Fan, Y. Liao and Q. Guan, "Characterization and evaluation of dewatering properties of PADB, a highly efficient cationic flocculant", Ind.Eng.Chem.Res., vol. 53, pp. 2572-2582, 2014.

[14] J. Long, H. Li, Z. Xu and J.H. Masliyah, "Improving oil sands processability using a temperature-sensitive polymer", Energy Fuels, vol. 25, pp. 701-707, 2011.

[15] H. Li, J. Zhou, R. Chow, A. Adegoroye and A.S. Najafi, "Enhancing treatment and geotechnical stability of oil sands fine tailings using thermo-sensitive poly(n-isopropyl acrylamide)", Can.J.Chem.Eng., vol. 93, pp. 1780-1786, 2015.

[16] L.G. Reis, R.S. Oliveira, T.N. Palhares, L.S. Spinelli, E.F. Lucas, D.R.L. Vedoy, E. Asare and J.B.P. Soares, "Using acrylamide/propylene oxide copolymers to dewater and densify mature fine tailings", Minerals Engineering, vol. 95, pp. 29-39, 2016.

[17] L. Botha, S. Davey, B. Nguyen, A.K. Swarnakar, E. Rivard and J.B.P. Soares, "Flocculation of oil sands tailings by hyperbranched functionalized polyethylenes (HBfPE)", Minerals Eng, vol. 108, pp. 71-82, 2017.

[18] L. Botha, D. Vedoy and J. Soares, "Novel hyperbranched functionalized polyethylenes for the treatment of oil sands tailings", in 19th International Seminar on Paste and Thickened Tailings, 2016.

[19] T.C. Chung, Functionalization of polyolefins, San Diego: Academic Press, 2002.

[20] L.K. Johnson, S. Mecking and M. Brookhart, "Copolymerization of ethylene and propylene with functionalized vinyl monomers by palladium(II) catalysts", J.Am.Chem.Soc., vol. 118, pp. 267-268, 1996.

[21] S. Mecking, "Mechanistic studies of the palladium-catalyzed copolymerization of ethylene and a-olefins with methyl acrylate", J.Am.Chem.Soc., vol. 120, pp. 888-899, 1998.

[22] G. Chen, X.S. Ma and Z. Guan, "Synthesis of functional olefin copolymers with controllable topologies using a chain-walking catalyst", J.Am.Chem.Soc., vol. 125, pp. 6697-6704, 2003.

[23] Z. Dong and Z. Ye, "Hyperbranched polyethylenes by chain walking polymerization: Synthesis, properties, functionalization, and applications", Polym.Chem., vol. 3, pp. 286-301, 2012.

[24] Z. Ye and S. Li, "Hyperbranched polyethylenes and functionalized polymers by chain walking polymerization with PD-diimine catalysis", Macromol.React.Eng., vol. 4, pp. 319-332, 2010.

[25] T.C. Chung, W. Janvikul, R. Bernard and G.J. Jiang, "Synthesis of ethylene-propylene rubber graft copolymers by borane approach", Macromolecules, vol. 27, pp. 26-31, 1994.

[26] T.C. Chung, W. Janvikul, R. Bernard, R. Hu, C.L. Li, S.L. Liu and G.J. Jiang, "Butyl rubber graft copolymers: synthesis and characterization", Polymer, vol. 36, pp. 3565-3574, 1995.

[27] T.C. Chung, "Synthesis of functional polyolefin copolymers with graft and block structures", Prog.Polym.Sci. (Oxford), vol. 27, pp. 39-85, 2002.

[28] J.S. Wang and K. Matyjaszewski, "Controlled/living radical polymerization. Atom transfer radical polymerization in the presence of transition-metal complexes", J.Am.Chem.Soc., vol. 117, pp. 5614-5615, 1995.

[29] M. Kato, M. Kamigaito, M. Sawamoto and T. Higashimura, "Polymerization of methyl methacrylate with the carbon tetrachloride/dichlorotris-(triphenylphosphine)ruthenium(II) /methylaluminum bis(2,6-di-tert-butylphenoxide) initiating system: possibility of living radical polymerization", Macromolecules, vol. 28, pp. 1721-1723, 1995.

[30] K. Matyjaszewski and J. Xia, "Atom transfer radical polymerization", Chem.Rev., vol. 101, pp. 2921-2990, 2001.

[31] V. Coessens, T. Pintauer and K. Matyjaszewski, "Functional polymers by atom transfer radical polymerization", Progress in Polymer Science, vol. 26, pp. 337-377, 2001.

[32] M. Kamigaito, T. Ando and M. Sawamoto, "Metal-catalyzed living radical polymerization", Chem.Rev., vol. 101, pp. 3689-3745, 2001.

[33] K. Matyjaszewski and N.V. Tsarevsky, "Nanostructured functional materials prepared by atom transfer radical polymerization", Nat.Chem., vol. 1, pp. 276-288, 2009.

[34] K.A. Davis and K. Matyjaszewski, Statistical, gradient block and graft copolymers by controlledliving radical polymerizations, Berlin; New York: Springer, 2002, pp. 191.

[35] K. Matyjaszewski, "Atom transfer radical polymerization: From mechanisms to applications", Isr.J.Chem., vol. 52, pp. 206-220, 2012.

[36] W.J. Wang, L. Pingwei, B.G. Li and Z. Shiping, "One-step synthesis of hyperbranched polyethylene macroinitiator and its block copolymers with methyl methacrylate or styrene via ATRP", J.Polym.Sci.Part A, vol. 48, pp. 3024-3032, 2010.

[37] Y. Inoue, T. Matsugi, N. Kashiwa and K. Matyjaszewski, "Graft copolymers from linear polyethylene via atom transfer radical polymerization", Macromolecules, vol. 37, pp. 3651-3658, 2004.

[38] H. Kaneko, J. Saito, N. Kawahara, S. Matsuo, T. Matsugi and N. Kashiwa, "Polypropylene-graft-poly(methyl methacrylate) Graft Copolymers: Synthesis and Compatibilization of Polypropylene/Polylactide", in Controlled/Living Radical Polymerization: Progress in ATRP, American Chemical Society, 2009, pp. 357-371.

[39] X.S. Wang, N. Luo and S.K. Ying, "Synthesis of EPDM-g-PMMA through atom transfer radical polymerization", Polymer, vol. 40, pp. 4515-4520, 1999.

[40] V.M.C. Coessens and K. Matyjaszewski, "Fundamentals of atom transfer radical polymerization", J.Chem.Educ., vol. 87, pp. 916-919, 2010.

[41] J. Xia and K. Matyjaszewski, "Controlled/living radical polymerization. Homogeneous reverse atom transfer radical polymerization using AIBN as the initiator", Macromolecules, vol. 30, pp. 7692-7696, 1997.

[42] K. Yamamoto, H. Tanaka, M. Sakaguchi and S. Shimada, "Well-defined poly(methyl methacrylate) grafted to polyethylene with reverse atom transfer radical polymerization initiated by peroxides", Polymer, vol. 44, pp. 7661-7669, 2003.

[43] R. Ma, Z. Song, Y. Hou, Y. Liu, B. Xing, Z. Tan and F. Bao, "Synthesis of norbornene and methyl methacrylate graft copolymers with high norbornene content by using mixed catalytic system", Macromol Sci. Part A Pure Appl Chem, vol. 46, pp. 193-201, 2009.

[44] D.J. Haloi, K. Naskar and N.K. Singha, "Poly(meth)acrylate grafted EPDM via reverse atom transfer radical polymerization: A single pot process", Eur Polym J, vol. 49, pp. 4098-4107, 2013.

Chapter 3

3 Ethylene/Propylene/Diene Terpolymers Grafted with Poly(methyl acrylate) by Reverse Atom Transfer Radical Polymerization

This chapter describes the synthesis of ethylene-propylene-diene terpolymers (EPDM) grafted with poly(methyl acrylate) by reverse atom transfer radical polymerization. The poly(methyl acrylate) graft molecular weights and densities were controlled by varying the concentration and conversion of methyl acrylate, as well as the concentration of initiator. The grafted copolymers were characterized by Fourier-transform infrared spectroscopy, proton nuclear magnetic resonance, and gel permeation chromatography. Copolymers with graft molecular weights varying from 12 to 179 kDa and grafting densities from 11 to 53% were made following this procedure.

3.1 Introduction

Polyolefins are one of the most useful commodity polymers today because of their wide range of applications, but they are hydrophobic and incompatible with polar compounds. Copolymers of ethylene and polar comonomers, however, combine the advantages of functional comonomers with the versatility and low cost of polyolefins [1]. Functional polyethylenes may be made by coordination polymerization of ethylene and polar monomers, but this method is limited by low catalyst activities and insufficient degrees of functionalization [1]. Brookhart et al. developed late

transition metal catalysts that were less oxophilic than Ziegler–Natta and metallocene catalysts, traditionally used to make commodity polyethylenes. Late transition metal catalysts may be used to polymerize ethylene and polar monomers such as acrylates, ethers, and hydroxyls, and also to make branched polyethylenes via the chain walking mechanism [2-6].

Hyperbranched functional polyethylenes have been used as high performance UV-curable cross linkers, inorganic nanofillers, and vehicles for drug delivery [5,6]. Botha et al. [7] were the first to use functional polyethylenes as flocculants to treat mineral tailings. They used a Pd-diimine catalyst to synthesize hyperbranched functional polyethylenes (HB*f*PE) with molecular weights averages up to 7,000 and methyl acrylate incorporation of 12 mol % to 50 mol % (Figure 3-1) [7].

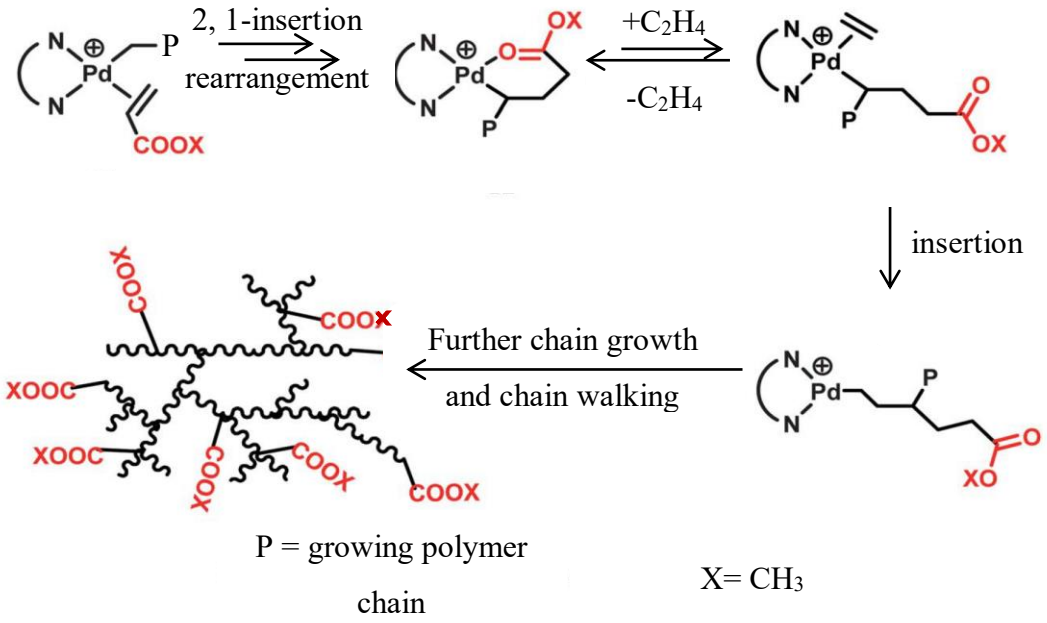

Figure 3-1: Copolymerization of ethylene and methyl acrylate with a Pd-diimine catalyst [7].

Botha et al. [7] hydrolyzed these copolymers in a post-polymerization step, generating anionic functional groups that enabled the polymer to be dispersed in water. The authors showed that these copolymers could densify oil sands tailings more effectively than conventional polyacrylamide flocculants, especially copolymers with higher fractions of functional groups. Unfortunately, HB*f*PE flocculants had molecular weights that were much lower than polyacrylamide flocculants commonly used in the industry for this application (~ 17 million) [8].

Several publications are available on the synthesis and applications of graft functionalized polyolefins [1, 9-11]. Hydroboration of high molecular weight rubbers, such as ethylene/propylene/diene monomer (EPDM) terpolymers, is one of the methods used to make functional polyolefins with higher molecular weights [9]. This procedure, however, faces challenges such as long polymerization times and sensitivity of boranes to air [1,11]. Graft copolymerization by controlled free radical polymerization can overcome these difficulties.

Atom transfer radical polymerization (ATRP) was independently discovered by Matyjaszeweski's [12] and Sawamoto's [13] groups in 1995. The literature on ATRP has grown rapidly to include a large variety of monomers [14-18]. Atom transfer radical polymerization is a controlled radical polymerization method that can make polymers with predetermined molecular weights and narrow molecular weight distributions by reducing chain transfer and termination reactions [19]. Many graft copolymers have been synthesized by ATRP using *grafting from* or *grafting to* approaches [14].

One of the advantages of ATRP is that it can polymerize monomers with many functionalities such as hydroxyl, amino, and esters [15,16]. It can also be used to graft polar polymer chains to polyolefin backbones to broaden their applications [14-16, 20-23]. The synthesis of functional polyolefin graft copolymers by ATRP is a two-step process: first, a halide group is bonded to the polyolefin backbone, then grafts are grown from the halide groups [24]. Reverse ATRP, on the other hand, needs only one step to make graft copolymers (Figure 3-2). First, a thermal initiator, such as azobisisobutyronitrile (AIBN), is decomposed to generate primary free radicals ($I^{\bullet}$). Then, the primary radicals either react with the transition metal complex in higher oxidation state (XMt^{n+1}/L) to make dormant species (I-X) and transition metal complexes in lower oxidation state (XMt^{n}/L), or react with monomer molecules to form polymer radicals ($I\text{-}P_1^{\bullet}$), which are rapidly deactivated by reaction with XMt^{n+1}/L, forming XMt^{n}/L and dormant species $I\text{-}P_1\text{-}X$. Subsequently, the dormant $I\text{-}P_n\text{-}X$ species are activated by reactions with XMt^{n}/L and the polymerization proceeds as in normal ATRP [25]. Haloi et al. showed how reverse ATRP could be used to graft poly(meth)acrylate onto EPDM backbones to enhance the properties of EPDM [26]. The synthesis method we used herein shares similarities with this previous publication.

Initiation:

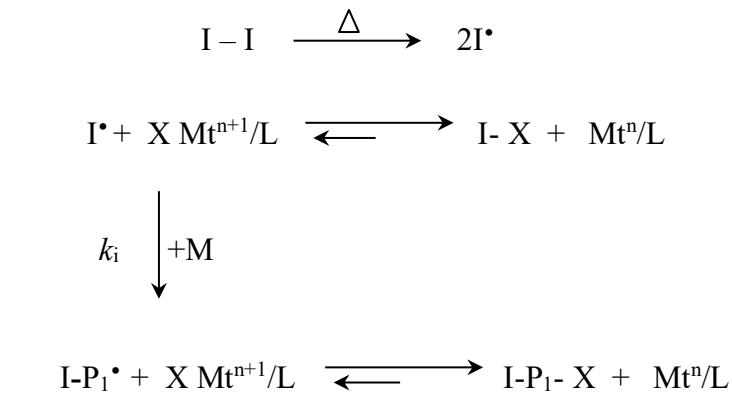

Propagation:

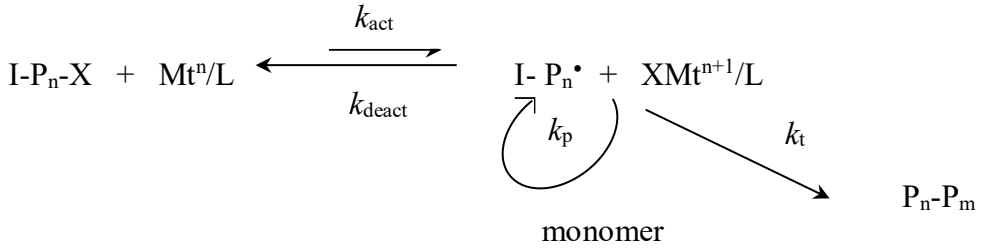

Figure 3-2: Reverse ATRP mechanism. I-I: initiator, I•: primary radical, M: monomer, k_i: initiation rate constant, k_{act}: activation rate constant, k_{deact}: deactivation rate constant, k_p: propagation rate constant, k_t: termination rate constant, I-P_nX: dormant species, Mt^n/L: activator, I-P_n•: polymer radical, X-Mt^{n+1}/L: deactivator, P_n-P_m: dead chain [25].

In the present investigation, poly(methyl acrylate) (PMA) side chains of different molecular weights were grafted onto EPDM backbones via reverse ATRP to make functional polyolefin graft copolymers with high molecular weights and high fractions of functional groups. Even though similar graft copolymers have been made before, this is the first time that the synthesis of grafts of PMA were added to EPDM backbones by reverse ATRP. The detailed characterization methods, particularly regarding the systematic variation of graft length and density – and related calculations – are also new. Moreover, the applications of these polymers as flocculants to treat oil sands tailings, as discussed in our companion article [27], opens new doors for the application of these new materials. These materials provide an alternative to the promising flocculants made by Botha

et al. [7], but eliminate the limitation of low molecular weights faced by the direct synthesis of hyperbranched functional polyethylenes.

3.2 Experimental

3.2.1 Materials

Ethylene–propylene–diene (EPDM) elastomers NORDEL IP 4520 (4.9 wt % ethylidene-norbornene, 50 wt % ethylene, 45.1 wt % propylene, Mooney viscosity at 125 ºC $ML_{1+4} = 20$) and NORDEL IP 4570 (4.9 wt % ethylidene-norbornene, 50 wt % ethylene, 45.1 wt % propylene, Mooney viscosity at 125 ºC $ML_{1+4} = 70$) were donated by the Dow Chemical Company. Azobisisobutyronitrile (AIBN) (98 %), copper(II) bromide ($CuBr_2$) (99 %), N,N,N′,N″,N″-pentamethyldiethylenetriamine (PMDETA) (99 %), and methyl acrylate (MA) (99 %) were purchased from Sigma-Aldrich and used without further purification. Toluene (99.8 %) from Sigma-Aldrich was used as a solvent in all syntheses. Hexane, acetone, and tetrahydrofuran (THF) were used to extract the grafted polymer from the homopolymer and unreacted reagents.

3.2.2 Synthesis of EPDM-*g*-PMA

Poly(methyl acrylate) was grafted from EPDM chains by reverse ATRP. The molecular weight and density of the grafts were controlled by varying the concentration and conversion of methyl acrylate, and the concentration of initiator. Two EPDM samples having the same chemical composition but different average molecular weights (M_b = 210 000 and 115 000) were used as backbones.

In a typical polymerization, AIBN (initiator), $CuBr_2$ (catalyst), and N,N,N′,N″,N″-pentamethyldiethylenetriamine (PMDETA, ligand) were dissolved in 2 mL of acetone. Then, 1.0 g of EPDM, dissolved in 20 mL of toluene, was mixed with the previous solution. The flask containing the mixture was stirred and purged with N_2 for 20 min before being immersed into an oil bath at 90 °C. After stirring the solution for 20 min, methyl acrylate (purged with N_2 for 20 min) was added using a syringe and a transfer needle to make EPDM-*g*-PMA. The polymerization continued from 8 to 48 hours. The polymer was precipitated in methanol, washed with additional

methanol, and dried at 60 °C for 24 hours. Hexane was used to extract ungrafted EPDM chains from the product, and acetone to extract ungrafted PMA, both by stirring the mixture for 24 h. The remaining fraction was recovered as the desired EPDM-*g*-PMA product. These three fractions were dried at 60 °C for 24 hours.

3.2.3 Purification of EPDM-*g*-PMA

Reverse ATRP needs a high catalyst-to-radical initiator ratio [28]. The catalyst is only partially soluble in most polymerization solvents [29] and since it is toxic, it must be removed from the product. Purification methods, such as flowing the polymer solution through silica gel or alumina columns or liquid-liquid extraction have been used to remove catalyst residues from the polymer product [30,31].

We used liquid-liquid extraction to extract $CuBr_2$ from EPDM-*g*-PMA. In a typical extraction, the graft copolymer was first dissolved in dichloromethane, which is immiscible with water. Deionized water was then added to the organic phase, creating two liquid phases (water on top of dichloromethane). The catalyst, $CuBr_2$, diffused from the organic to the water phase, and was removed using a syringe. Purified EPDM-*g*-PMA was collected from the organic phase by precipitating it in isobutanol.

3.2.4 Characterization of EPDM-*g*-PMA

Three fractions—EPDM, PMA, and EPDM-*g*-PMA—were recovered and weighed for each polymerization. Mass balances were used to calculate methyl acrylate conversion, graft molecular weights and densities, and EPDM-*g*-PMA molecular weight. EPDM-*g*-PMA graft densities were also measured by ^{1}H NMR, and EPDM-*g*-PMA molecular weights by gel permeation chromatography (GPC). These measurements are compared with the mass balance estimates in the Results and Discussion section.

The molecular weight distributions (MWD) of the products were measured by GPC at 40 ^{o}C using THF as eluent, with a flow rate of 0.5 mL·min^{-1}. The GPC 270Max dual detector (viscometer plus light scattering) was calibrated using a multidetector calibration method based on refractive index, low angle light scattering, and right angle light scattering data. It is notoriously difficult to

determine the absolute MWDs of non-linear polymers, and the EPDM-*g*-PMA samples made herein are no exception. This should be kept in mind when analysing the values of the molecular weight averages reported in this chapter. More importantly, however, is the comparison of the relative changes in molecular weight as a function of polymerization conditions, which allows us to design copolymers with different graft densities and molecular weights. For this purpose, GPC is a reliable guide.

The EPDM-*g*-PMA samples were characterized by Fourier transform-infrared spectroscopy (FTIR) using an Agilent Technologies, Cary 600 series FTIR spectrometer. The spectra were recorded from 400 to 4000 cm^{-1} after 64 scans.

The graft copolymers were also characterized by ^{1}H NMR in $CDCl_3$ using a u5 VNMRS 500 MHz spectrometer. The (-OCH_3) proton in the methyl acrylate, the unsaturated proton in the norbornene unit, and the proton in the methyl acrylate of the terminal group ($CHBrCOOCH_3$) of EPDM-*g*-PMAs were identified using their resonances at 3.6, 5.2, and 3.75 ppm, respectively. The amount of MA incorporated into the EPDM-*g*-PMAs was estimated from the integrated area under the appropriate peak intensities.

3.3 Results and Discussion

3.3.1 Polymer Synthesis

Figure 3-3 shows how the PMA grafts are envisioned to grow from the EPDM backbones by reverse ATRP. The thermal initiator (AIBN) is decomposed at 90 °C to generate primary free radicals. The EPDM pendant double bonds react with the primary initiators to form macroinitiators (I-P$^{\bullet}$). The graft polymerization starts when macroinitiators or the propagating radicals (I-P$^{\bullet}$ or I-P-P′$_1^{\bullet}$) abstract halogen atoms (Br) from the metal halide ($CuBr_2$) to form metal species in lower oxidation states and dormant macromolecular species (I-P-Br and I-P-P′$_1$-Br). The formed transition metal in lower oxidation state then promote the ATRP process.

Initiation:

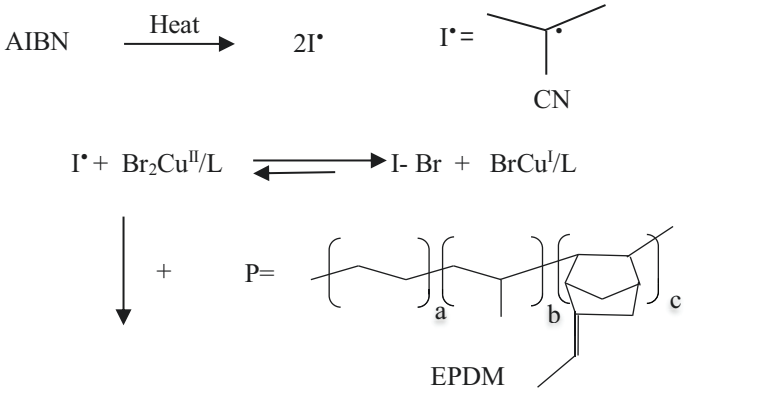

Propagation:

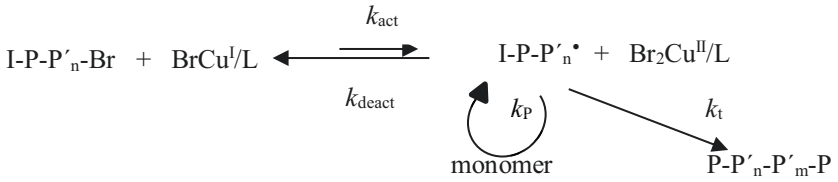

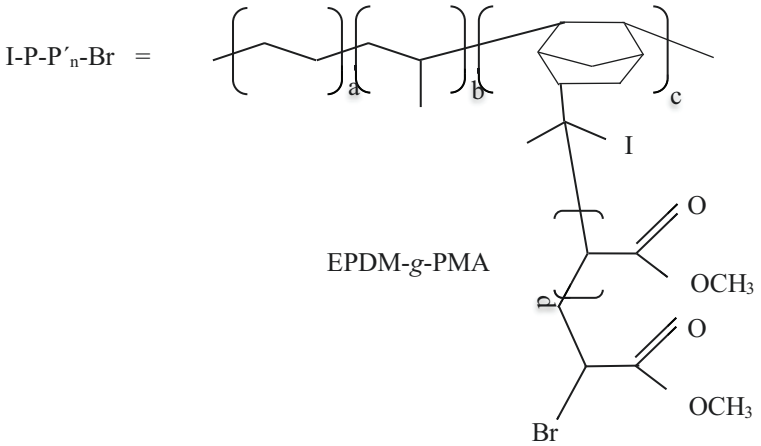

Figure 3-3: Graft copolymerization of methyl acrylate on EPDM by reverse ATRP.

Table 3-1 lists the synthesis conditions for all EPDM-*g*-PMA samples and some of their average properties.

Table 3-1: Polymerization conditions for EPDM-*g*-PMA synthesis and their properties.

Polymer[a]	$[MA]_0$	$[AIBN]_0$[b]	AIBN/EPDM	Time	Graft molecular weights	Graft density	EPDM-*g*-PMA
	mol/L	mol/L	mol%	h	M_g (kDa)	ρ_g (%)	M_w (kDa)
EPDM-*g*-PMA-210-12-11	5.0	0.00526	0.00785	8	12	11	321
EPDM-*g*-PMA-210-24-11	5.0	0.00526	0.00785	12	24	11	432
EPDM-*g*-PMA-210-49-14	7.6	0.00300	0.00785	24	49	14	795
EPDM-*g*-PMA-210-93-11	7.6	0.00300	0.00785	48	93	11	1082
EPDM-*g*-PMA-210-147-16	9.6	0.00121	0.00785	24	147	16	2217
EPDM-*g*-PMA-210-178-16	9.6	0.00121	0.00785	48	178	16	2640
EPDM-*g*-PMA-210-34-28	5.0	0.00450	0.00662	24	34	28	1022
EPDM-*g*-PMA-210-94-29	7.6	0.00253	0.00662	24	94	29	2537
EPDM-*g*-PMA-210-101-32	7.6	0.00253	0.00662	48	101	32	2969
EPDM-*g*-PMA-210-175-28	9.6	0.00105	0.00662	24	175	28	4393
EPDM-*g*-PMA-210-48-37	5.0	0.00360	0.00540	48	48	37	1725
EPDM-*g*-PMA-210-150-37	9.6	0.00086	0.00540	24	150	37	4949
EPDM-*g*-PMA-210-96-53	7.6	0.00170	0.00445	48	96	53	4554
EPDM-*g*-PMA-210-178-53	9.6	0.00070	0.00445	48	178	53	8256
EPDM-*g*-PMA-115-95-15	7.6	0.00300	0.00785	48	95	15	750
EPDM-*g*-PMA-115-143-14	9.6	0.00121	0.00785	24	143	14	1010
EPDM-*g*-PMA-115-179-13	9.6	0.00121	0.00785	48	179	13	1156

[a] EPDM-*g*-PMA-M_b-M_g-ρ_g: M_b = average molecular weight of the backbone (kDa), M_g = average molecular weight of the PMA grafts (kDa), ρ_g = percentual graft density.

[b] Initial $[AIBN]_0/[CuBr_2]_0/[PMDETA]_0$ ratio = 1/1.5/3.

Assuming that the concentration of polymer radicals is constant [32,33],

$$\ln\frac{[M]_0}{[M]} = k_p\,[P^\bullet]t = k_p^{app}t \tag{3-1}$$

where k_p^{app} is the apparent propagation rate constant.

In the ideal case of ATRP without termination reactions and constant $[P^\bullet]$, a plot of $\ln([M]_0/[M])$ versus time will give a straight line with slope equal to k_p^{app}.

Three series of EPDM-*g*-PMA samples were made using different concentrations of methyl acrylate (5.0 to 9.6 M) and polymerization times varying from 8 to 48 h. The EPDM average molecular weight was kept the same (M_b = 210 kDa) in all polymerizations. These polymers were made to find out how the concentration of MA varied as a function of polymerization time and to verify whether Equation (3-1) applied to our polymerization system. We calculated these concentrations through a mass balance using the three fractions separated according to Figure 3-4. Hexane was used to extract the ungrafted EPDM, and acetone to extract the ungrafted PMA from the product. The remaining fraction was the desired EPDM-*g*-PMA product.

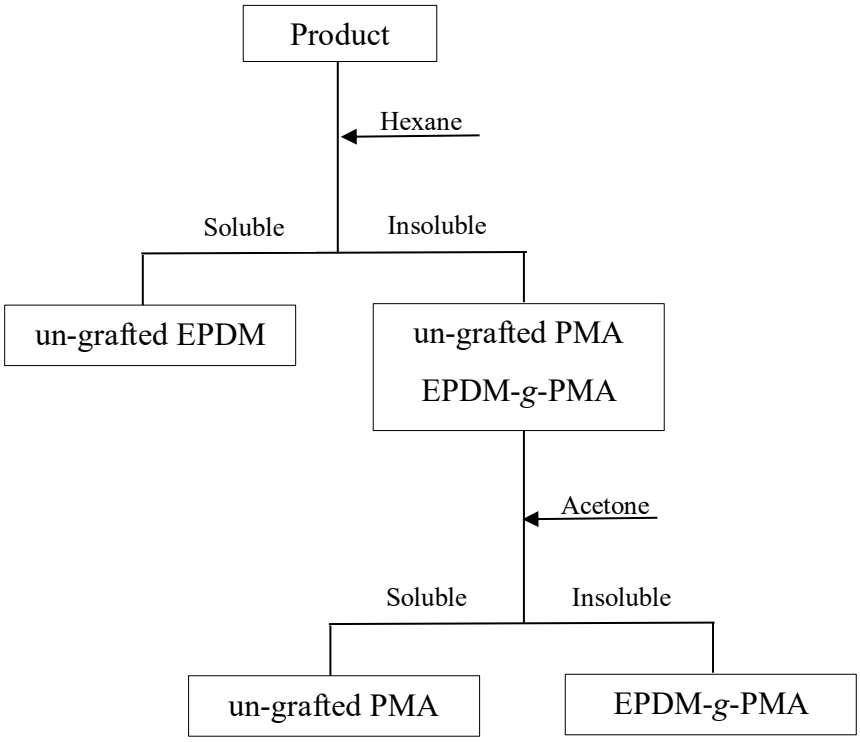

Figure 3-4: Product purification process steps.

Table 3-2 lists the mass of three fractions—ungrafted EPDM, ungrafted PMA, and EPDM-*g*-PMA—for each polymerization run.

Table 3-2: Masses of different fractions of the EPDM-*g*-PMA samples.

Polymer	ungrafted EPDM	ungrafted PMA	EPDM-*g*-PMA
	g	g	g
EPDM-*g*-PMA-210-12-11	0.28	4.77	0.92
EPDM-*g*-PMA-210-24-11	0.25	9.04	1.10
EPDM-*g*-PMA-210-28-13	0.32	10.32	1.18
EPDM-*g*-PMA-210-32-11	0.30	11.73	1.19
EPDM-*g*-PMA-210-40-14	0.43	13.10	3.00
EPDM-*g*-PMA-210-12-13	0.21	4.2	1.45
EPDM-*g*-PMA-210-23-15	0.236	7.62	2.24
EPDM-*g*-PMA-210-36-14	0.28	12.03	2.96
EPDM-*g*-PMA-210-49-14	0.19	16.25	3.63
EPDM-*g*-PMA-210-93-11	0.21	31.75	5.13
EPDM-*g*-PMA-210-42-15	0.31	13.79	3.45
EPDM-*g*-PMA-210-70-15	0.17	22.81	5.27
EPDM-*g*-PMA-210-91-15	0.21	29.8	6.48
EPDM-*g*-PMA-210-147-16	0.11	47.31	10.87
EPDM-*g*-PMA-210-178-16	0.11	56.88	13.06

*Initial $[AIBN]_0/[CuBr_2]_0/[PMDETA]_0$ ratio = 1/1.5/3.

The mass of EPDM that reacted with methyl acrylate was calculated with the expression,

$$m_{EPDM_r} = m_{EPDM_0} - m_{EPDM} \tag{3-2}$$

where m_{EPDM_0} is the mass of EPDM added to the reactor at the beginning of the polymerization and m_{EPDM} is the mass of ungrafted EPDM, extracted as the hexene-soluble fraction (Figure 3-4).

The mass of methyl acrylate grafted onto EPDM backbones, m_{MA_g}, was calculated as,

$$m_{MA_g} = m_{EPDM-g-PMA} - m_{EPDM_r} \tag{3-3}$$

where $m_{EPDM-g-PMA}$ is the mass of grafted EPDM, recovered as the acetone-insoluble fraction (Figure 3-4).

The mass of reacted methyl acrylate is given by the sum,

$$m_{MA_r} = m_{PMA} + m_{MA_g} \tag{3-4}$$

where m_{PMA} is the mass of ungrafted PMA, recovered in the acetone-soluble fraction (Figure 3-4).

The mass of unreacted methyl acrylate was calculated by subtracting the mass of reacted methyl acrylate from the mass of methyl acrylate added to the reactor at the beginning of the polymerization,

$$m_{MA} = m_{MA_0} - m_{MA_r} \tag{3-5}$$

Finally, the concentration of unreacted methyl acrylate at the end of each polymerization was calculated with the expression,

$$[MA] = \frac{m_{MA}/M_{MA}}{V} \tag{3-6}$$

where M_{MA} is the molar mass of methyl acrylate, and V is the reaction volume.

Combining all expressions in a single mass balance equation, we get,

$$[MA] = \frac{m_{MA_0} + m_{EPDM_0} - (m_{PMA} + m_{EPDM-g-PMA} + m_{EPDM})}{VM_{MA}} \tag{3-7}$$

Figure 3-5 shows how $\ln([MA]_0/[MA])$ varied as a function of time with different initial methyl acrylate concentrations. For each series, the plot of $\ln([MA]_0/[MA])$ versus time was linear. This implies that the concentration of polymer radicals was nearly constant during the polymerizations, and confirms that the graft polymerizations followed the desired ATRP mechanism.

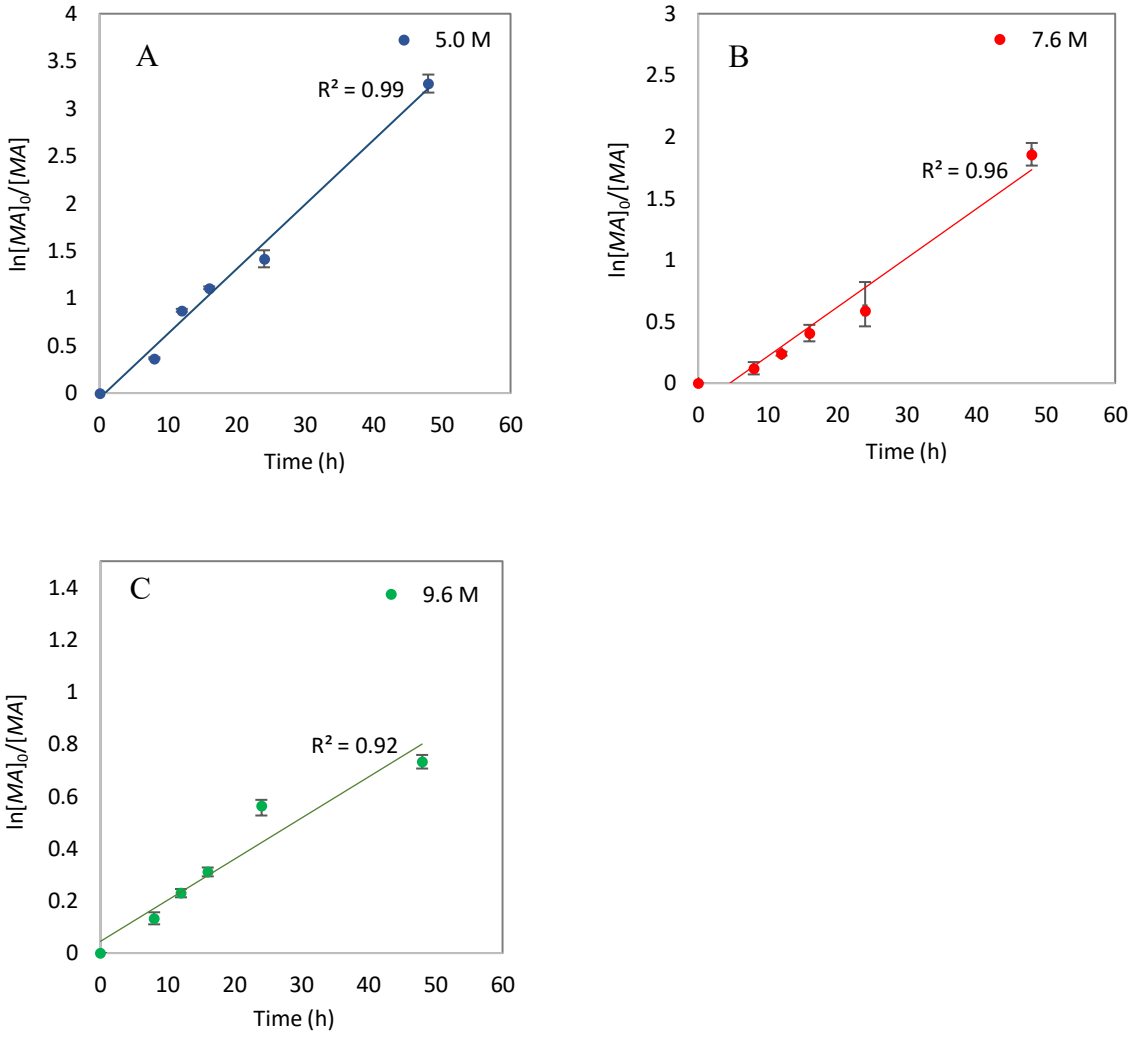

Figure 3-5: ln($[MA]_0/[MA]$) versus polymerization time. Polymerization conditions: T = 90 °C, initial $[AIBN]_0/[CuBr_2]_0/[PMDETA]_0$ ratio = 1/1.5/3. a) $[MA]_0$ = 5.0 M, and $[AIBN]_0$ = 0.00526 M, b) $[MA]_0$ = 7.6 M, and $[AIBN]_0$ = 0.0030, and c) $[MA]_0$ = 9.6 M, and $[AIBN]_0$ = 0.00121.

3.3.2 Composition Characterization of EPDM-*g*-PMA

Figure 3-6 compares the FTIR spectra of EPDM, PMA, and EPDM-*g*-PMA-210-178-16 (a graft polymer made of EPDM with M_b = 210 000, graft molecular weight of 178 000, and graft density of 16 %). In the spectrum of the ungrafted EPDM, the 757 cm^{-1} band is assigned to methylene groups –(CH_2–CH_2)– in the backbone. The 1376 and 1448 cm^{-1} bands are –C–H methyl (–CH_3) and methylene (–CH_2–) bending frequencies, respectively. Symmetric and asymmetric stretching vibration of the methylene group at 2850 cm^{-1} and 2919 cm^{-1} were also observed [34].

In the FTIR spectra of PMA, the band at 1730 cm^{-1} is assigned to the characteristic carbonyl stretching frequency (C=O). The bands at 2952 cm^{-1} and 2998 cm^{-1} are assigned to symmetric and asymmetric stretching of –C–H bending of methyl (CH_3O) groups, which are attached to an oxygen atom. Also, ten additional vibrations were observed from1650 to 750 cm^{-1}, which are allocated to PMA. More details regarding these vibrations are described by J. K. Haken and R. L. Werner [35].

In the EPDM-*g*-PMA sample, the bands at 2850 cm^{-1}, 2919 cm^{-1} are allocated to the symmetric and asymmetric stretching vibration of the methylene group, respectively, that is not connected to the inverted ester group. These bands are assigned to the EPDM part of the grafted copolymer. In addition, the band identified at 1729 cm^{-1} is assigned to the carbonyl stretching frequency; the band at 2952 cm^{-1} was also observed, which is assigned to symmetric stretching of –C–H bending of CH_3O groups. These bands are assigned to the PMA part of the grafted copolymer. Having these bands together in the FTIR spectra of purified EPDM-*g*-PMA confirmed the successful grafting of PMA chains onto EPDM backbones.

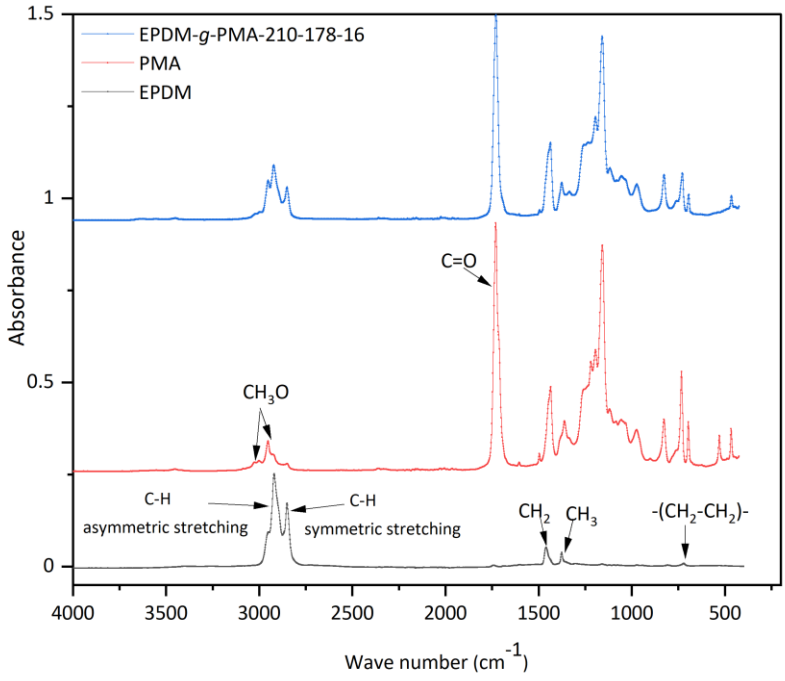

Figure 3-6: FTIR spectra of EPDM, PMA and EPDM-*g*-PMA.

^{1}H NMR spectra were used to characterize the chemical composition of the EPDM and purified EPDM-*g*-PMAs with different graft molecular weights and densities. The ^{1}H NMR spectra of EPDM and EPDM-*g*-PMAs with different graft molecular weights and densities are compared in Figure 3-7. The resonances of the methyl (–CH_3), methylene (–CH_2–), methine (>CH–), and unsaturated (=CH–) protons of the EPDM were identified [36]. In addition, the resonances at 1.5, 1.7, 1.9, 2.3 and 3.6 ppm belong to PMA protons (repeating unit CH_2–CH–$COOCH_3$) that are part of the EPDM-*g*-PMA. The resonance of the terminal group CHBr–$COOCH_3$ is also presented at 3.75 ppm [37].

Figure 3-7 also shows that the intensity of peaks associated with methyl acrylate units (represented by the resonances at 1.5, 1.7, 1.9, 2.3, and 3.6 ppm) increase as the methyl acrylate content in the polymer increases. The fractions of methyl acrylate in EPDM-*g*-PMAs were calculated from the ^{1}H NMR spectra using the intensity of the (–OCH_3) resonance at 3.6 ppm [38]. Increasing the concentration and conversion of methyl acrylate, increased the incorporation of methyl acrylate in the graft copolymer up to 174 mol %.

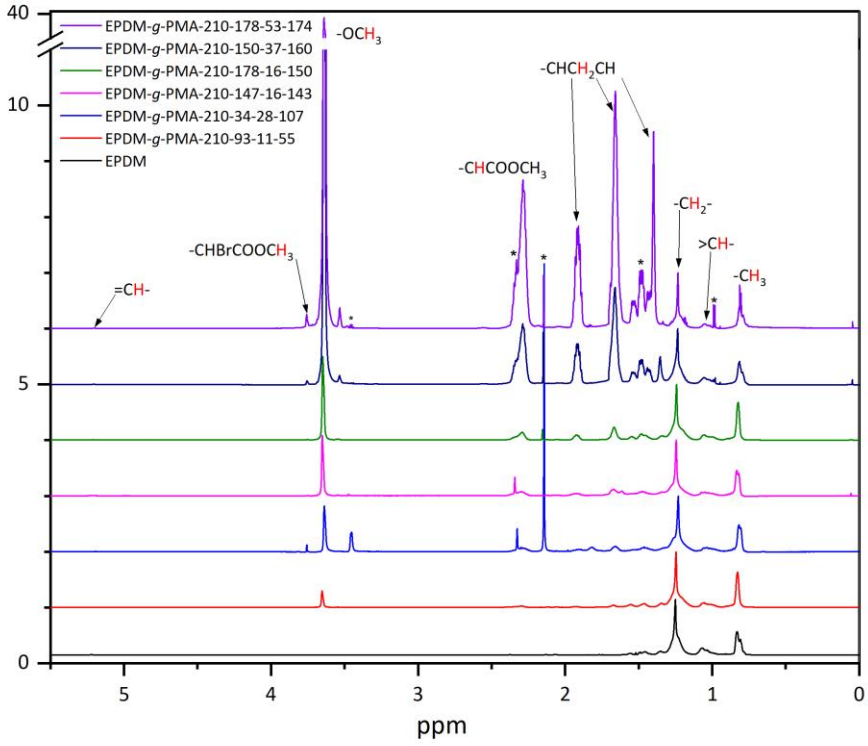

Figure 3-7: ^{1}H NMR spectra of EPDM and EPDM-*g*-PMA with different graft molecular weights and densities. Polymers are labeled as EPDM-*g*-PMA-M_b-M_g-ρ_g-M_{MA} where M_b is the average molecular weight of the backbone in kDa, M_g is the average molecular weight of the PMA grafts in kDa, ρ_g is the percentual graft density, and M_{MA} is mol% of MA incorporated in the grafted copolymer. The asterix (*) indicates residual solvent signals for methanol, acetone, hexane, toluene, and isobutanol.

Figure 3-8 is the close-up view of the ^{1}H NMR spectra of the (=CH–) resonance at 5.2 ppm, and the terminal group (CHBr–$COOCH_3$) resonance at 3.75 ppm for EPDM and EPDM-*g*-PMAs with different graft molecular weights and densities. The intensities of peaks related to diene groups decrease (Figure 3-8a) and the intensity associated with MA groups increase (Figure 3-8b) as the graft densities of the copolymer increase. The graft densities of the EPDM-*g*-PMA samples were measured as the ratio of the intensity of the peak for CHBr-$COOCH_3$ (3.75 ppm) to the intensity of the (=CH–) protons of EPDM (5.2 ppm). Decreasing the ratio of initiator to EPDM backbone increased the graft densities of the graft copolymer up to 53 % (Table 3-1).

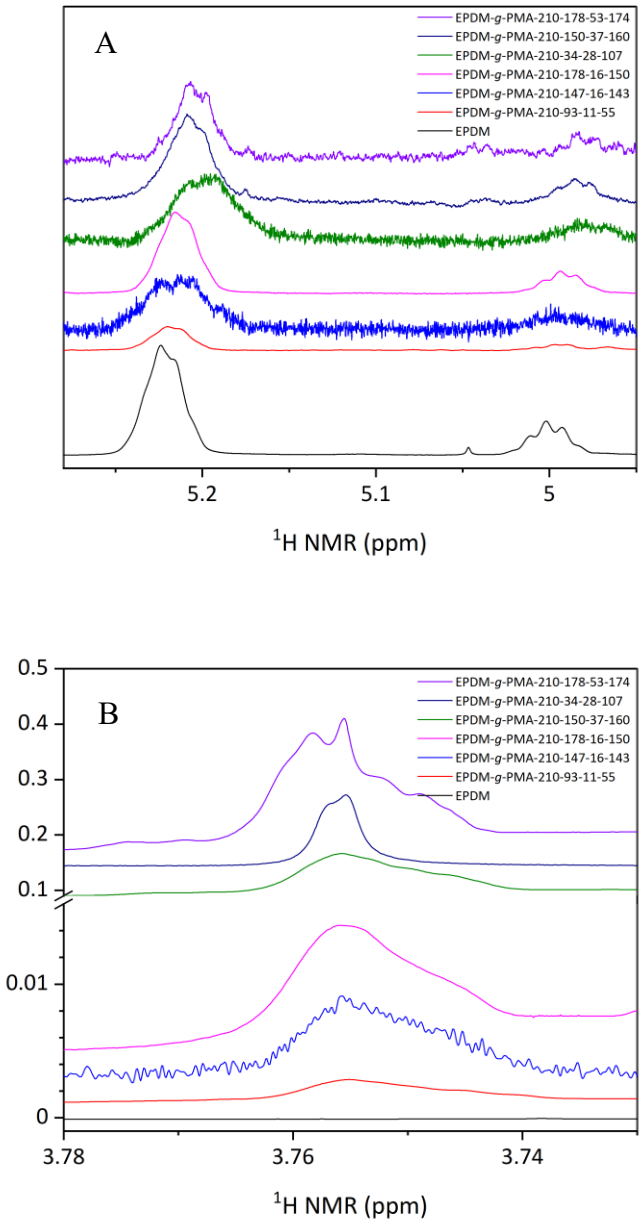

Figure 3-8: Close-up view of ^{1}H NMR spectrum of the EPDM and EPDM-*g*-PMAs with different graft molecular weights and densities: a) resonance of the unsaturated (=CH–) protons, and b) resonance of the terminal group (CHBr-$COOCH_3$) protons.

The EPDM-*g*-PMA graft densities were also estimated by mass balance using the equation,

$$\rho_g(\%) = \frac{n_g}{n_d} \times 100 \tag{3-8}$$

where n_g is the number of moles of PMA grafts and n_d is the number of moles of diene molecules (pendant double bonds) in the EPDM backbones.

The number of moles of diene molecules in the EPDM backbones is given by,

$$n_d = \frac{w_{ENB}}{M_{ENB}} \tag{3-9}$$

where, w_{ENB} is the mass fraction of ethylidene norbornene in the EPDM backbone and M_{ENB} is the molar mass of ethylidene norbornene.

The number of moles of grafted PMA chains is given by dividing the number of moles of MA molecules grafted onto EPDM by the degree of polymerization of the grafts,

$$n_g = \frac{n_{MA}}{DP_n} \tag{3-10}$$

The number of moles of MA molecules grafted onto EPDM is given by,

$$n_{MA} = \frac{m_{MA_g}}{M_{MA}} \tag{3-11}$$

Assuming that the initiation step is fast, that all chains start growing at the same time, and that they keep growing at the same rate, the degree of polymerization of the grafts is given by,

$$DP_n = \frac{[MA]_0}{[I]_0} x \tag{3-12}$$

where, $[I]_0$ is the initial concentration of initiator and x is the conversion of MA,

$$x = \frac{m_{MA_r}}{m_{MA_0}} \tag{3-13}$$

All these equations can be combined in a single expression to calculate the graft density percentage of EPDM-*g*-PMA,

$$\rho_g(\%) = \frac{m_{MA_0}}{w_{ENB}} \frac{m_{MA_g}}{m_{MA_r}} \frac{[I]_0}{[MA]_0} \frac{M_{ENB}}{M_{MA}} \times 100 \tag{3-14}$$

Figure 3-9 shows that the graft density of EPDM-*g*-PMAs obtained with mass balance calculations agree with the values measured by ^{1}H NMR, with the coefficient of determination of 0.95, confirming that the produced EPDM-*g*-PMAs are graft copolymers and not mixtures of the EPDM and PMA. As the results obtained with the two methods agree, the graft densities listed in Table 3-1 were calculated using Equation (3-14).

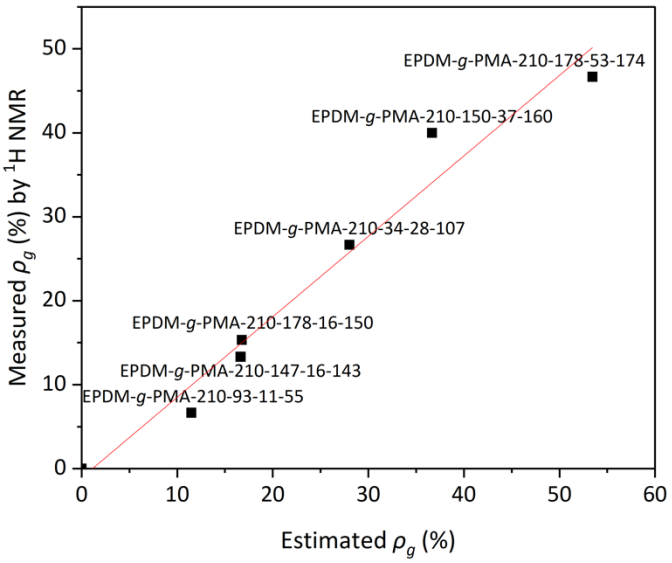

Figure 3-9: Measured ρ_g (%) by ^{1}H NMR versus estimated ρ_g (%) calculated by mass balance.

3.3.3 Molecular Weight Characterization of EPDM-*g*-PMA

The number and weight average molecular weights, M_n and M_w, of the EPDM-*g*-PMA samples were measured by GPC to verify the formation of EPDM-*g*-PMAs (Table 3-1). Due to the limitations of our GPC columns, measurements, samples with M_w > 2500 kDa could not be analyzed. Mass balances were also used to calculate M_n and M_w the EPDM-*g*-PMA samples, and the measured and estimated values were compared.

To estimate the M_n of the EPDM-*g*-PMA samples, we first need to calculate the average number of moles of diene in an EPDM sample of number average molecular weight M_n^{EPDM},

$$n_d = \frac{M_n^{EPDM} \times w_{ENB}}{M_{ENB}} \tag{3-15}$$

The number of grafted PMA chains in the whole polymer is, therefore,

$$n_g = n_d \times \rho_g = \frac{M_n^{EPDM} \times w_{ENB}}{M_{ENB}} \times \rho_g \tag{3-16}$$

Consequently, the number average molecular weight of the grafted polymer is,

$$M_n^{EPDM-g-PMA} = M_n^{EPDM} + n_g \times M_g \tag{3-17}$$

Combining all equations above, we get,

$$M_n^{EPDM-g-PMA} = M_n^{EPDM} + \frac{M_n^{EPDM} \times w_{ENB}}{M_{ENB}} \times \rho_g \times M_g \tag{3-18}$$

A more elaborate calculation is needed to estimate the M_w of the EPDM-*g*-PMA samples. In this case, the molecular weight distribution information for the EPDM backbone were used as the starting point (Figure 3-10).

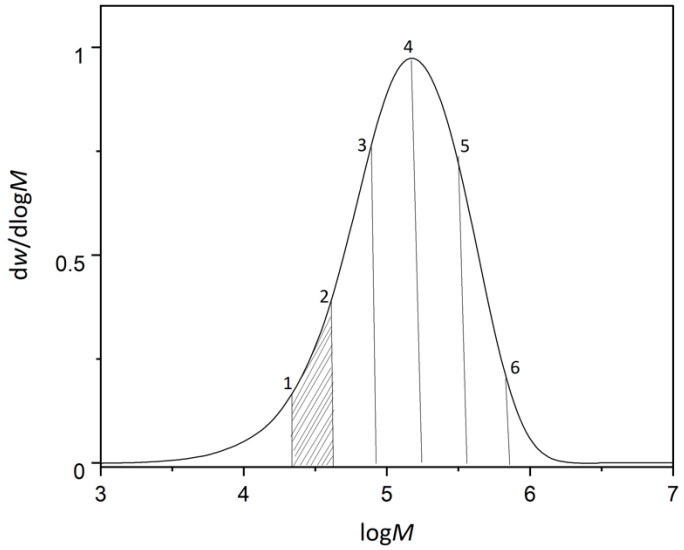

Figure 3-10: EPDM (M_b = 210 kDa) molecular weight distribution.

Figure 3-10 shows the molecular weight distribution of the EPDM sample with M_b = 210 kDa, as measured by GPC, discretized in bins of different molecular weights. The weight fraction of polymer in each bin, w_i, is calculated with the trapezoidal rule,

$$w_i = \frac{(\mathrm{d}w/\mathrm{d}logM)_i + (\mathrm{d}w/\mathrm{d}logM)_{i+1}}{2} \times (\log M_{i+1} - \log M_i) \tag{3-19}$$

The average number of moles of diene in EPDM chains of average molecular weight M_i is,

$$n_{di} = \frac{M_i \times w_{ENB}}{M_{ENB}} \tag{3-20}$$

The number of grafted chains, n_{gi}, in an EPDM of average molecular weight of M_i is,

$$n_{gi} = n_{di} \times \rho_g = \frac{M_i \times w_{ENB}}{M_{ENB}} \times \rho_g \tag{3-21}$$

The average molecular weight of the grafted polymer is given by,

$$M_i^{EPDM-g-PMA} = M_i + n_{gi} \times M_g = M_i + \frac{M_i \times w_{ENB}}{M_{ENB}} \times \rho_g \times M_g \tag{3-22}$$

where the molecular weight of the PMA grafts, M_g, were calculated using the ATRP equation,

$$DP_n = \frac{M_g}{M_{MA}} = \frac{[MA]_0}{[I]_0} x \tag{3-23}$$

Consequently, the weight average molecular weight of EPDM-*g*-PMAs, $M_w^{EPDM-g-PMA}$, is,

$$M_w^{EPDM-g-PMA} = \frac{\sum_{i=1}^{n} (M_i + \frac{M_i \times w_{ENB}}{M_{ENB}} \times \rho_g \times M_g)^2 N_i}{\sum_{i=1}^{n} (M_i + \frac{M_i \times w_{ENB}}{M_{ENB}} \times \rho_g \times M_g) N_i} \tag{3-24}$$

where N_i is the number of moles of chain with molecular weight $M_i^{EPDM-g-PMA}$, which is related to its weight fraction by the expression,

$$w_i = \frac{N_i M_i}{\sum_{i=1}^{n} N_i M_i} \tag{3-25}$$

Finally, the weight average molecular weight of EPDM-*g*-PMAs can be calculated with the expression,

$$M_w^{EPDM-g-PMA} = \frac{\sum_{i=1}^{n} (M_i + \frac{M_i \times w_{ENB}}{M_{ENB}} \times \rho_g \times M_g)^2 \frac{w_i}{M_i}}{\sum_{i=1}^{n} (M_i + \frac{M_i \times w_{ENB}}{M_{ENB}} \times \rho_g \times M_g) \frac{w_i}{M_i}} \tag{3-26}$$

Figure 3-11 compares the M_n and M_w of EPDM-*g*-PMAs estimated with Equation 3-18 and 3-26, respectively, with the values measured by GPC. The averages obtained with these two methods agree reasonably well, with the coefficient of determination of 0.93 and 0.95 respectively, considering the complexity of the GPC measurements and the polymerization process itself. This indicates that the grafting process follow the desired ATRP kinetics in this investigation. Since the results obtained with the two methods agree relatively well, the M_w values listed in Table 3-1 were calculated using Equation 3-26.

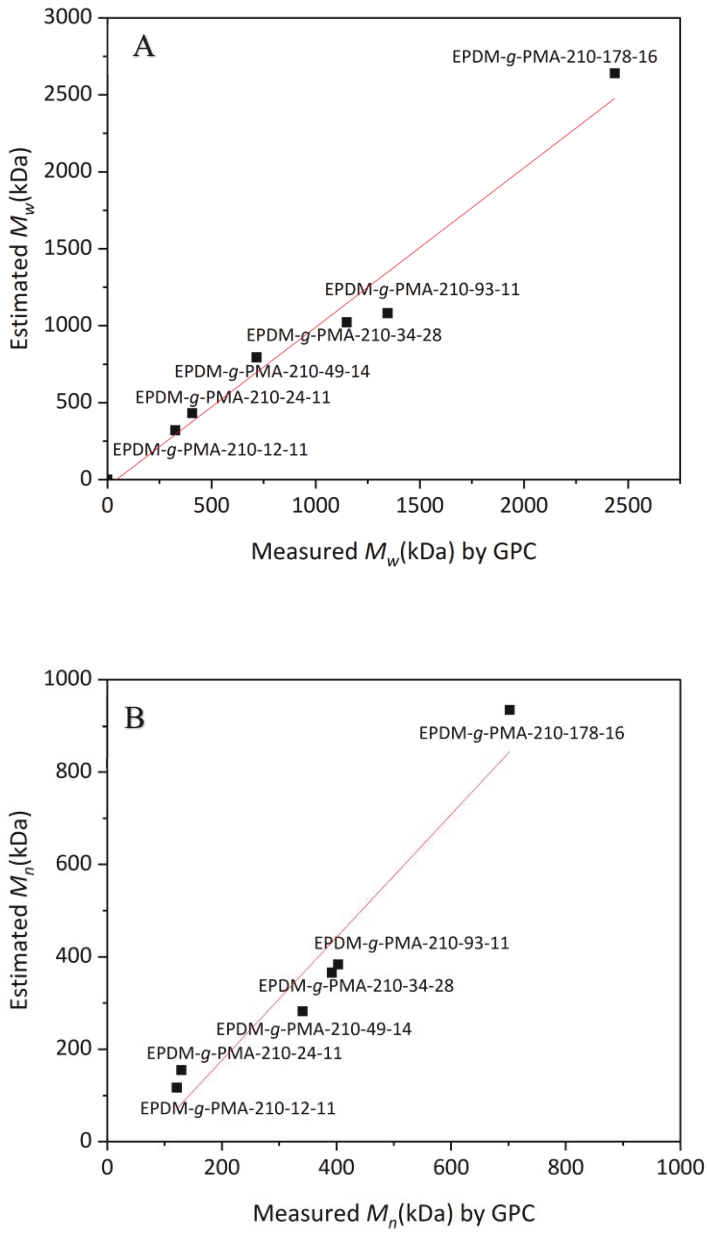

Figure 3-11: Estimated versus measured average molecular weights of EPDM-*g*-PMA samples: a) M_w, and b) M_n.

3.4 Conclusions

Graft copolymers of poly(methyl acrylate) and EPDM, EPDM-*g*-PMAs, were synthesized by grafting PMA side chains onto EPDM backbone with various graft molecular weights and densities via reverse ATRP. The graft molecular weight was controlled by varying methyl acrylate

concentration (5.0 to 9.6 M) and polymerization time (8 to 48h). EPDM-*g*-PMAs with a wide range of graft molecular weights (M_g = 12 to 179 kDa) were synthesized using this approach. The graft density was controlled by varying the ratio of initiator to EPDM backbone (0.00785 to 0.00445 mol %), permitting the production of EPDM-*g*-PMAs with graft densities varying from 11 to 53 %.

Graft densities and molecular weights of the EPDM-*g*-PMA samples were estimated theoretically using ATRP kinetics and also measured by ^{1}H NMR, and GPC. Measurements and estimates for these properties agreed well, confirming that the EPDM-*g*-PMA samples were synthesised successfully with controllable graft lengths and densities.

Controlling the microstructure of EPDM-*g*-PMA is essential to tailor its performance as a flocculant and dewatering agent for oil sands tailings, and supposedly other mineral tailings. In next chapter, we showed that EPDM-*g*-PMA (after hydrolysis) reached its best performance when the PMA grafts were long, but the grafting density was low. The synthesis method described in this chapter teaches how to control the microstructure of these graft copolymers and, therefore, how to regulate their flocculation and dewatering performances.

References

[1] T.C. Chung, Functionalization of polyolefins. Published in San Diego by Academic Press, 2002; ISBN:9780080477930.

[2] L.K. Johnson, S. Mecking and M. Brookhart, "Copolymerization of ethylene and propylene with functionalized vinyl monomers by palladium(II) catalysts", J.Am.Chem.Soc., vol. 118, pp. 267-268, 1996.

[3] S. Mecking, "Mechanistic studies of the palladium-catalyzed copolymerization of ethylene and a-olefins with methyl acrylate", J.Am.Chem.Soc., vol. 120, pp. 888-899, 1998.

[4] G. Chen, X.S. Ma and Z. Guan, "Synthesis of functional olefin copolymers with controllable topologies using a chain-walking catalyst", J.Am.Chem.Soc., vol. 125, pp. 6697-6704, 2003.

[5] Z. Dong and Z. Ye, "Hyperbranched polyethylenes by chain walking polymerization: Synthesis, properties, functionalization, and applications", Polym.Chem., vol. 3, pp. 286-301, 2012.

[6] Z. Ye and S. Li, "Hyperbranched polyethylenes and functionalized polymers by chain walking polymerization with PD-diimine catalysis", Macromol.React.Eng., vol. 4, pp. 319-332, 2010.

[7] L. Botha, S. Davey, B. Nguyen, A.K. Swarnakar, E. Rivard and J.B.P. Soares, "Flocculation of oil sands tailings by hyperbranched functionalized polyethylenes (HBfPE)", Minerals Eng, vol. 108, pp. 71-82, 2017.

[8] H. Li, J. Long, Z. Xu and J.H. Masliyah, "Synergetic role of polymer flocculant in low-temperature bitumen extraction and tailings treatment", Energy Fuels, vol. 19, pp. 936-943, 2005.

[9] T.C. Chung, W. Janvikul, R. Bernard and G.J. Jiang, "Synthesis of ethylene-propylene rubber graft copolymers by borane approach", Macromolecules, vol. 27, pp. 26-31, 1994.

[10] T.C. Chung, W. Janvikul, R. Bernard, R. Hu, C.L. Li, S.L. Liu and G.J. Jiang, "Butyl rubber graft copolymers: synthesis and characterization", Polymer, vol. 36, pp. 3565-3574, 1995.

[11] T.C. Chung, "Synthesis of functional polyolefin copolymers with graft and block structures", Prog Polym Sci (Oxford), vol. 27, pp. 39-85, 2002.

[12] J.S. Wang and K. Matyjaszewski, "Controlled/living radical polymerization. Atom transfer radical polymerization in the presence of transition-metal complexes, J.Am.Chem.Soc., vol. 117, pp. 5614-5615, 1995.

[13] M. Kato, M. Kamigaito, M. Sawamoto and T. Higashimura, "Polymerization of methyl methacrylate with the carbon tetrachloride/dichlorotris-(triphenylphosphine)ruthenium(II) /methylaluminum bis(2,6-di-tert-butylphenoxide) initiating system: possibility of living radical polymerization", Macromolecules, vol. 28, pp. 1721-1723, 1995.

[14] K. Matyjaszewski and J. Xia, "Atom transfer radical polymerization" Chem.Rev., vol. 101, pp. 2921-2990, 2001.

[15] V. Coessens, T. Pintauer and K. Matyjaszewski, "Functional polymers by atom transfer radical polymerization", Progress in Polymer Science, vol. 26, pp. 337-377, 2001.

[16] M. Kamigaito, T. Ando and M. Sawamoto, "Metal-catalyzed living radical polymerization", Chem.Rev., vol. 101, pp. 3689-3745, 2001.

[17] K. Matyjaszewski and N.V. Tsarevsky, "Nanostructured functional materials prepared by atom transfer radical polymerization", Nat.Chem., vol. 1, pp. 276-288, 2009.

[18] K.A. Davis and K. Matyjaszewski, Statistical, gradient block and graft copolymers by controlledliving radical polymerizations. Published in Berlin ;New York by Springer, 2002; pp. 191; ISBN:3540432442.

[19] K. Matyjaszewski, "Atom transfer radical polymerization: From mechanisms to applications", Isr.J.Chem., vol. 52, pp. 206-220, 2012.

[20] W.J. Wang, L. Pingwei, B.G. Li and Z. Shiping, "One-step synthesis of hyperbranched polyethylene macroinitiator and its block copolymers with methyl methacrylate or styrene via ATRP", J.Polym.Sci.Part A, vol. 48, pp. 3024-3032, 2010.

[21] Y. Inoue, T. Matsugi, N. Kashiwa and K. Matyjaszewski, "Graft copolymers from linear polyethylene via atom transfer radical polymerization", Macromolecules, vol. 37, pp. 3651-3658, 2004.

[22] H. Kaneko, J. Saito, N. Kawahara, S. Matsuo, T. Matsugi and N. Kashiwa, "Polypropylene-graft-poly(methyl methacrylate) Graft Copolymers: Synthesis and Compatibilization of

Polypropylene/Polylactide", in Controlled/Living Radical Polymerization: Progress in ATRP, American Chemical Society, 2009, pp. 357-371.

[23] X.S. Wang, N. Luo and S.K. Ying, "Synthesis of EPDM-g-PMMA through atom transfer radical polymerization", Polymer, vol. 40, pp. 4515-4520, 1999.

[24] V.M.C. Coessens and K. Matyjaszewski, "Fundamentals of atom transfer radical polymerization", J.Chem.Educ., vol. 87, pp. 916-919, 2010.

[25] J. Xia and K. Matyjaszewski, "Controlled/living radical polymerization. Homogeneous reverse atom transfer radical polymerization using AIBN as the initiator", Macromolecules, vol. 30, pp. 7692-7696, 1997.

[26] D.J. Haloi, K. Naskar, N.K. Singha, "Poly(meth)acrylate grafted EPDM via reverse atom transfer radical polymerization: A single pot process", European Polymer Journal, vol. 49, pp. 4098-4107, 2013.

[27] Z. Rostami Najafabadi and J.B.P. Soares, "Flocculation and dewatering of oil sands tailings with a novel functionalized polyolefin flocculant", Separation and Purification Technology, vol. 274, pp. 119018, 2021.

[28] W. Tang and K. Matyjaszewski, "Kinetic Modeling of Normal ATRP, Normal ATRP with [CuII], Reverse ATRP and SR&NI ATRP", Macromol.Theory Simul., vol. 17, pp. 359-375, 2008.

[29] J.S. Wang and K. Matyjaszewski, "Controlled/Living Radical Polymerization. Atom Transfer Radical Polymerization in the Presence of Transition-Metal Complexes", J.Am.Chem.Soc., vol. 117, pp. 5614-5615, 1995.

[30] K. Matyjaszewski, T. Pintauer and S. Gaynor, "Removal of copper-based catalyst in atom transfer radical polymerization using ion exchange resins", Macromolecules, vol. 33, pp. 1476-1478, 2000.

[31] A.M. Kasko, A.M. Heintz and C. Pugh, "The effect of molecular architecture on the thermotropic behavior of poly[11-(4′-cyanophenyl-4′-phenoxy)undecyl acrylate] and its relation to polydispersity", Macromolecules, vol. 31, pp. 256-271, 1998.

[32] G. Coullerez, A. Carlmark, E. Malmström and M. Jonsson, "Understanding copper-based atom-transfer radical polymerization in aqueous media", J Phys Chem A, vol. 108, pp. 7129-7131, 2004.

[33] W. Tang and K. Matyjaszewski, "Kinetic modeling of normal ATRP, normal ATRP with [CuII], reverse ATRP and SR & NI ATRP", Macromol.Theory Simul., vol. 17, pp. 359-375, 2008.

[34] J.R. Riba Ruiz, T. Canals and R. Cantero, "Supervision of Ethylene Propylene Diene M-Class (EPDM) Rubber Vulcanization and Recovery Processes Using Attenuated Total Reflection Fourier Transform Infrared (ATR FT-IR) Spectroscopy and Multivariate Analysis", Appl.Spectrosc., vol. 71, pp. 141-151, 2017.

[35] J.K. Haken and R.L. Werner, "Infrared spectrum of polymethyl acrylate", Brit.Poly.J., vol. 3, pp. 263-265, 1971.

[36] K. Ute, R. Niimi, K. Hatada and A.C. Kolbertb, "Characterization of Ethylene—Propylene—Diene Terpolymers (EPDM) by 750 MHz On-line SEC-NMR", vol. 5, pp. 47-59, 1999.

[37] G. Lligadas, J.S. Ladislaw, T. Guliashvili and V. Percec, "Functionally terminated poly(methyl acrylate) by SET-LRP initiated with CHBr3 and CHI3", J.Polym.Sci.Part A, vol. 46, pp. 278-288, 2008.

[38] C.S. Popeney, D.H. Camacho and Z. Guan, "Efficient incorporation of polar comonomers in copolymerizations with ethylene using a cyclophane-based Pd(II) α-diimine catalyst", J.Am.Chem.Soc., vol. 129, pp. 10062-10063, 2007.

Chapter 4

4 Flocculation and Dewatering of Oil Sands Tailings with a Novel Functionalized Polyolefin Flocculant

This work investigates the impact of the molecular weight and grafting density of hydrolyzed poly(methyl acrylate) grafted onto ethylene-propylene-diene copolymer backbones (EPDM-*g*-HPMA) on the flocculation and dewatering of oil sands mature fine tailings through a central composite experimental design by measuring initial settling rate, capillary suction time, supernatant turbidity, and sediment solids content. Flocculants with high molecular weight grafts and low grafting densities reduced the initial settling rates, decreased supernatant turbidities, and increased the solids content of the flocculated sediments. The capillary suction time, however, depended mostly on the charge density and on the hydrophobicity of the grafted copolymer. The effect of the EPDM backbone molecular weight was also investigated. Shorter backbones resulted in flocculants that dispersed more easily in water and settled the sediments faster. In addition, they decreased the supernatant turbidity and increased the solids content in the sediments. EPDM-*g*-HPMA flocculants with graft molecular weight of 179 kDa and grafting density of 13 % are outstanding filtration aids, helping generate sediments with 43 % solids content and outperforming a reference commercial polyacrylamide flocculant.

4.1 Introduction

Natural bitumen deposits are found in many countries, including Canada, Venezuela, the United States, and Russia. Alberta ranks third in proven global crude oil reserves (166 billion barrels),

after Saudi Arabia and Venezuela [1]. Bitumen is most commonly extracted from oil sands using the Clark hot water extraction process. In this process, the oil sands ores are first mined, then crushed, and finally mixed with warm water and caustic at 75-80 °C to make a slurry that is transferred to a primary separation vessel to liberate and aerate bitumen aggregates. The bitumen froth, recovered in the primary separation vessel, is transferred to the froth treatment stage to recover more bitumen. The slurry residues, called tailings, are transported to tailing ponds for solid-liquid separation [2].

Oil sands tailings are aqueous suspensions of coarse sands (particles greater than 44 μm), fine solids and clays (particles less than 44 μm), and 1 to 5 wt. % residual bitumen, with pH varying from 8 to 9 [3]. In the pond, the coarse particles settle fast, but the fine solids remain in suspension. After three to five years, the concentration of the suspended fine solids reaches 30 to 40 wt. %, which is known as mature fine tailings (MFT). It may take centuries to consolidate untreated MFT [4]. Tailings ponds and their operating structures covered about 257 km^2 of Alberta's oil sands region in 2016 [5]. Unfortunately, only a small fraction of this large area has been reclaimed because there is no effective way to separate the suspended solids from the water in tailing ponds. Different chemical and mechanical methods have been developed to treat oil sands tailings: consolidated tailings, paste technology, filtration, thin lift dewatering, centrifugation, rim ditching, and wet landscape reclamation. Unfortunately, none of these methods can dewater tailings above the 75 wt. % solids required for land reclamation [4, 6].

Paste technology uses polymer flocculants to treat different types of mining wastes. For oil sands tailings, it is often combined with other treatments such as coagulation and centrifugation. Most studies have used commercial polyacrylamide (PAM) or partially hydrolyzed anionic polyacrylamide (HPAM) [7]. Despite their fast settling and initial water release rates, both flocculants are shear sensitive, disperse poorly in tailings, cannot flocculate fine clay particles effectively, and retain large amounts of water in the sediments [8].

Some investigators have developed inorganic-organic hybrid PAM flocculants such as Al-PAM [9, 10] and Fe-PAM [11]. Although Al-PAM flocculated fines more effectively than HPAM [12], health and biocompatibility concerns hinder their industrial implementation [13]. Another modified acrylamide-based flocculant, the temperature-sensitive poly- N-isopropylacrylamide (PNIPAM), has also been evaluated because it becomes hydrophobic above its lower critical

solution temperature (LCST) of 32 °C, repelling the water trapped in the sediments [14]. PNIPAM flocculates finer particles, consolidates sediments, and generates supernatants with lower turbidities than HPAM [15]. However, heating large volumes of MFT/PNIPAM suspensions above 32 ºC is necessary for optimal performance, making this flocculant less attractive from an economic perspective.

Other researchers have shown that polyacrylamide-*graft*-poly(propylene oxide) (PAM-*g*-PPO) flocculates and dewaters MFT more effectively than commercial HPAM, likely because of the hydrophobic PPO grafts. This flocculant is also less shear sensitive and easier to mix with MFT because of its lower molecular weight. Unfortunately, high dosages (up to 10,000 ppm) were needed to achieve optimal performance, which might restrict its applications in large scale [16].

Wang et al. [17] assessed the effect of polymer topology on the flocculation of clays by comparing hyperbranched cationic temperature-sensitive poly(2-amino-ethyl methacrylamide hydrochloride block N-isopropylacrylamide) P($AEMA_{12}$-*b*-$NIPAM_{90}$) to linear cationic temperature-sensitive P($AEMA_8$-*st*-$NIPAM_{75}$). The hyperbranched polymer was a more effective flocculant and produced clearer supernatants, which the authors attributed to the better contact of the cationic groups in the hyperbranched polymer with the clay surfaces [17]. Since the linear and hyperbranched polymers had similar molecular weights, their performance differences were attributed to their distinct branching topologies.

Botha et al. [18, 19] combined the desired features of hyperbranched topology and hydrophobicity in a new hyperbranched functionalized polyethylene containing polar groups and used it to treat oil sands tailings. The authors showed that in the presence of cations in the process water, the polar functional groups in the hyperbranched functionalized polyethylene adsorbed onto the surface of the clay particles, causing them to flocculate. Because of the hydrophobic polyethylene core, less water was retained in the sediments. The hyperbranched functionalized polyethylene improved flocculation and dewatering performance with respect to a commercial HPAM, but was limited by its low molecular weights of only up to 7000 g/mol and its insufficient polar group density [18, 19]. In our recent investigation [20], this limitation was eliminated by grafting poly(methyl acrylate) (PMA) side chains onto high molecular weight ethylene-propylene-diene (EPDM) backbones via reverse atom transfer radical polymerization (RATRP) to produce the novel (EPDM-*g*-PMA) flocculants that are the main subject of this article.

Atom transfer radical polymerization (ATRP) is a controlled radical polymerization method that can make polymers with narrow molecular weight distributions by reducing chain transfer and termination reactions. This process occurs in the presence of initiator/dormant macromolecular species containing an easily transferable halide atom and a catalyst. The catalyst (or activator) is a metal in lower oxidation state with a suitable ligand. Polymerization starts when the halide atom transfers from the initiator to the catalyst to form a free radical and a metal halide with higher oxidation state (deactivator). An equilibrium, which is mostly shifted towards the side with low radical concentration, is quickly established. As a result, the likelihood of chain termination or transfer occurring is minimized. This equilibrium can be reached through two main approaches: *normal* ATRP and *reverse* ATRP [21].

Atom transfer radical polymerization has been used to synthesize functional polyolefin graft copolymers for different applications [22-28] in a two-step process: first, halide groups are attached to polyolefin backbones, and then grafts are grown from these groups [29]. Reverse ATRP, on the other hand, requires only one step to make polyolefin graft copolymers [30-32]. In this process, the combination of a thermal initiator, a metal halide in its higher oxidation states, and a ligand to bind the catalyst initiates the polymerization.

In this article, we used a series of partially hydrolyzed poly(methyl acrylate) grafted onto ethylene-propylene-diene copolymer backbones (EPDM-*g*-HPMA) [20] to flocculate mature fine tailings. These flocculants had HPMA grafts with distinct molecular weights and different densities. The objective of this study was to find out how these variables affected the flocculation and dewatering performance of these novel polymers. Two EPDM samples of different molecular weights were also compared to study the effect of backbone length on the performance of the flocculants. The flocculation and dewatering performance of the novel copolymers were investigated using a central composite design by measuring initial settling rate, capillary suction time, supernatant turbidity, and sediment solids content. Through our analysis, we found out that among our flocculants, those with high molecular weight grafts and low grafting densities were better flocculants and dewatering agents. Understanding how graft molecular weight and density affect the efficiency of these flocculants is essential to design better polymers for the treatment of oil sands and other mineral tailings.

4.2 Experimental Details

4.2.1 Materials

Anhydrous methanol (99.8 %), potassium hydroxide (≥ 85 % KOH basis), calcium chloride (≥ 96 %), and anhydrous dicholoromethane (≥ 99.8 %) were purchased from Sigma-Aldrich and used without further purification. The commercial HPAM (Magnafloc 1100, M_w = 17.5 MDa, 27 % charge density) was donated by Kemira. The MFT sample was donated by Imperial Oil. Deionized water was used for all flocculation experiments.

4.2.2 Experimental Design

Central composite designs can be used to build a second order model for the response variables without needing a complete three-level factorial design, thus reducing experimental time and costs. This design allow us to determine which variables have the greatest influence on process performance. In addition, this information can be used to adjust the critical variables required to improve the process [33].

In this study, a central composite experimental design was used to assess the effect of selected polymer architecture parameters on the flocculation and dewatering of oil sands tailings with EPDM-*g*-PMA [33]. The performance of the novel graft copolymers was quantified by measuring the initial settling rate (ISR), capillary suction time (CST), supernatant turbidity, and sediment solids content. A multiple linear regression model with quadratic and interaction terms was used to evaluate these responses

$$Y_i = b_0 + \sum_1^n b_i X_i + \sum_1^n b_{ii} X_i^2 + \sum_1^{n-1} \sum_{i+1}^n b_{ij} X_i X_j \qquad (4\text{-}1)$$

where Y_i is the ith predicted response, X_i and X_j are the coded values for the independent variables, and b_0, b_i, b_{ii}, and b_{ij} are constants.

4.2.3 Synthesis of EPDM-*g*-PMA

Poly(methyl acrylate) was grafted onto EPDM via reverse ATRP. The graft molecular weights and densities were controlled by varying the concentration and conversion of methyl acrylate and the concentration of initiator. Two EPDM samples having the same comonomer composition (4.9 wt.% 5-ethylidene-2-norbornene, 50 wt. % ethylene, and 45.1 wt. % propylene) and different weight average molecular weights (M_w = 210 000 and 115 000) were used as backbones [20].

In a typical polymerization, the desired masses of AIBN (initiator), $CuBr_2$ (catalyst), and N,N,N′,N″,N″-pentamethyldiethylenetriamine (PMDETA, ligand) were dissolved in 2 mL of acetone. One gram of EPDM, dissolved in 20 mL of toluene, was then mixed with the previously prepared solution. The flask containing the resulting mixture was stirred under N_2 for 20 min before being immersed into an oil bath at 90 °C. After stirring the solution at 90 °C for 20 min, methyl acrylate (previously purged with N_2 for 20 min) was added to the solution to grow the PMA grafts on the EPDM backbones. The polymerization was allowed to continue from 24 to 48 h before being stopped by precipitating the polymer and with excess methanol. After washing with methanol, the polymer was dried at 60 °C for 24 h. Finally, ungrafted EPDM and PMA were extracted from the product by first stirring it in hexane (to remove the EPDM) and acetone (to extract the PMA) for 24 h. These three fractions were dried at 60 °C for 24 h. More details regarding the synthesis and characterization of the EPDM-*g*-PMA samples are described in our upcoming publication on the synthesis of EPDM-*g*-PMA copolymers [20]. However, a similar procedure is described in the paper by Haloi et al. [32], with the main exception that they used methacrylate instead of methyl acrylate to make for the grafts.

4.2.4 EPDM-*g*-PMA Base Hydrolysis

All EPDM-*g*-PMA copolymers were hydrolyzed according to the reaction

$$\text{R-COOCH}_3 \xrightarrow[\text{H}_2\text{O}]{\text{K}^+\text{OH}^-} \text{R-COOH} + \text{CH}_3\text{OH} \qquad (4\text{-}2)$$

which converts acrylate into carboxylic groups [34] and enable the polymer to be dispersed in water. Approximately 2.0 g of EPDM-*g*-PMA were dissolved in 150 mL of dichloromethane. A desired amount of KOH solution (2.0 M) in methanol was added to the EPDM-*g*-PMA solution and left at 60 °C for 24 h to ensure near complete hydrolysis. Then, 100 mL of deionized water was added to the solution at 60 °C. The polymer was dispersed into the water phase, while dichloromethane and methanol were evaporated. The polymer aqueous solution after hydrolysis was used to flocculate the MFT samples. This is an expedient way to make these flocculants because it avoid an additional step of polymer recovery from solution.

4.2.5 Settling and Flocculation Tests

Dean-Stark extraction was used to measure the amounts of the bitumen, solids, and water of the MFT sample, atomic absorption spectroscopy (Varian 220FS) to quantify the concentration of major ions in the MFT process water (obtained by centrifuging 200 g of MFT sample for 30 minutes), and a Malvern Mastersizer 3000 to measure particle size distribution.

Flocculation tests used 100 mL of diluted tailings (5, 10, and 20 wt. % solids) and either the novel EPDM-*g*-HPMAs or a commercial HPAM. Deionized water was used to make diluted tailings, a standard procedure reported in the literature [9, 35, 36]. All settling tests were done in the presence of 1000 ppm Ca^{2+} (from a 1 M $CaCl_2$ stock solution). For the case of anionic flocculants, it is usual to add divalent anions to act as salt bridges between the polymer and the negatively charged clay surfaces [37-40]. The dosage of 1000 ppm Ca^{2+} used in this investigation was previously determined from a set of experiments on the MFT of Imperial Oil, by monitoring flocculation and dewatering performance of MFT at different Ca^{2+} dosages. Mature fine tailings diluted to 5 wt. % solids were dosed with 2000 ppm of flocculant, while those with 10 and 20 wt % solids were treated with 4000 ppm of flocculant. All dosages were based on the solids content of the MFT.

The best dosages for EPDM-*g*-HPMAs were determined in flocculation screening tests using EPDM-*g*-HPMA with different graft molecular weights (M_g = 34 to 175 kDa) and densities (ρ_g = 16 to 50 %). MFT samples diluted to 5, 10, and 20 wt. % solids were dosed with 250–10000 ppm of different EPDM-*g*-HPMA flocculants and ISR, CST, supernatant turbidity, and sediment solids content were measured. The results show that MFT diluted to 5 wt. % solids were overdosed when

more than 2000 ppm was used, while MFT with 10 and 20 wt % solids were overdosed with more than 4000 ppm. Therefore, a dosage o 2000 ppm was selected to treat MFT diluted to 5 wt. % solids, and 4000 ppm was selected to treat MFT diluted to 10 and 20 wt % solids.

The polymer solution and the MFT were mixed in a 250 mL glass beaker equipped with a Heidolph Hei-Torque Precision 200 overhead mixer with a four-blade impeller (4.8 cm diameter). The MFT suspension was premixed at 600 rpm for 2 min to disperse the solids uniformly. After the premixing period, a desired amount of flocculant was added to the MFT, followed by 1000 ppm of Ca^{2+} while mixing at 20 rpm for 2 min. The best mixing parameters for EPDM-*g*-HPMAs were obtained by varying the mixing speed and monitoring the suspension torque in real-time. For the reference HPAM, we adopted the original mixing conditions of 650 rpm for 2 min, followed by slow mixing 230 rpm for 8 min [16].

After the mixing procedure was completed, the suspension was slowly transferred to a 100 mL graduated cylinder to measure the ISR. Settling rates were recorded every minute during the first 10 min, and then recorded every 10 min over 3 h. The ISR was calculated by plotting the tangent of the settling curve for the first 2 min [41].

Capillary suction time was measured to assess the dewaterability of the sludge [42] using a Triton 319 multi-purpose instrument. At the start of the settling tests, a sample volume of 5 mL was added to the CST funnel, and the capillary flow of water in the filter paper was recorded. These measurements were repeated three times in order to quantify the experimental error.

After 24 h of settling, the supernatant was separated from the sediments and its turbidity measured using a Hach 2100 AN turbidimeter. Finally, the sediments were transferred to a pre-weighted drying pan, dried in an oven at 60 °C for 24 h, and weighed to calculate the solids content.

4.2.6 Filter Press Operation

Pressure filtration was carried out in a filter press equipment (OFI Testing Equipment, Inc.) consisting of four 0.2-L stainless-steel cylindrical filtering units. This system can be pressurized up to 250 psig. Triton chromatographic paper with a filtration area of $12cm^2$ and 5 micron pore size was used as the filtration medium.

In a typical procedure, 100 mL of undiluted tailings was flocculated with EPDM-*g*-HPMA (2000 to 10000 ppm) in the presence of 1000 ppm Ca^{2+}. Undiluted tailings and flocculant were mixed at 20 rpm for 2 mins. After mixing, the flocculated sediments were transferred to the filter press cylinder. The pressure was adjusted to 5 psig, and the treated MFT was filtered for 1 hour. The formed filter cake was dried for 24 h in an oven at 60 °C to calculate the final solids content.

4.3 Results and Discussion

4.3.1 MFT Sample Composition

Table 4-1 lists the composition of the MFT sample from Imperial Oil. The sample contained 31.3 wt. % solids, 90 % of which were fine particles with characteristic dimensions below 46 µm. It also shows that the most abundant ions in MFT process water were Na^{+}, K^{+}, Ca^{2+}, Mg^{2+}.

Table 4-1: MFT sample composition.

Characterization technique		
Dean stark analysis (wt. %)	Bitumen	0.2
	Solids	31.3
	Water	68.6
Major ions measured by atomic absorption spectroscopy (ppm)	Na^{+}	118.3
	Ca^{++}	37.3
	Mg^{++}	19.8
	K^{+}	15.3
Particle size distribution Volume average (µm)	d10	1.12
	d50	6.82
	d90	46.4
Particle size distribution Number average (µm)	d10	0.35
	d50	0.49
	d90	0.92
pH		8.0

4.3.2 Effect of Graft Molecular Weight and Density of EPDM-*g*-HPMA on Flocculation

4.3.2.1 Initial Settling Rate (ISR)

EPDM-*g*-HPMA with different graft molecular weights (M_g) and graft densities (ρ_g) were used to flocculate MFT diluted to 5 wt. % solids. Settling tests were done in the presence of 1000 ppm Ca^{2+} and 2000 ppm of flocculant. Table 4-2 shows the ISR values for a wide range of graft average molecular weights (M_g = 34 to 175 kDa) and densities (ρ_g = 11 to 53 %). In this set of flocculants, the weight average molecular weight of the backbone was kept the same, M_b = 210 kDa. Graft density is defined as the average fraction of diene units per chain that were grafted with a PMA chain. For instance, ρ_g = 11 % indicates that only 11 out of 100 diene units in the EPDM chain became grafted with PMA chains.

Table 4-2: ISR for 5 wt. % MFT treated with EPDM-*g*-HPMA.

Polymer*	Graft molecular weights M_g (kDa)	Graft density ρ_g (%)	ISR (m/h)
EPDM-*g*-HPMA-210-93-11	93	11	1.12
EPDM-*g*-HPMA-210-49-14	49	14	0.69
EPDM-*g*-HPMA-210-147-16	147	16	1.57
EPDM-*g*-HPMA-210-34-28	34	28	0.68
EPDM-*g*-HPMA-210-101-32	101	32	0.94
EPDM-*g*-HPMA-210-94-29	94	29	0.90
EPDM-*g*-HPMA-210-175-28	175	28	1.05
EPDM-*g*-HPMA-210-48-37	48	37	0.78
EPDM-*g*-HPMA-210-150-37	150	37	0.98
EPDM-*g*-HPMA-210-96-53	96	53	0.74

* Polymers are labeled as EPDM-*g*-HPMA-M_b-M_g-ρ_g, where M_b is the average molecular weight of the backbone in kDa, M_g is the average molecular weight of the PMA grafts in kDa, and ρ_g is the percentual graft density.

Table 4-3 summarizes the analysis of variance for the ISR experiments. Insignificant predictors were dropped out from the model.

Table 4-3: ANOVA table for ISR.

Source of Variation	Sum of Squares	Degrees of Freedom	Mean Squares	F	P	Comments*
1) M_g (L: linear)	0.3696	1	0.3696	39.3591	0.0032	significant
M_g (Q: uadratic)	0.0002	1	0.0002	0.0288	0.8733	
2) ρ_g (L)	0.1479	1	0.1479	15.7478	0.0165	significant
ρ_g (Q)	0.0028	1	0.0028	0.2985	0.6138	
1L by 2L	0.1329	1	0.1329	14.1524	0.0197	significant
Error	0.0375	4	0.0093			
Total SS	0.6372	9				

* 95% confidence interval.

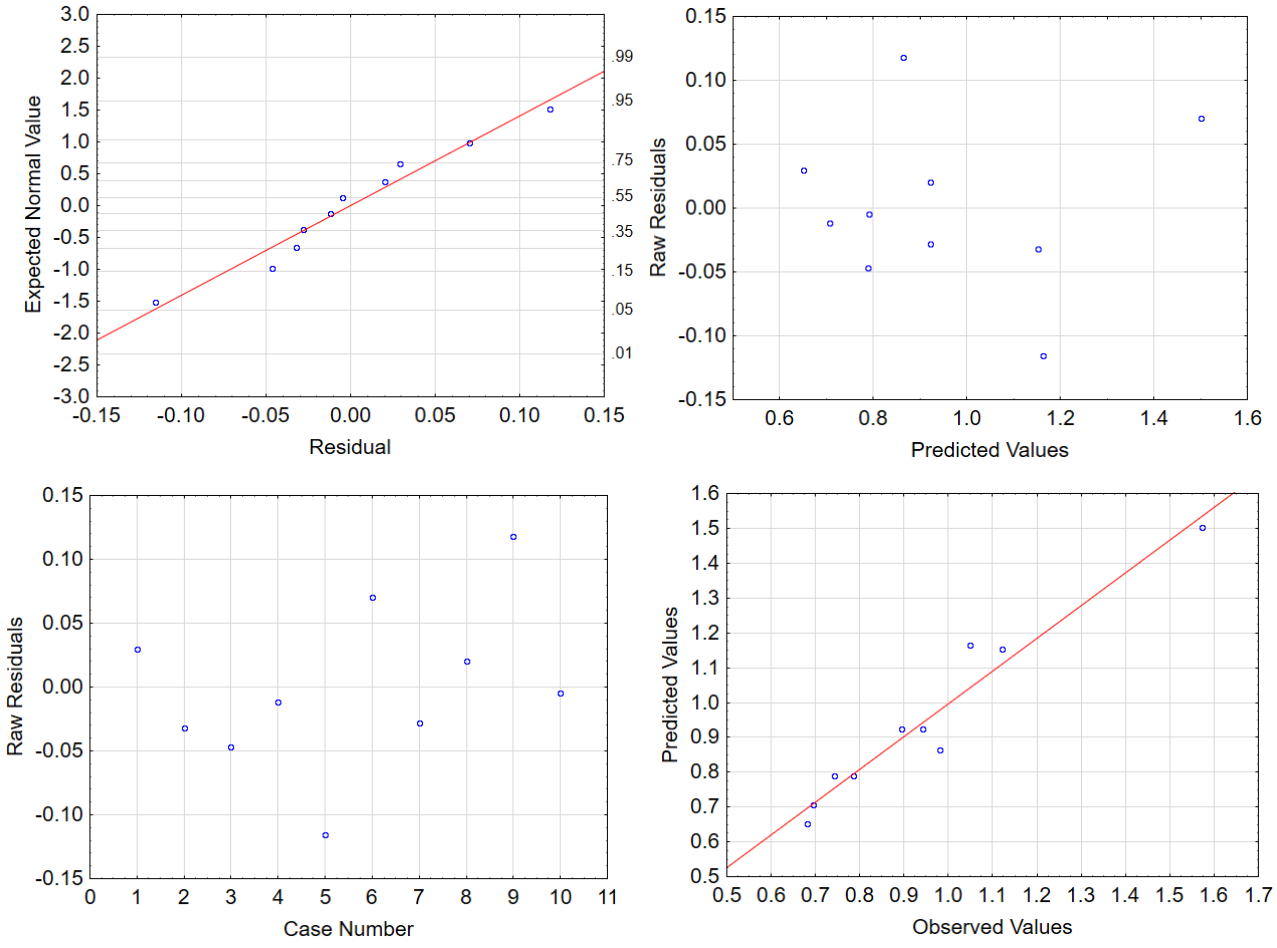

Figure 4-1: ISR model plots: a) normal plot, b) scatterplot of the standardized residuals as a function of the standardized predicted values, c) residuals versus run number, d) predicted versus observed values.

The residuals (measurements versus predictions) were plotted as a function of the expected normal values to check for model adequacy (Figure 4-1a). The linear trend indicates that the data follows a normal distribution. Moreover, the scatterplot of the standardized residuals as a function of the standardized predicted values shows that the variance of the residuals across all levels of the independent variables is randomly distributed (Figure 4-1b). The residuals were also plotted versus case number in Figure 4-1c, showing that the independent variables were not correlated with each other. Finally, the plot of predicted versus observed values (Figure 4-1d) confirms that the model is adequate. Since all multiple linear regression assumptions were met, Equation (4-3) was derived based on the significant predictors,

$$ISR = 0.029 + 0.018\ \rho_g + 0.012\ M_g - 0.2887\times10^{-3}\ M_g\ \rho_g \qquad (4\text{-}3)$$

where M_g is the graft average molecular weight and ρ_g is the graft density.

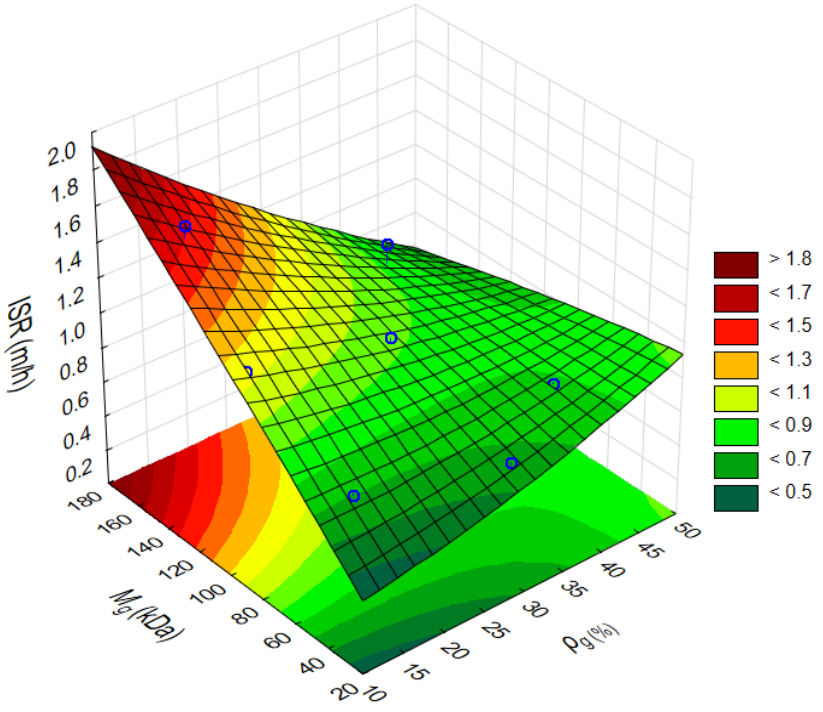

Figure 4-2: Surface response plot for ISR as a function of graft molecular weight and density.

Figure 4-2, the surface plot generated with Equation (4-3), shows that ISR increases as M_g increases for EPDM-*g*-HPMA flocculants with $\rho_g < 40\%$, which may be attributed to more effective interactions between suspended clay particles and the acrylic functional groups in the HPMA grafts. This suggests that longer grafts (with more functional groups) interact more effectively with clay particles and form larger fast-settling flocs. Interestingly, the opposite behaviour is observed when the grafting density is higher than 40%: for these flocculants, ISR decreases as the grafts get longer.

To confirm the dependency of ISR on graft molecular weights and densities of EPDM-*g*-HPMA flocculants, the dependency of ISR changes with the mass percentage of HPMA in EPDM-*g*-HPMA were assessed.

Figure 4-3 shows that ISR is not a function of the HPMA fraction in EPDM-*g*-HPMA. The EPDM-*g*-HPMA flocculants (210-49-14 and 210-96-53) that had the lowest and second highest HPMA fractions led to the lowest ISRs of all flocculants in Figure 4-3. In addition, EPDM-*g*-HPMA flocculants 210-147-16 and 210-101-32, with similar HPMA fractions, have largely different ISRs.

The structure of the EPDM-*g*-HPMA flocculants, however, influences the ISR values. For instance, EPDM-*g*-HPMA 210-96-53, 210-150-37, and 210-175-28 have the highest HPMA fractions of all samples in Figure 4-3. For these polymers, increasing M_g and decreasing ρ_g causes the ISR to increase. Comparing EPDM-*g*-HPMA 210-101-32 and 210-147-16 leads to the same conclusion. These results agree with the correlation among M_g, ρ_g, and ISR shown in Figure 4-2, where the performance of the EPDM-*g*-HPMA flocculants is a function of M_g and ρ_g, but not of HPMA fraction.

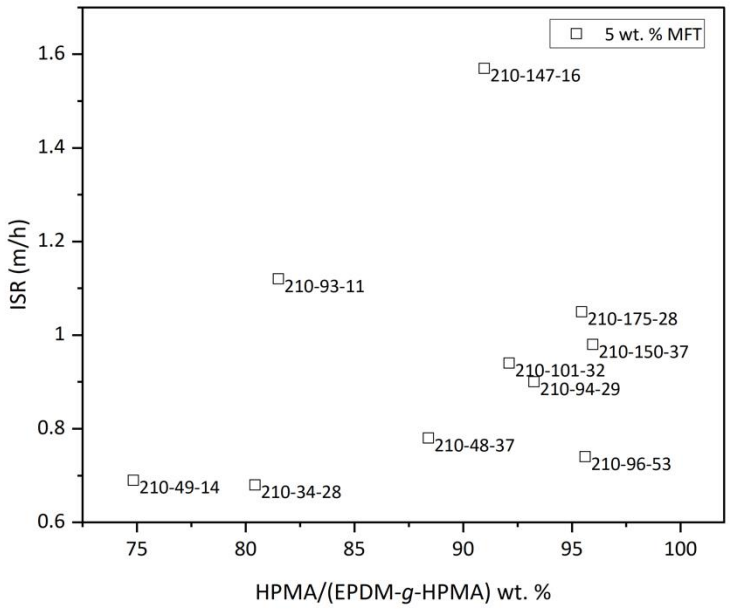

Figure 4-3: ISR for 5 wt. % MFT treated with EPDM-g-HPMA of different graft molecular weights and densities versus mass percentage of HPMA in EPDM-*g*-HPMA.

Figure 4-4, comparing the performance of two flocculants with the same graft density but different molecular weights (M_g = 49 and 147 kDa), is a powerful visual demonstration of how the molecular weight of the HPMA grafts affect floc size. This behaviour is typical of other flocculants with different graft molecular weights.

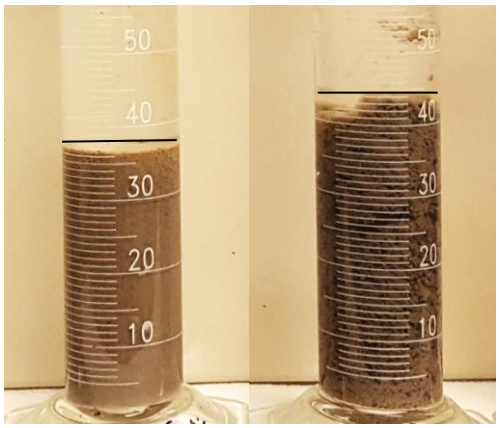

Figure 4-4: Flocculation of 5 wt. % MFT using EPDM-*g*-HPMA with different graft molecular weights: a) EPDM-*g*-HPMA-210-49-14 (M_g = 49 kDa), b) EPDM-*g*-HPMA-210-147-16 (M_g = 147 kDa).

Figure 4-5 compares flocculation results with less diluted MFT (10 and 20 wt. % solids) with 4000 ppm of a EPDM-*g*-HPMA with high molecular weight grafts and low graft density (M_g = 147 kDa, ρ_g =16 %). Since large flocs were formed almost immediately in these experiments, it was not possible to quantify the ISR values.

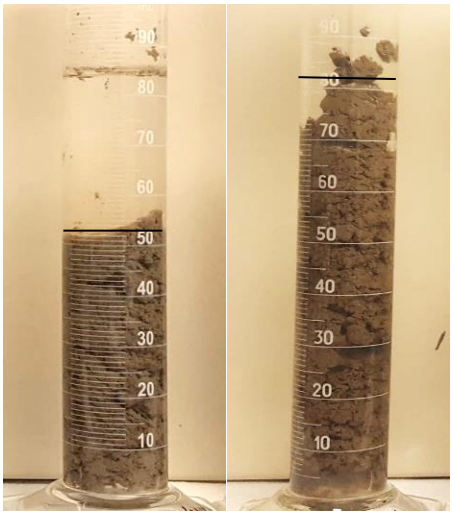

Figure 4-5: Flocculation of MFT with EPDM-*g*-HPMA-210-147-16: a) 10 wt.% MFT, b) 20 wt.% MFT.

4.3.2.2 Capillary suction time (CST)

Capillary suction time measures how easy it is for sediments to release water. In a typical experiment, a sample aliquot is poured into a funnel to form a sediment bed. Once a thin porous filter paper is put underneath the funnel, the capillary suction pressure starts draining the water trapped in the sediments radially through the filter paper. The water flow rate depends on the height, permeability, and water-holding capacity of the sediment bed [43].

In the following experiments, we quantified the influence of graft molecular weight and density of EPDM-*g*-HPMAs on MFT dewatering with a systematic statistical approach. Table 4-4 shows the CST of the sediments for 5, 10 and 20 wt. % MFT treated with different EPDM-*g*-HPMA flocculants.

Table 4-4: CST of the sediments for 5, 10 and 20 wt. % MFT treated with EPDM-*g*-HPMAs.

Polymer	Graft molecular weights	Graft density	CST (s)		
	M_g (kDa)	ρ_g (%)	5 wt %	10 wt %	20 wt %
EPDM-*g*-HPMA-210-93-11	93	11	91.52	131.43	151.31
EPDM-*g*-HPMA-210-49-14	49	14	102.43	132.43	237.17
EPDM-*g*-HPMA-210-147-16	147	16	45.51	85.51	102.12
EPDM-*g*-HPMA-210-34-28	34	28	121.32	159.32	245.25
EPDM-*g*-HPMA-210-101-32	101	32	77.35	107.26	123.27
EPDM-*g*-HPMA-210-94-29	94	29	82.41	112.26	122.56
EPDM-*g*-HPMA-210-175-28	175	28	39.12	83.32	107.51
EPDM-*g*-HPMA-210-48-37	48	37	95.36	127.65	148.06
EPDM-*g*-HPMA-210-150-37	150	37	57.43	87.43	97.23
EPDM-*g*-HPMA-210-96-53	96	53	51.54	91.29	105.89

Similarly to the procedure followed for ISR, we conducted an analysis of variance for the CST response (ANOVA tables are available in Appendix A). The accuracy of the models was assessed by analyzing their residuals based on multiple linear regression assumptions. To address non-normality in the residuals, we modeled log(CST) versus the predictors to find a model that satisfied the assumptions of linear regression models [33]. The residual plots (Appendix A) show that the model met all required assumptions. Equation (4-4) to Equation (4-6) are the final expressions based on the significant predictors for 5, 10, and 20 wt. % MFT samples, respectively.

$$\log(CST)_{5\%} = 2.115 + 0.009\ \rho_g - 0.200 \times 10^{-3}\ \rho_g^2 - 0.003\ M_g \quad (4\text{-}4)$$

$$\log(CST)_{10\%} = 2.218 + 0.004\ \rho_g - 0.103 \times 10^{-3}\ \rho_g^2 - 0.002\ M_g \quad (4\text{-}5)$$

$$\log(CST)_{20\%} = 2.426 + 0.004\ \rho_g - 0.144 \times 10^{-3}\ \rho_g^2 - 0.003\ M_g \quad (4\text{-}6)$$

Figure 4-6 compares the log(CST) models for MFT samples of all concentrations. Capillary suction times decrease (indicating faster dewatering) when the molecular weight of the grafts increase for all graft densities. Moreover, the lowest CST values were reached at particular combinations of graft molecular weight and density. This behaviour suggests that one of the significant factors in dewaterability of the flocs is the total charge density of the copolymer.

Figure 4-7 shows how log(CST) changes with the mass percentage of HPMA in EPDM-*g*-HPMA. The hydrolyzed PMA graft is the main source of charges in the EPDM-*g*-HPMA flocculants: increasing the HPMA content in the grafted copolymer also causes the charge density to increase.

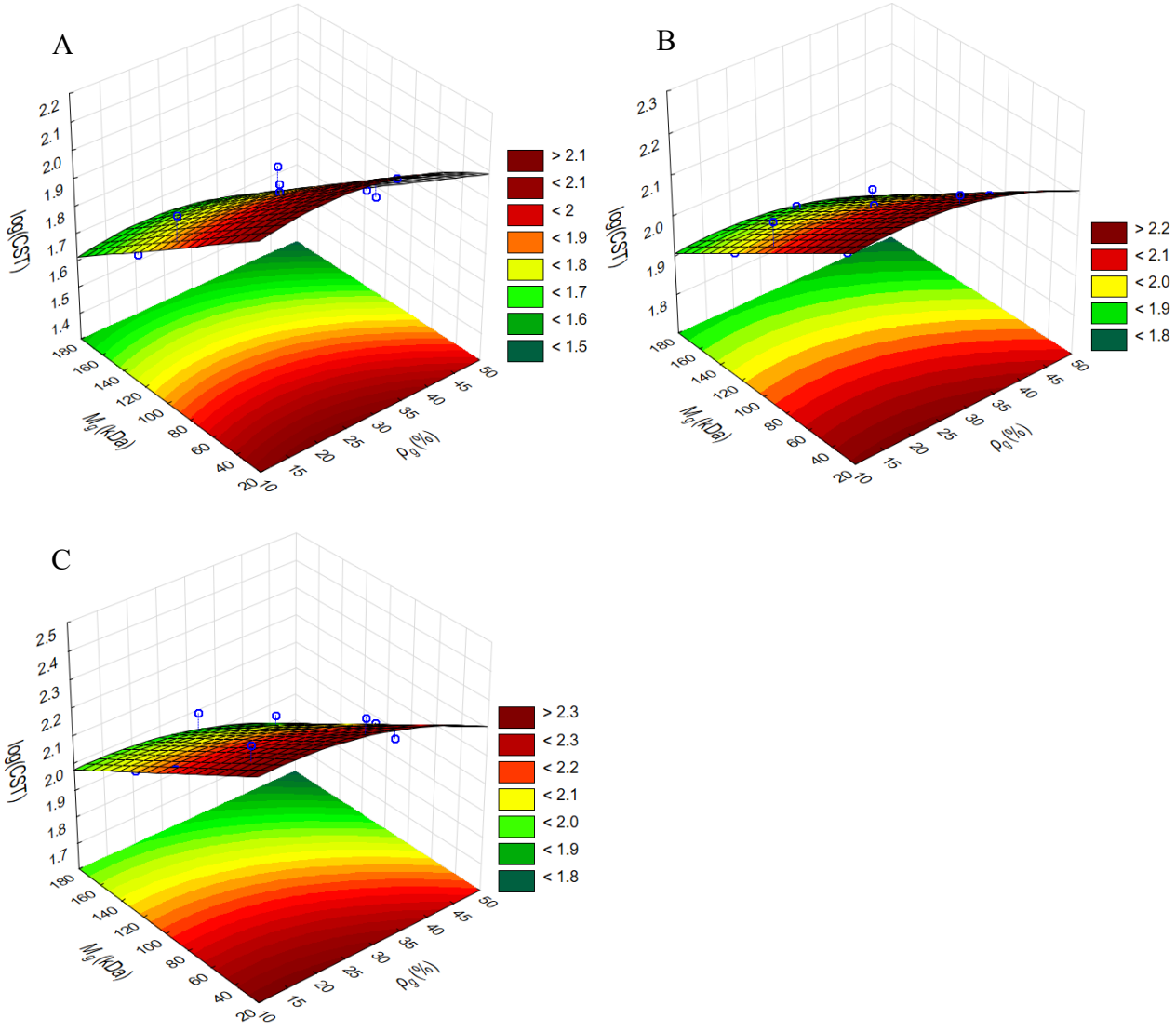

Figure 4-6: Surface response of log(CST) for diluted MFT treated with EPDM-*g*-HPMA of different graft molecular weights and densities: a) 5 wt. % MFT, b) 10 wt. % MFT, c) 20 wt. % MFT.

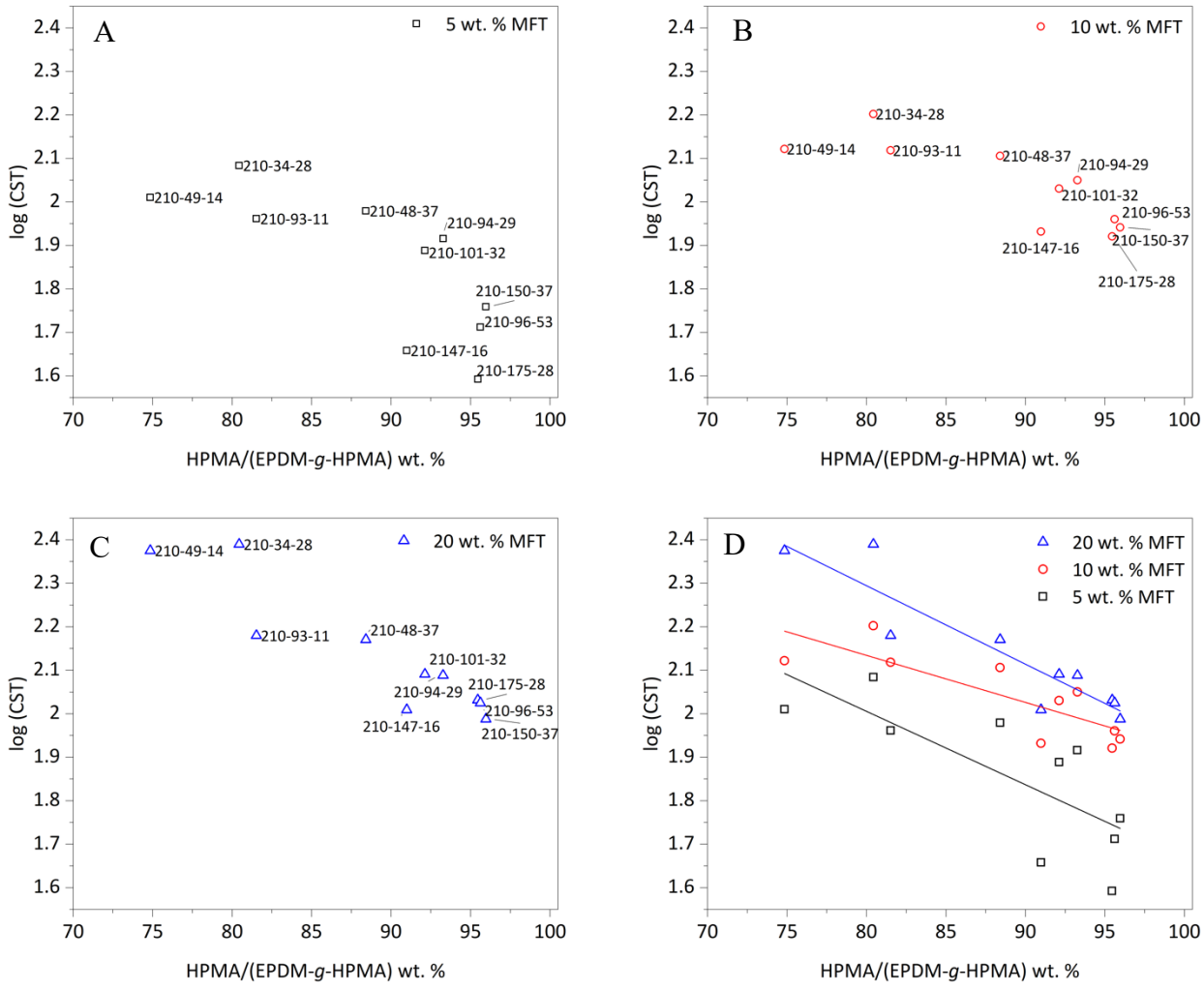

Figure 4-7: log(CST) for diluted MFT treated with EPDM-*g*-HPMA of different graft molecular weights and densities versus mass percentage of HPMA in EPDM-*g*-HPMA: a) 5 wt. % MFT, b) 10 wt. % MFT, c) 20 wt. % MFT, d) MFT samples of all concentrations.

4.3.2.3 Supernatant turbidity

Measuring the supernatant turbidity allows us to determine how effectively the flocculant captures the finest particles in suspension. In the following experiments, we quantified the influence of graft molecular weight and density of EPDM-*g*-HPMAs on capturing fine particles with a systematic statistical approach. Table 4-5 shows the supernatant turbidity of 5, 10, and 20 wt. % MFT samples treated with EPDM-*g*-HPMAs after 24 h of settling.

Table 4-5: Supernatant turbidity for 5, 10 and 20 wt. % MFT treated with EPDM-*g*-HPMAs.

Polymer	Graft molecular weights	Graft density	Supernatant turbidity (NTU), T		
	M_g (kDa)	ρ_g (%)	5 wt. %	10 wt. %	20 wt. %
EPDM-*g*-PMA-210-93-11	93	11	23.5	62.2	126
EPDM-*g*-PMA-210-49-14	49	14	251	187.6	385.1
EPDM-*g*-PMA-210-147-16	147	16	23.9	13.09	29.5
EPDM-*g*-PMA-210-34-28	34	28	466	333.5	243.4
EPDM-*g*-PMA-210-101-32	101	32	96	76.8	116.8
EPDM-*g*-PMA-210-94-29	94	29	96	85	135.4
EPDM-*g*-PMA-210-175-28	175	28	62	16.5	50.3
EPDM-*g*-PMA-210-48-37	48	37	187	112.2	301.5
EPDM-*g*-PMA-210-150-37	150	37	75	95	163.7
EPDM-*g*-PMA-210-96-53	96	53	216	128	171.7

Turbidity data were transformed by taking the logarithm of the numerical data to address non-normality in the residuals. Like the previous response variables, we conducted an ANOVA study, dropped out insignificant predictors, and assessed the accuracy of the models by analyzing their residuals based on multiple linear regression assumptions (see Appendix A). Equation (4-7) to Equation (4-9) quantify these relations for 5, 10, and 20 wt. % MFT samples, respectively.

$$\log(T)_{5\%} = 2.025 - 0.006\,\rho_g - 0.972\times10^{-3}\,M_g + 0.176\times10^{-3}\,M_g\,\rho_g \quad (4\text{-}7)$$

$$\log(T)_{10\%} = 1.046 - 0.008\,\rho_g - 0.005\,M_g + 0.110\times10^{-3}\,M_g\,\rho_g \quad (4\text{-}8)$$

$$\log(T)_{20\%} = 0.988 - 0.006\,\rho_g - 0.004\,M_g + 0.803\times10^{-3}\,M_g\,\rho_g \quad (4\text{-}9)$$

Figure 4-8 shows the output of the $\log(T)$ model for MFT samples of all concentrations. The supernatant turbidity decreases for longer grafts (higher M_g) and lower graft density (ρ_g). Supernatant turbidity is mainly controlled by the stability of clays in the MFT. Bridging the negatively-charged clay particles in MFT destabilizes and settles them, causing the supernatant turbidity to decrease. Acrylic acid groups in side chains of EPDM-*g*-HPMA in the presence of Ca^{2+} cations in the water facilitate bridging flocculation and lower supernatant turbidity. Increasing graft density, however, may lead to overdosing, which explains why the turbidity starts increasing

for highly grafted polymers [44]. Under this condition, the solids get covered in excess flocculant chains and steric and/or electrostatic repulsion are getting higher that may stabilize clay particles and cause higher supernatant turbidity.

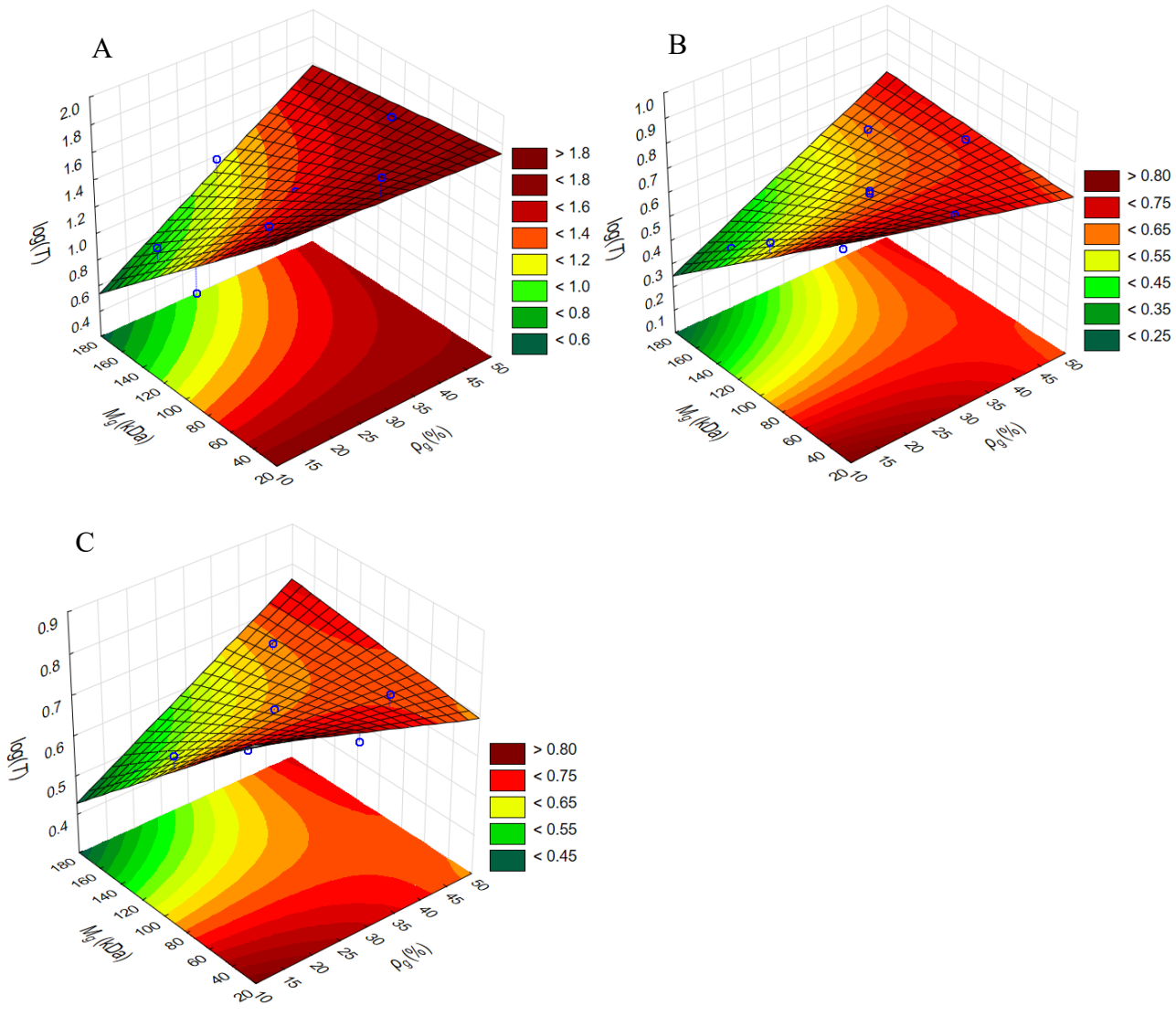

Figure 4-8: Surface response of log(T) for diluted MFT treated with EPDM-g-HPMAs with different graft molecular weights and densities: a) 5 wt. % MFT, b) 10 wt. % MFT, c) 20 wt. % MFT.

Similarly to ISR, no trend was observed between supernatant turbidity and the mass percentage of HPMA in EPDM-*g*-HPMA flocculants. Figure 4-9 shows that EPDM-*g*-HPMA with the same HPMA content may produce supernatants with vastly different turbidities. Compare, for instance,

EPDM-*g*-HPMA 210-96-53, 210-150-37, and 210-175-28, which have the highest HPMA content: as the M_g increases and the ρ_g decreases, the supernatant turbidity is decreases. A similar conclusion is reached by comparing EPDM-*g*-HPMA 210-101-32 and 210-146-16. These results agree with the correlation shown in Figure 4-8: the turbidity of supernatants released with EPDM-*g*-HPMA flocculants is a function of M_g and ρ_g, but not of HPMA content.

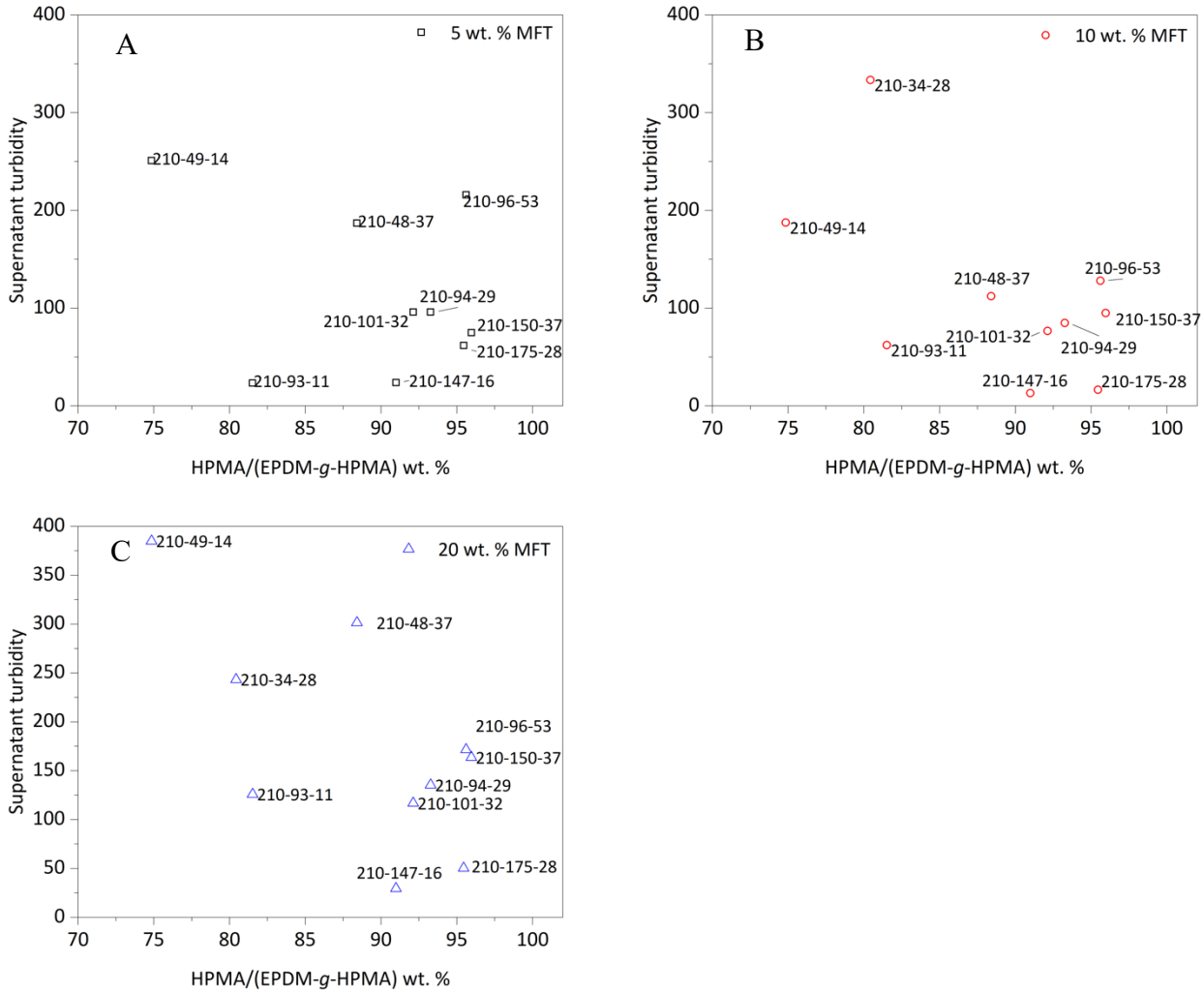

Figure 4-9: Supernatant turbidity for diluted MFT treated with EPDM-*g*-HPMA of different graft molecular weights and densities versus mass percentage of HPMA in EPDM-*g*-HPMA: a) 5 wt. % MFT, b) 10 wt. % MFT, c) 20 wt. % MFTs.

4.3.2.4 Sediment solids content

Table 4-6 shows the sediment solids content for 5, 10 and 20 wt. % MFT samples treated with EPDM-*g*-HPMAs at different graft molecular weights and densities after 24 h.

Table 4-6: Sediment solids content for 5, 10 and 20 wt. % MFT treated with EPDM-*g*-HPMAs.

Polymer	**Graft molecular weights**	**Graft density**	**Solids content, *S***		
	***M*$_g$ (kDa)**	**ρ_g (%)**	**5 wt. %**	**10 wt. %**	**20 wt. %**
EPDM-*g*-PMA-210-93-11	93	11	20.8	18.71	17.11
EPDM-*g*-PMA-210-49-14	49	14	14.27	13.47	15.6
EPDM-*g*-PMA-210-147-16	147	16	21.8	21.65	23.65
EPDM-*g*-PMA-210-34-28	34	28	13.47	11.7	15
EPDM-*g*-PMA-210-101-32	101	32	18.27	15.9	19.46
EPDM-*g*-PMA-210-94-29	94	29	18.27	16.52	18.59
EPDM-*g*-PMA-210-175-28	175	28	19.1	18.63	24.11
EPDM-*g*-PMA-210-48-37	48	37	15.4	12.11	16.13
EPDM-*g*-PMA-210-150-37	150	37	18.37	16.59	19.97
EPDM-*g*-PMA-210-96-53	96	53	15.1	14.7	17.46

Equation (4-10) to Equation (4-12) are the final formulae including only the significant predictors for 5, 10, and 20 wt. % MFT samples, respectively. Details of the ANOVA study are presented in the Appendix A.

$$S_{5\%} = 7.529 + 0.173\, M_g - 0.365\times10^{-3}\, M_g^2 + 0.085\, \rho_g - 0.001\, M_g \rho_g \quad (4\text{-}10)$$

$$S_{10\%} = 7.235 + 0.155\, M_g - 0.267\times10^{-3}\, M_g^2 + 0.0361\, \rho_g - 0.001\, M_g \rho_g \quad (4\text{-}11)$$

$$S_{20\%} = 11.925 + 0.0833\, M_g + 0.628\times10^{-3}\, \rho_g^2 - 0.742\times10^{-3}\, M_g \rho_g \quad (4\text{-}12)$$

Figure 4-10 shows how the solids content varies as a function of graft molecular weight and density. For all three MFT loadings, increasing graft molecular weight and decreasing graft density lead to the recovery of sediments with higher solids contents.

Interestingly, each of the EPDM-*g*-HPMA that was used to treat MFT loadings with concentration from 5 to 20 wt. % produced sediments with similar solids contents. This observation indicates that the post-flocculation solids content is a function of graft molecular weights and densities, but is less dependent on the MFT concentration. The MFT concentration, however, determines the amount of sediments collected at the end of the sedimentation. Figure 4-4b, Figure 4-5a and Figure 4-5b depict the volume of sediments obtained when 5, 10, and 20 wt. % MFT were treated with the same flocculant, EPDM-*g*-HPMA-210-147-16. It is clear that by increasing the MFT concentration, the volume of sediment also increases from 45 to more than 80 mL. The solids contents of all sediments, however, were almost the same, varying only from 21.65 to 23.65, as listed in Table 4-6.

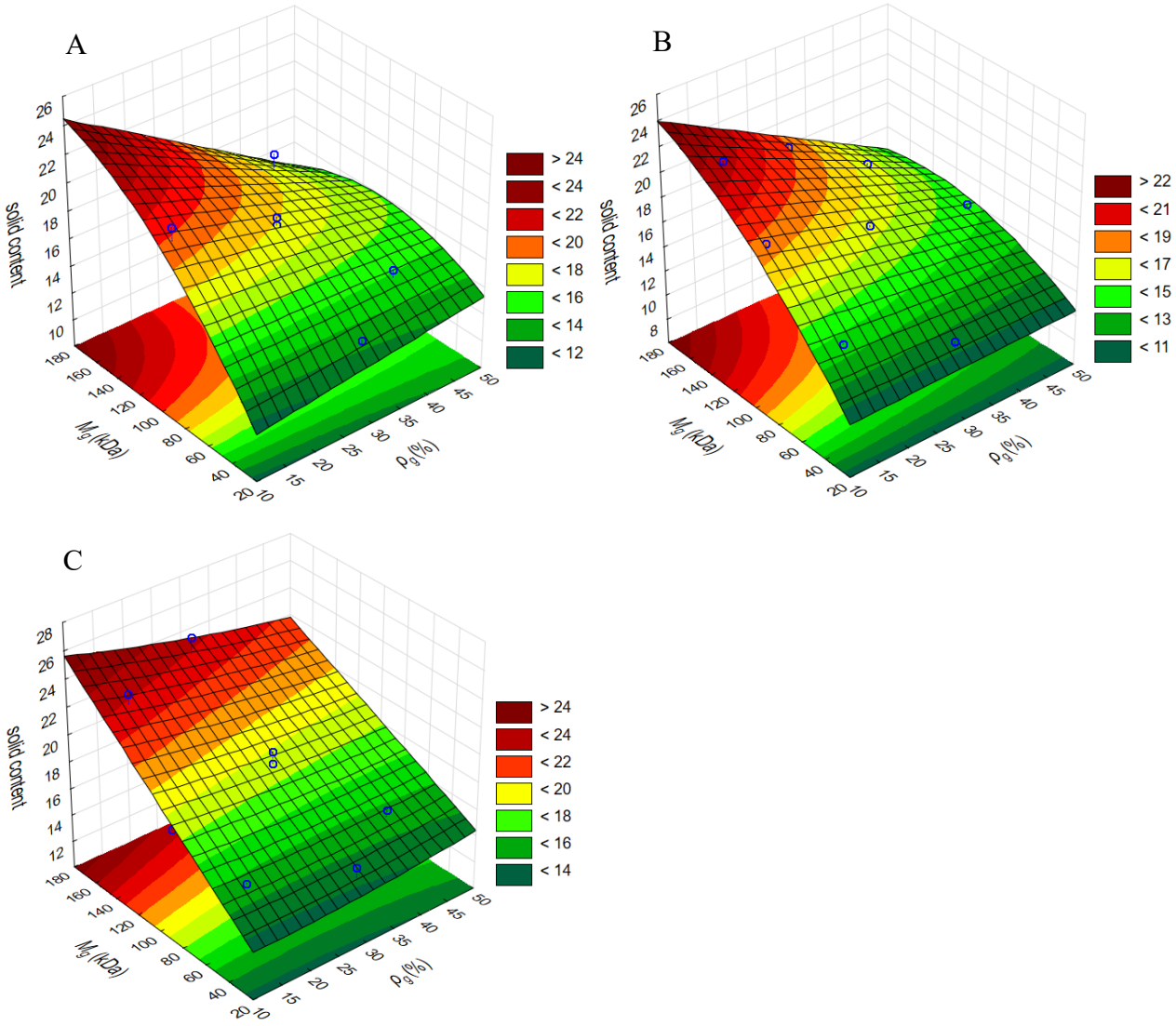

Figure 4-10: Surface response of sediment solids content for diluted MFT treated with EPDM-*g*-HPMA of different graft molecular weights and densities: a) 5 wt. % MFT, b) 10 wt. % MFT, and c) 20 wt. % MFT.

No trend was observed between solids content and the mass percentage of HPMA in EPDM-*g*-HPMA flocculants, as shown in Figure 4-11. EPDM-*g*-HPMA flocculants with the same HPMA content led different solids contents. Comparing EPDM-*g*-HPMA 210-96-53, 210-150-37, and 210-175-28, which have the highest HPMA content, shows that by increasing M_g and decreasing ρ_g, the solids content increases.

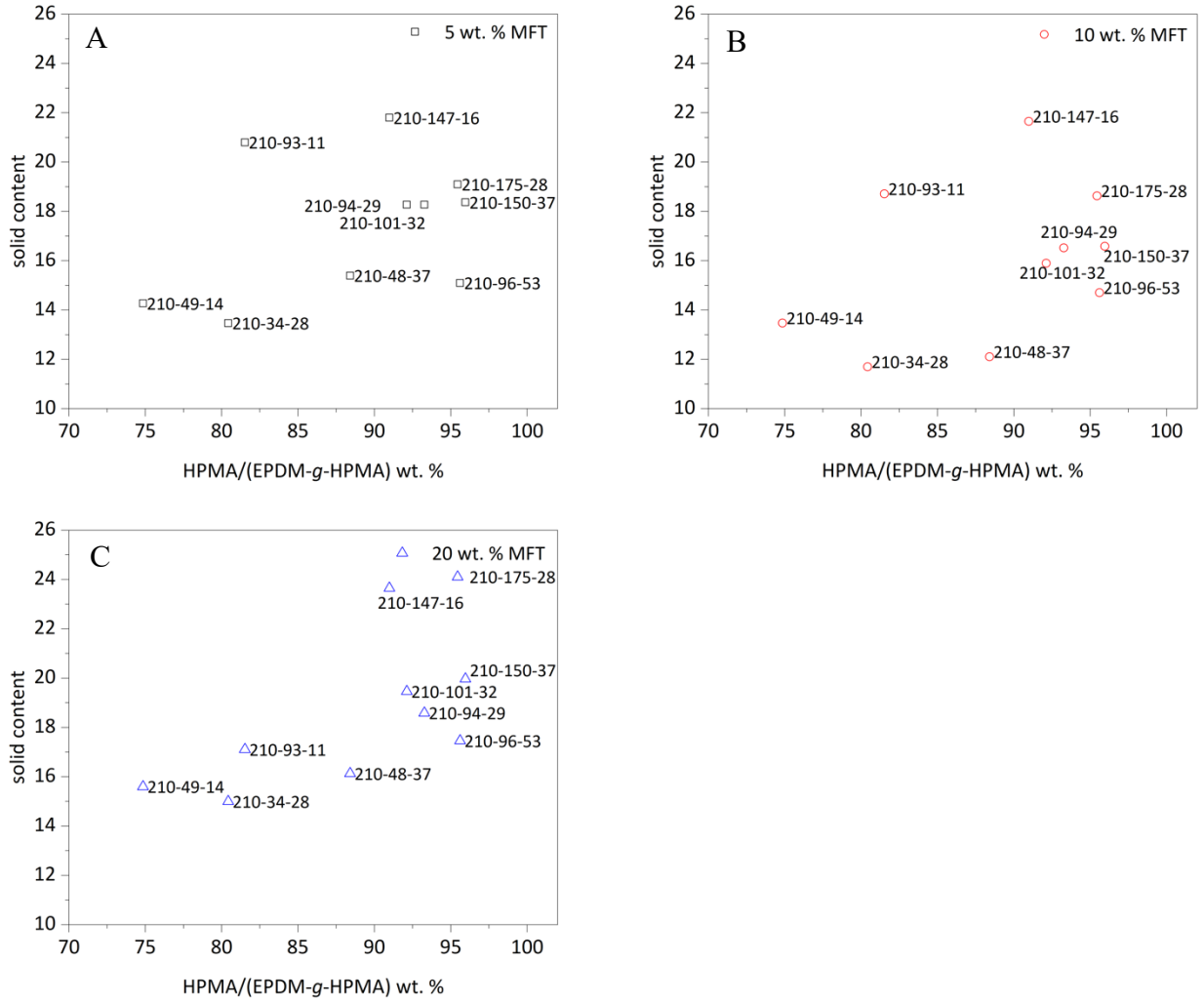

Figure 4-11: Solids content for diluted MFT treated with EPDM-*g*-HPMA of different graft molecular weights and densities versus mass percentage of HPMA in EPDM-*g*-HPMA: a) 5 wt. % MFT, b) 10 wt. % MFT, c) 20 wt. % MFT.

4.3.3 Effect of Backbone Length of EPDM-*g*-HPMA on Flocculation

Two different EPDM samples with weight average molecular weights (M_b) of 115 and 210 kDa were used as backbones to make two series of EPDM-*g*-HPMAs. In the experiments discussed above, EPDM-*g*-HPMA flocculants with high M_g and low ρ_g performed better. Based on those findings, three flocculants with high M_g (93 to 179 kDa) and low ρ_g (~15 %) from each series (M_b = 115 and 210 kDa) were compared (Table 4-7). Settling rate, capillary suction time, turbidity, and sediment solids content were measured to study the effect of backbone length on flocculation performance.

Table 4-7: EPDM-*g*-HPMAs properties.

Polymer	Graft molecular weights M_g (kDa)	Graft density ρ_g (%)
EPDM-*g*-HPMA-210-93-11	93	11
EPDM-*g*-HPMA-115-95-15	95	15
EPDM-*g*-HPMA-210-147-16	147	16
EPDM-*g*-HPMA-115-143-14	143	14
EPDM-*g*-HPMA-210-177-16	177	16
EPDM-*g*-HPMA-115-179-13	179	13

4.3.3.1 Settling rate

Both series of EPDM-*g*-HPMA flocculants (M_b = 115 and 210 kDa) listed in Table 4-7 were used to flocculate 5 wt. % solids MFT in the presence of 1000 ppm Ca^{2+} at a dosage of 2000 ppm. Figure 4-12 compares settling rates over 50 min for the EPDM-*g*-HPMAs series and HPAM. For all graft molecular weights, EPDM-*g*-HPMA-115 outperformed EPDM-*g*-HPMA-210, but not HPAM. This behavior was expected, considering the molecular weight differences between HPAM and the EPDM-*g*-HPMA series. High molecular weight PAM promotes faster settling rates because they have more units available in the polymer chains for adsorption onto the clay surface. Longer chains can flocculate clay particles that are more widely separated through the bridging mechanism.

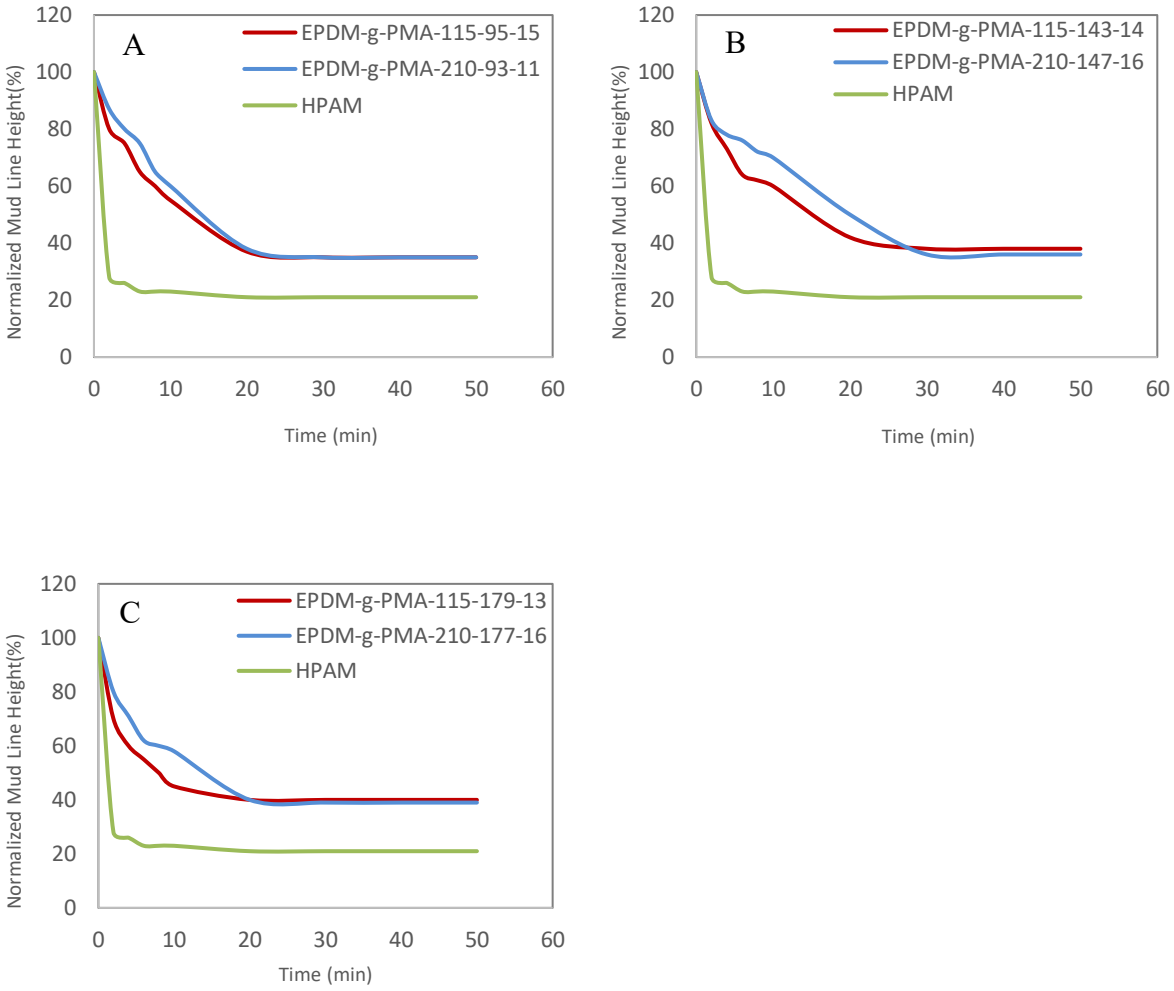

Figure 4-12: Settling rates for 5 wt. % MFT treated with HPAM and EPDM-*g*-HPMA with two different backbones (M_b = 115 and 210 kDa) at graft molecular weights (M_g): a) M_g = 100 kDa, b) M_g = 150 kDa, c) M_g = 180 kDa.

Interestingly, EPDM-*g*-HPMA flocculants with shorter backbones formed bigger flocs than the EPDM-*g*-HPMA with longer backbones (Figure 4-13).

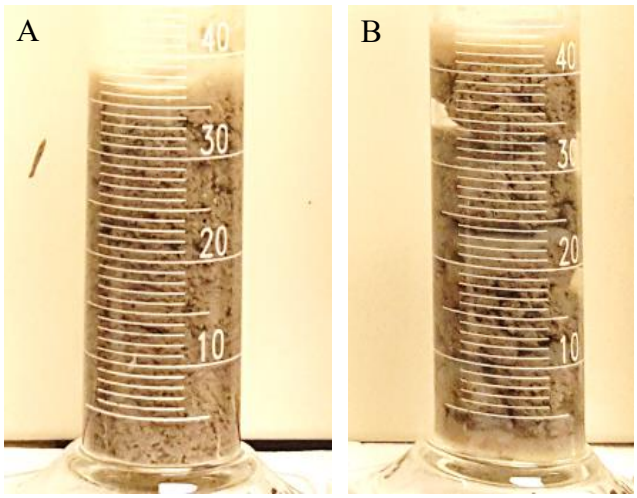

Figure 4-13: Flocculation of 5 wt. % MFT using EPDM-*g*-HPMA with the same graft molecular weight and density, but different backbone length: a) EPDM-*g*-HPMA-210-177-16, M_b = 210 kDa, b) EPDM-*g*-HPMA-115-179-13, M_b = 115 kDa.

The formation of bigger flocs that sediment faster may be correlated to how well the flocculant is dispersed in water. Table 4-8 shows that for all graft molecular weights (M_g = 93 to 179 kDa), the EPDM-*g*-HPMA-115 flocculants produced supernatants with lower turbidity. We may assume that this reflect their higher dispersability in water, which is expected since these flocculants are less hydrophobic than the EPDM-*g*-HPMA-210. As a result, interactions between the polymer functional groups and the clay surfaces may be more effective and lead to the formation of larger flocs that settle faster.

Table 4-8: Turbidity of anionic EPDM-*g*-HPMAs suspension in water.

Polymer	**Turbidity (NTU)**
EPDM-*g*-HPMA-210-93-11	826
EPDM-*g*-HPMA-115-95-15	731
EPDM-*g*-HPMA-210-147-16	466
EPDM-*g*-HPMA-115-143-14	319
EPDM-*g*-HPMA-210-177-16	175
EPDM-*g*-HPMA-115-179-13	95

4.3.3.2 Capillary Suction Time (CST)

Figure 4-14a shows that for all graft molecular weights, the CST was lower for 5 wt. % MFT treated with EPDM-*g*-HPMA-210. Since EPDM-*g*-HPMA-210 flocculants have longer hydrophobic backbones, they can more effectively expel water from the flocs. These results are consistent with settling rate results for EPDM-*g*-HPMA-210 generating more compact mudlines (Figure 4-12). This supports our hypothesis that longer hydrophobic backbones enhance the dewaterability and consolidation of the sediments. The EPDM-*g*-HPMA flocculants with longer grafts (M_g = 150 and 180 kDa) also outperform HPAM due to their higher hydrophobicities.

Figure 4-14b, and Figure 4-14c show that capillary suction times for 10 and 20 wt. % MFTs are higher than those for 5 wt. % MFT. However, similarly to 5 wt. % MFT, EPDM-*g*-HPMA-210 flocculants with M_g = 100 to 180 KDa have lower CST values than EPDM-*g*-HPMA-115 flocculants. These figures also show that flocculants with longer grafts lead to lower CSTs. Interestingly, the CST values of the sediments made with both EPDM-*g*-HPMAs series with M_g= 180 kDa are lower than for the reference PAM. These results highlight how adding hydrophobic segments to polymer flocculants can help improve their dewatering behaviour.

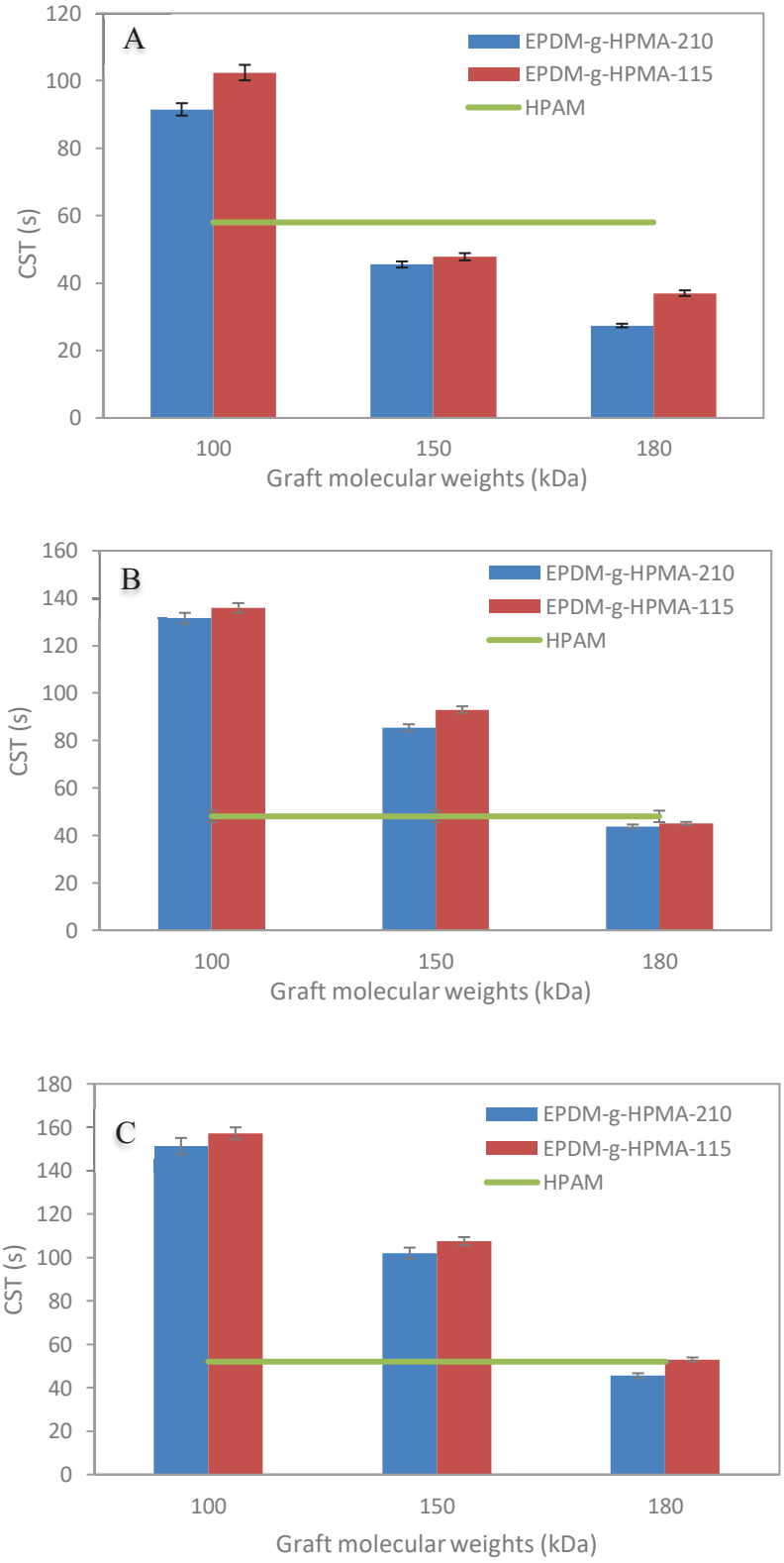

Figure 4-14: Cappilary suction times for diluted MFT treated with HPAM and EPDM-*g*-HPMA flocculants: a) 5 wt. % MFT, b) 10 wt. % MFT,) 20 wt. % MFT.

4.3.3.3 Supernatant turbidity

The supernatants turbidities of 5 wt. % MFT treated with different flocculants after 24 h of sedimentation is compared in Figure 4-15a. The first striking difference is that all EPDM-*g*-HPMA flocculants produced supernatants with much lower turbidities than the reference PAM. EPDM-*g*-HPMA-210 flocculants generated supernatants with slightly higher turbidity than its shorter-backbone counterparts, EDPM-*g*-HPMA-115, but the differences were almost negligible. It may be speculated that the presence of a longer EPDM backbone in the EPDM-*g*-HPMA-210 series imparts higher hydrophobicity to these polymers, causing them to disperse less effectively in the MFT and capture fewer fine particles.

Not surprisingly, when more concentrated MFT suspensions were used (10 and 20 wt. %), the supernatant turbidity increased, as depicted in Figure 4-15b, and Figure 4-15c, but the same trends were still observed: 1) all EPDM-*g*-HPMA outperformed the reference PAM and, 2) EPDM-*g*-HPMA-115 flocculants produced supernatants with lower turbidities than EPDM-*g*-HPMA-210. In both series, increasing M_g led to a decrease in supernatant turbidity, which highlights how the functional groups on the grafted chains interact with the fine clay particles.

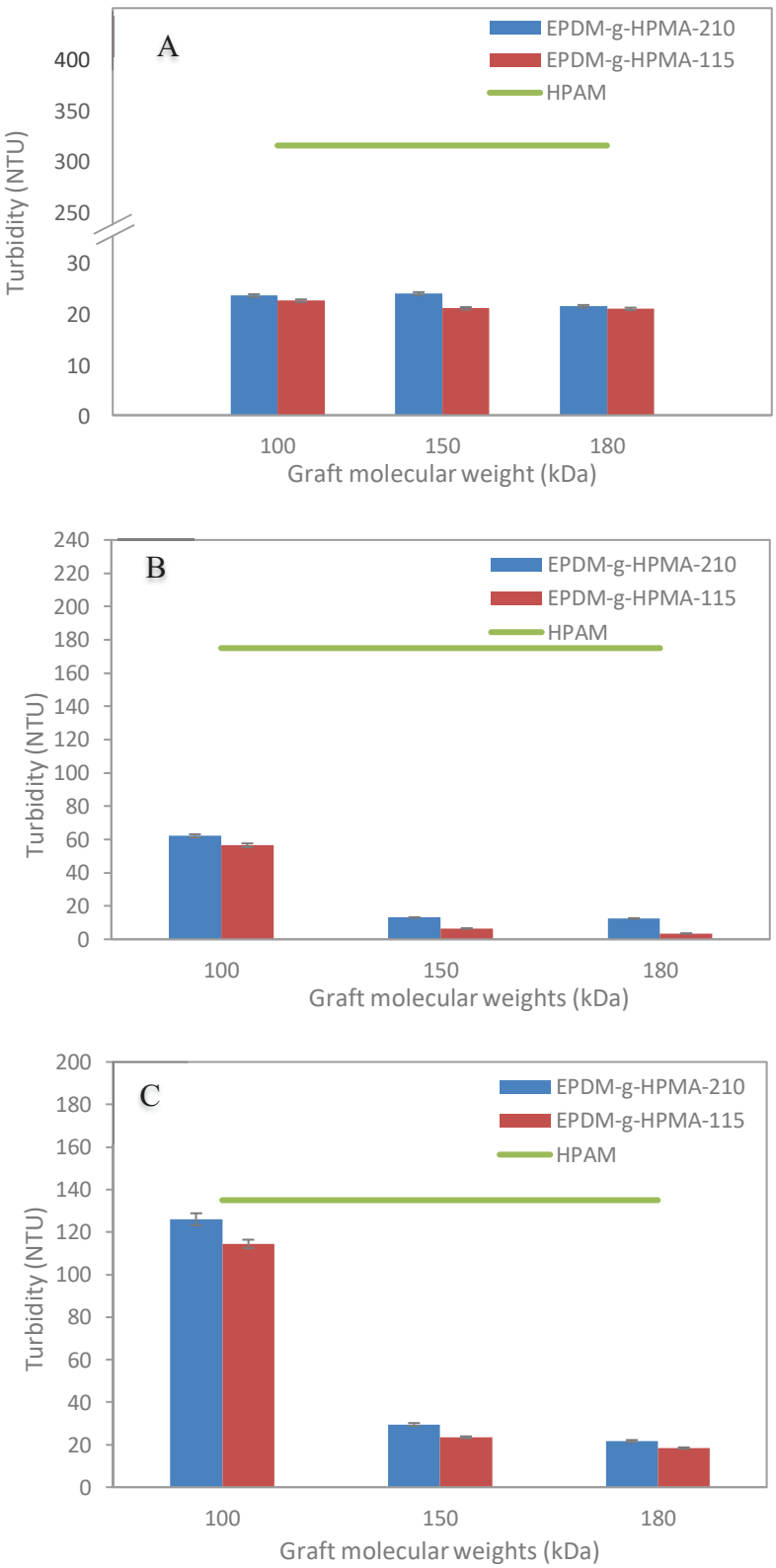

Figure 4-15: Supernatent turbidity of diluted MFT treated with HPAM and EPDM-*g*-HPMA flocculants: a) 5 wt. % MFT, b) 10 wt. % MFT,) 20 wt. % MFT.

4.3.3.4 Sediment solids content

Figure 4-16a compares the sediment solids content measured after 24 h for 5 wt. % MFT treated with 2000 ppm of EPDM-*g*-HPMAs and HPAM in the presence of 1000 ppm Ca^{2+}. All EPDM-*g*-HPMA outperformed the reference PAM. In addition, sediments with higher solids contents were achieved for EPDM-*g*-HPMA-115 than with EPDM-*g*-HPMA-210, although the difference was relatively small. The molecular weight of the grafts also seems to play a minor role on the final solids content.

As shown in Figure 4-16b, and Figure 4-16c, 10 and 20 wt. % MFT treated with 4000 ppm of EPDM-*g*-HPMAs show similar trends: the shorter the EPDM backbone, the higher the solids contents of the sediments. For 10 wt. % MFT suspensions, both EPDM-*g*-HPMAs series having $M_g \geq 150$ kDa produced sediments with more solids than HPAM. For 20 wt. % MFT suspensions, however, only EPDM-*g*-HPMA-115 with grafts of M_g=180 kDa outperformed the reference HPAM.

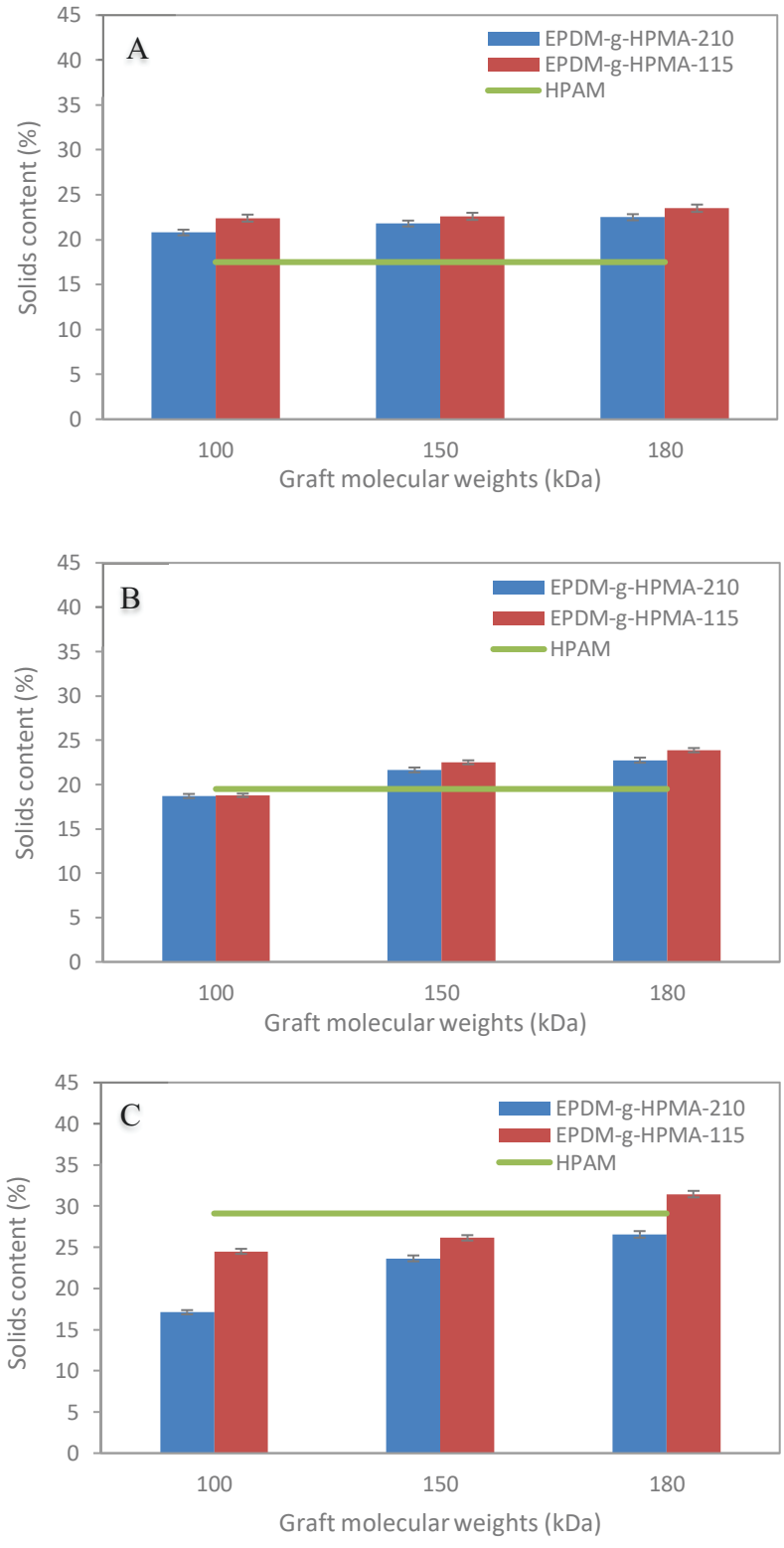

Figure 4-16: Sediment solids content for diluted MFT treated with HPAM and EPDM-*g*-HPMA flocculants: a) 5 wt. % MFT, b) 10 wt. % MFT,) 20 wt. % MFT.

4.3.3.5 Filtration of Flocculated Sediments

In the experiments discussed above, EPDM-*g*-HPMA-115-179-13 produced sediments with more solids than HPAM for all MFT suspensions. Based on those findings, undiluted MFT was treated with 2000 ppm of HPAM, and different dosages (2000 to 10000 ppm) of EPDM-*g*-HPMA-115-179-13 in the presence of 1000 ppm Ca^{2+} (Figure 4-17). A dosage of 2000 ppm of EPDM-*g*-HPMA-115-179-13 was not enough to flocculate the MFT. Increasing it to 4000 ppm produced sediments with 36.16 % solids, but higher dosages up to 10000 only increased the solids slightly to 39.53 %. This observation is not uncommon with polymeric flocculants, which see their effectiveness plateau or even decrease after they reach an optimum surface coverage of the suspended solids. For polymer dosages of 4000 to 10000 ppm, EPDM-*g*-HPMA-115 outperformed HPAM.

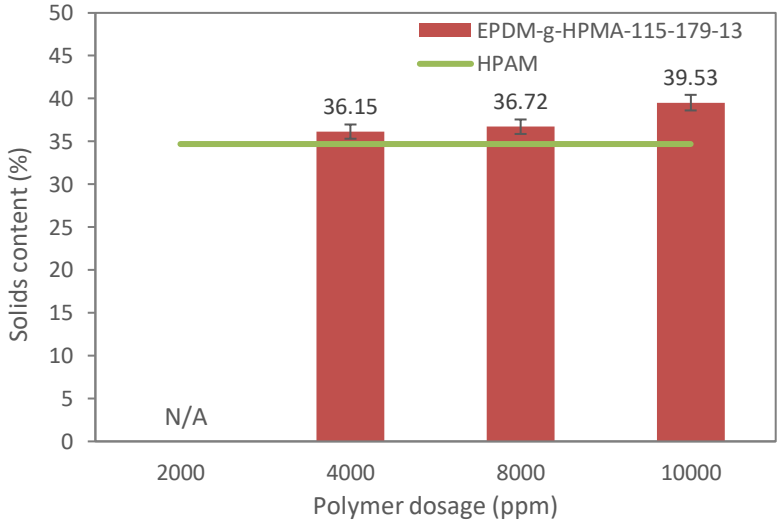

Figure 4-17: Sediment solids contents for undiluted MFT treated with 2000 ppm of HPAM, and different dosages of EPDM-*g*-HPMA-115-179-13.

The solids content of the sediments can be further increased by filtration [12] after flocculation. Immediately after settling, the flocculated sediments were filtered in a filter press at 5 psig. The filter cake samples formed after 1 h were dried for 24 h in an oven at 60 °C to obtain the final solids content. Figure 4-18 shows that cohesive filter cakes were formed with 40 % solids content for HPAM, and 43 % solids content for all EPDM-*g*-HPMA-115-179-13 dosages.

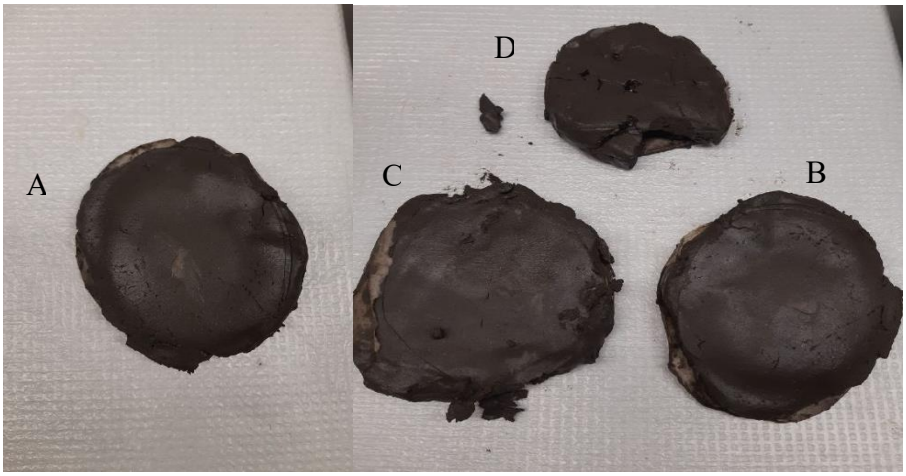

Figure 4-18: Filter cakes for flocculation of undiluted MFT with: a) 2000 ppm HPAM, b) 4000 ppm EPDM-*g*-HPMA-115-179-13, c) 8000 ppm EPDM-*g*-HPMA-115-179-13, and d) 10000 ppm EPDM-*g*-HPMA-115-179-13.

EPDM-*g*-HPMA-115-179-13 is the best candidate among this series of EPDM-*g*-HPMA flocculants because it can produce sediments with higher solids contents than HPAM. Based on those findings, EPDM-*g*-HPMA-115-179-13 was hydrolyzed with process water to assess the effect of process water on its performance. Undiluted MFT was treated with 2000 ppm of HPAM and 4000 ppm of EPDM-*g*-HPMA-115-179-13 in the presence of 1000 ppm Ca^{2+}. This treatment produced sediments with solids content of 37.14 % and 35.1 % for EPDM-*g*-HPMA-115-179-13 and HPAM respectively. EPDM-*g*-HPMA-115-179-13 also performed better than HPAM as a filtration aid. It formed a filter cake with 47 % solids content, while it was 43% for HPAM. Both flocculants with process water showed slightly higher solids content than those with deionized water.

4.4 Conclusions

In this work, the impact of graft molecular weights (M_g) and graft densities (ρ_g) of a series of EPDM-*g*-HPMA polymers on the flocculation and dewatering of MFT were investigated through a systematic statistical approach. The initial settling rate (ISR) for 5 wt. % MFT was lower for EPDM-*g*-HPMAs with higher M_g and low ρ_g. Flocculants with high M_g and low ρ_g performed even better for 10 and 20 wt. % MFT due to the fast formation of larger flocs that settled quickly. Based on the CST measurements, a balance between M_g and ρ_g of the EPDM-*g*-HPMAs is required for fast dewatering of the sediments. The turbidity was significantly decreased by increasing M_g and decreasing ρ_g for MFT samples of all concentrations. Sediments solids content measurements show that the highest solids content were achieved using EPDM-*g*-HPMAs with high M_g and low ρ_g.

Based on these results, high molecular weight poly(methyl acrylate) side chains with low graft density were added to two different EPDM backbones with different weight average molecular weights of 115 and 210 kDa to find out the effect of backbone length on the flocculation and dewatering of MFT in comparison with a reference HPAM. Initial settling rate, CST, turbidity, and solids content results for these two series of EPDM-*g*-HPMA showed that their flocculation properties depended significantly on their backbone lengths. Flocculants with shorter EPDM backbones seemed to disperse more effectively in water and, consequently, improve the settling rate of the suspended clay particles, decrease supernatant turbidity, and increase the solids content of sediments. On the other hand, the longer hydrophobic EPDM backbones expelled water from the flocs faster, and generating more compact mudlines.

Although EPDM-*g*-HPMAs with lower M_b = 115 kDa enhanced the settling rate of the clay particles, but it is still lower than HPAM. The CST results show that both series of EPDM-*g*-HPMAs with high M_g (180 kDa) dewatered MFT faster than HPAM. Both series also produced supernatants with lower turbidity than HPAM, which shows the capability of these flocculants in capturing more fine particles.

References

[1] L. Gross, T.L. Joly and C. Westman, Extracting home in the oil sands : settler colonialism and environmental change in subarctic Canada. Published in Milton by Routledge, 2020; ISBN:1351127438.

[2] J. Masliyah, Z. Zhou, Z. Xu, J. Czarnecki and H. Hamza, "Understanding water-based bitumen extraction from athabasca oil sands", Can.J.Chem.Eng., vol. 82, pp. 628-654, 2004.

[3] L. Botha and J.B.P. Soares, "The Influence of Tailings Composition on Flocculation", Can.J.Chem.Eng., vol. 93, pp. 1514-1523, 2015.

[4] K.L. Kasperski and R.J. Mikula, "Waste streams of mined oil sands: Characteristics and remediation", Elements, vol. 7, pp. 387-392, 2011.

[5] Alberta Energy Regulator, "State of Fluid Tailings Management for Mineable Oil Sands", Alberta Energy Regulator, 2019.

[6] J.H. Masliyah, Z. Xu, J.A. Czarnecki and M. Dabros, Handbook on theory and practice of bitumen recovery from Athabasca Oil Sands. Published in Cochrane, Alberta by Kingsley Knowledge Pub., 2013; ISBN:9781926832036.

[7] H. Li, J. Long, Z. Xu and J.H. Masliyah, "Synergetic role of polymer flocculant in low-temperature bitumen extraction and tailings treatment", Energy Fuels, vol. 19, pp. 936-943, 2005.

[8] D.R.L. Vedoy and J.B.P. Soares, "Water-soluble polymers for oil sands tailing treatment: A Review", Can.J.Chem.Eng., vol. 93, pp. 888-904, 2015.

[9] X.W. Wang, X. Feng, Z. Xu and J.H. Masliyah, "Polymer aids for settling and filtration of oil sands tailings", Can.J.Chem.Eng., vol. 88, pp. 403-410, 2010.

[10] H. Li, J. Long, Z. Xu and J.H. Masliyah, "Novel polymer aids for low-grade oil sand ore processing", Can.J.Chem.Eng., vol. 86, pp. 168-176, 2008.

[11] S. Wang, L. Alagha and Z. Xu, "Adsorption of organic–inorganic hybrid polymers on kaolin from aqueous solutions", Colloids Surf.Physicochem.Eng.Aspects, vol. 453, pp. 13-20, 2014.

[12] A. Alamgir, D. Harbottle, J. Masliyah and Z. Xu, "Al-PAM assisted filtration system for abatement of mature fine tailings", Chem.Eng.Sci., vol. 80, pp. 91-99, 2012.

[13] M. Hollósi, Z.M. Shen, A. Perczel and G.D. Fasman, "Stable intrachain and interchain complexes of neurofilament peptides: A putative link between Al3+ and Alzheimer disease", Proc.Natl.Acad.Sci.U.S.A., vol. 91, pp. 4902-4906, 1994.

[14] J. Long, H. Li, Z. Xu and J.H. Masliyah, "Improving oil sands processability using a temperature-sensitive polymer", Energy Fuels, vol. 25, pp. 701-707, 2011.

[15] H. Li, J. Zhou, R. Chow, A. Adegoroye and A.S. Najafi, "Enhancing treatment and geotechnical stability of oil sands fine tailings using thermo-sensitive poly(n-isopropyl acrylamide)", Can.J.Chem.Eng., vol. 93, pp. 1780-1786, 2015.

[16] L.G. Reis, R.S. Oliveira, T.N. Palhares, L.S. Spinelli, E.F. Lucas, D.R.L. Vedoy, E. Asare and J.B.P. Soares, "Using acrylamide/propylene oxide copolymers to dewater and densify mature fine tailings", Minerals Engineering, vol. 95, pp. 29-39, 2016.

[17] Y. Wang, Y. Kotsuchibashi, Y. Liu and R. Narain, "Temperature-responsive hyperbranched amine-based polymers for solid-liquid separation", Langmuir, vol. 30, pp. 2360-2368, 2014.

[18] L. Botha, D. Vedoy and J. Soares, "Novel hyperbranched functionalized polyethylenes for the treatment of oil sands tailings", in 19th International Seminar on Paste and Thickened Tailings, 2016.

[19] L. Botha, S. Davey, B. Nguyen, A.K. Swarnakar, E. Rivard and J.B.P. Soares, "Flocculation of oil sands tailings by hyperbranched functionalized polyethylenes (HBfPE)", Minerals Eng, vol. 108, pp. 71-82, 2017.

[20] Z. Rostami Najafabadi and J.B.P. Soares, "Ethylene/Propylene/Diene Terpolymers Grafted with Poly(methyl acrylate) via Reverse Atom Transfer Radical Polymerization", Macromol. Chem. Phys, vol. 222, article no. 2100189, 2021.

[21] K. Matyjaszewski, "Atom transfer radical polymerization: From mechanisms to applications", Isr.J.Chem., vol. 52, pp. 206-220, 2012.

[22] K. Matyjaszewski and J. Xia, "Atom transfer radical polymerization", Chem.Rev., vol. 101, pp. 2921-2990, 2001.

[23] V. Coessens, T. Pintauer and K. Matyjaszewski, "Functional polymers by atom transfer radical polymerization", Progress in Polymer Science, vol. 26, pp. 337-377, 2001.

[24] M. Kamigaito, T. Ando and M. Sawamoto, "Metal-catalyzed living radical polymerization", Chem.Rev., vol. 101, pp. 3689-3745, 2001.

[25] W.J. Wang, L. Pingwei, B.G. Li and Z. Shiping, "One-step synthesis of hyperbranched polyethylene macroinitiator and its block copolymers with methyl methacrylate or styrene via ATRP", J.Polym.Sci.Part A, vol. 48, pp. 3024-3032, 2010.

[26] Y. Inoue, T. Matsugi, N. Kashiwa and K. Matyjaszewski, "Graft copolymers from linear polyethylene via atom transfer radical polymerization", Macromolecules, vol. 37, pp. 3651-3658, 2004.

[27] H. Kaneko, J. Saito, N. Kawahara, S. Matsuo, T. Matsugi and N. Kashiwa, "Polypropylene-graft-poly(methyl methacrylate) Graft Copolymers: Synthesis and Compatibilization of Polypropylene/Polylactide", in Controlled/Living Radical Polymerization: Progress in ATRP, American Chemical Society, 2009, pp. 357-371.

[28] X.S. Wang, N. Luo and S.K. Ying, "Synthesis of EPDM-g-PMMA through atom transfer radical polymerization", Polymer, vol. 40, pp. 4515-4520, 1999.

[29] V.M.C. Coessens and K. Matyjaszewski, "Fundamentals of atom transfer radical polymerization", J.Chem.Educ., vol. 87, pp. 916-919, 2010.

[30] K. Yamamoto, H. Tanaka, M. Sakaguchi and S. Shimada, "Well-defined poly(methyl methacrylate) grafted to polyethylene with reverse atom transfer radical polymerization initiated by peroxides", Polymer, vol. 44, pp. 7661-7669, 2003.

[31] R. Ma, Z. Song, Y. Hou, Y. Liu, B. Xing, Z. Tan and F. Bao, "Synthesis of norbornene and methyl methacrylate graft copolymers with high norbornene content by using mixed catalytic system", J Macromol Sci Part A Pure Appl Chem, vol. 46, pp. 193-201, 2009.

[32] D.J. Haloi, K. Naskar and N.K. Singha, "Poly(meth)acrylate grafted EPDM via reverse atom transfer radical polymerization: A single pot process", Eur Polym J, vol. 49, pp. 4098-4107, 2013.

[33] J. Neter, W. Wasserman and M.H. Kutner, Applied linear statistical models : regression, analysis of variance, and experimental designs. Published in Homewood, IL by Irwin, 1990; pp. 1181; ISBN:025608338X.

[34] V. Theodorou, K. Skobridis, A.G. Tzakos and V. Ragoussis, "A simple method for the alkaline hydrolysis of esters", Tetrahedron Lett., vol. 48, pp. 8230-8233, 2007.

[35] H. Lu, L. Xiang, X. Cui, J. Liu, Y. Wang, R. Narain and H. Zeng, "Molecular Weight Dependence of Synthetic Glycopolymers on Flocculation and Dewatering of Fine Particles", Langmuir, vol. 32, pp. 11615-11622, 2016.

[36] K.C. Lister, H. Kaminsky and R.A. Hutchinson, "Evaluation of a novel polymeric flocculant for enhanced water recovery of mature fine tailings", Process., vol. 8, pp. 1-14, 2020.

[37] J. Long, H. Li, Z. Xu and J.H. Masliyah, "Role of colloidal interactions in oil sand tailings treatment", AIChE J., vol. 52, pp. 371-383, 2006.

[38] F.L. Motta, R. Gaikwad, L. Botha and J.B.P. Soares, "Quantifying the effect of polyacrylamide dosage, Na+ and Ca2+ concentrations, and clay particle size on the flocculation of mature fine tailings with robust statistical methods", Chemosphere, vol. 208, pp. 263-272, 2018.

[39] A. Pourmohammadbagher and J.M. Shaw, "Probing the Role of Water Chemistry on the Behavior of Clays in Process and Natural Environments Using Solution Calorimetry", Energy Fuels, vol. 30, pp. 5964-5969, 2016.

[40] A. Sworska, J.S. Laskowski and G. Cymerman, "Flocculation of the Syncrude fine tailings Part I. Effect of pH, polymer dosage and Mg2+ and Ca2+ cations", Int.J.Miner.Process., vol. 60, pp. 143-152, 2000.

[41] S. Wang, L. Zhang, B. Yan, H. Xu, Q. Liu and H. Zeng, "Molecular and surface interactions between polymer flocculant chitosan g polyacrylamide and kaolinite particles: Impact of salinity", J.Phys.Chem.C, vol. 119, pp. 7327-7339, 2015.

[42] M. Scholz, "Review of recent trends in Capillary Suction Time (CST) dewaterability testing research", Ind Eng Chem Res, vol. 44, pp. 8157-8163, 2005.

[43] L. Besra, D.K. Sengupta, B.P. Singh and S. Bhattacharjee, "A novel method based on Capillary Suction Time (CST) for assessment of dispersion characteristics of suspensions", J Am Ceram Soc, vol. 88, pp. 109-113, 2005.

[44] R. Hogg, "Flocculation and dewatering", Int.J.Miner.Process., vol. 58, pp. 223-236, 2000.

Chapter 5

5 Flocculation Efficiency and Spatial Distribution of Water in Oil Sands Tailings Flocculated with a Partially Hydrophobic Graft Copolymer

Partially hydrophobic polymers may dewater oil sands tailings more effectively than commercial hydrophilic flocculants. In this study we combine confocal microscopy and rheology to investigate how the graft density of ethylene-propylene-diene grafted with hydrolysed poly(methyl acrylate) (EPDM-*g*-HPMA) affect its dispersion in water and flocculation efficiency in terms of sediment solids content and long-term dewatering of oil sands tailings. Increasing the graft density from 30 % to 50 % makes the flocculant easier to disperse, increases the rate of initial dewatering, and also enhances the viscoelastic response of the flocculated sediments right after sedimentation. However, the long-term rheological properties of the flocculated sediments were similar for all flocculants. Tri-dimensional microscopic details of the spatial distribution of water within the flocculated sludge provide novel insights into the performance of the flocculants. Increasing the graft density in EPDM-*g*-HPMA traps more water within the individual flocs and consequently, decreases the post-flocculation dewatering rate.

5.1 Introduction

Alberta has the third largest proven crude oil reserve in the world. The tailings that are produced during hot water oil extraction methods are the well-known problem of oil sands. These tailings are a complex mixtures of water, clay, silt, sand, unrecovered bitumen, and organic solvents [1] ,which cover an area over 176 km^2 in Alberta [2]. Tailings contain negatively-charged clay particles. The larger particles (>44μm) settle under gravity, while the fines (<44μm) and ultra-fines (<0.2μm) undergo a limited consolidation and from colloidal suspension [3, 4] known as fluid fine tailings (FFT). After a certain time, the fines compact into a stable gel-like structure called mature fine tailings (MFT), which contains approximately 30 wt% solids [5].

Over the past few decades, several approaches have been proposed to expedite dewatering and solids consolidation in MFT [6-9]. Polymer flocculation has been commonly used to treat the oil sands tailings because of its low cost and immediate water release [10]. Electrostatic interactions, hydrogen bonding, and Van der Waals forces make the polymer chains adsorbed onto MFT particles and creating larger flocs that settle faster. The formation of large flocs is also linked to the bridging efficiency of the polymer [11].

Many natural and synthetic polymers have been used to flocculate MFT. Natural polymers degrade easily and are non-toxic, but are less effective than synthetic flocculants [12, 13]. Among the latter, industry has chosen high molecular weight polyacrylamide (PAM) because of its fast initial dewatering and floc settling rates [14, 15]. The performance of a flocculant, however, depends not only on initial dewatering and settling rates, but also on the rate of water release from the sediments during the consolidation period, which occurs on much longer time scale [16]. Since highly hydrophilic flocculants are likely to retain water in the sediments, it is reasonable to assume that a partially hydrophobic flocculant would help retain less water in the sediments [17, 18].

Recent studies on PAM modification involve the addition of hydrophobic groups to increase dewatering rates [19-25]. Partially hydrophobic flocculants, including UV-initiated [26, 27], thermosensitive [28, 29], CO_2 transitional polymers [30] and pH-responsive polymers, have been studied. Although most of them flocculated and dewatered tailings well, they are hard to scale up [31]. Most of these studies highlighted the advantages of hydrophobic modifications of PAM-based flocculants and discussed how they improved dewatering, but most polymers used

acrylamide as a comonomer, which is known to retain large amounts of water via hydrogen bonding [32-35].

To address this issue, a novel hybrid flocculant by reverse ATRP combining a hydrophobic ethylene/propylene/diene copolymer backbone and hydrolyzed poly(methyl acrylate) grafts (EPDM-*g*-HPMA) were synthesized [36]. The graft density of this polymer can be varied to obtain an optimum level of solubility and extended conformation of the polymer in solution. The functional groups in EPDM-*g*-HPMA are expected to adsorb to clay surfaces via hydrogen bonding that can undergo bridging flocculation. Although this mechanism is expected to be similar to that of hydrolyzed polyacrylamides, the extent of hydrogen bonding is expected to be less in the case of the EPDM-*g*-HPMA due to the absence of amide groups.

To characterize this novel polymer, the current study combines laser scanning confocal microscopy (LSCM) and rheology to quantify microscale rearrangements in oil sands tailings sediments flocculated with EPDM-*g*-HPMA with grafting densities varying between 30 % and 50 %. Our analysis demonstrated that graft density controls the dispersity if flocculant in water and the amount of retained water in the produced flocs. In addition, the *intra-floc* vs *inter-floc* water distribution in the flocculated sediments showed a clear effect of the polymer grafting density on the post flocculation long-term consolidation. Our results elucidate the fundamental of microscopic mechanisms for flocculation and dewatering of oil sands tailings and is a great help to develop effective flocculants for oil sands and other mineral tailings.

5.2 Materials and Methods

5.2.1 Materials

Three EPDM-*g*-HPMA samples with graft molecular weights of ~ 175 kDa and different graft densities of (~30, 40 and 50 %) were used in this study. Poly(methyl acrylate) was grafted on EPDM chains by reverse atom transfer radical polymerization (ATRP). The molecular weight and density of the grafts were controlled by varying the concentration and conversion of methyl acrylate, and the concentration of initiator. More details regarding the synthesis, characterization, and hydrolysis of the EPDM-*g*-HPMA flocculants were described in other publications [36, 37].

The mature fine tailings (MFT) sample used in the flocculation studies was received from Innotech tailings bank (Calgary, AB, Canada). The mass fractions of water (62.2 %), solids (36.77 %), and bitumen (1.03 %) in the raw MFT were determined by Dean-Stark analysis [38, 39].

5.2.2 Flocculation Methodology

The MFT was diluted to 5 wt% using deionized water and pre-mixed at 300 rpm for 1 min to get a homogeneous slurry. The flocculation tests used a mixture of the diluted MFT, 2000 ppm of EPDM-*g*-HPMAs, and 1000 ppm of Ca^{2+} (1M $CaCl_2$), totalling 1000 mL. A flat blade impeller (111.43 × 25.4 mm) attached to an overhead stirrer was used to mix the slurry without breaking the flocs [37]. The mixture was stirred at 30 rpm for 3 min. Immediately after the flocculation, about 100 mL of the mixture was transferred to a graduated cylinder to measure changes in mudline height, while the rest of the slurry was placed into a separating funnel for prolonged storage and sampling during the aging study. The above procedure was repeated thrice for all three polymer-treated MFT.

5.2.3 Microstructure Imaging of the Flocculant and the Flocculated Sediment by Confocal Microscopy

An inverted SP8X confocal laser scanning microscope (Leica Microsystems Inc, Canada) was used to image the flocculant dispersion in reflection mode, and the flocculated MFT sediments in a combination of reflection and fluorescence imaging techniques [40-42]. For all imaging, a 63× oil immersion objective with a numerical aperture of 1.4, a zoom factor of 1, a pinhole of 0.80 AU and an imaging format of 1024 × 1024 was used, with a final image pixel size of 180 nm × 180 nm. The polymer dispersion was imaged by detecting the reflection of 633 nm laser light from the polymer aggregates. In the case of flocculated MFT sediments, the fluorescence of bitumen features was imaged in a detection range 500 to 550 nm, upon excitation with 488 nm laser line [43-45], while the clay structures were imaged in the reflection mode similarly to the above-mentioned polymer dispersion. The stacks of 2D images were acquired from different spots throughout the sediment sample. The obtained stacks of 2D images were firstly processed in MATLAB using a pseudocode, and then the exported binarized 2D image stacks of the bitumen

and clay channels were further processed using the AVIZO® software to obtain their respective 3D surfaces [41]. The complete schematic of the image processing methodology for each of the channels is shown in Figure 5-1.

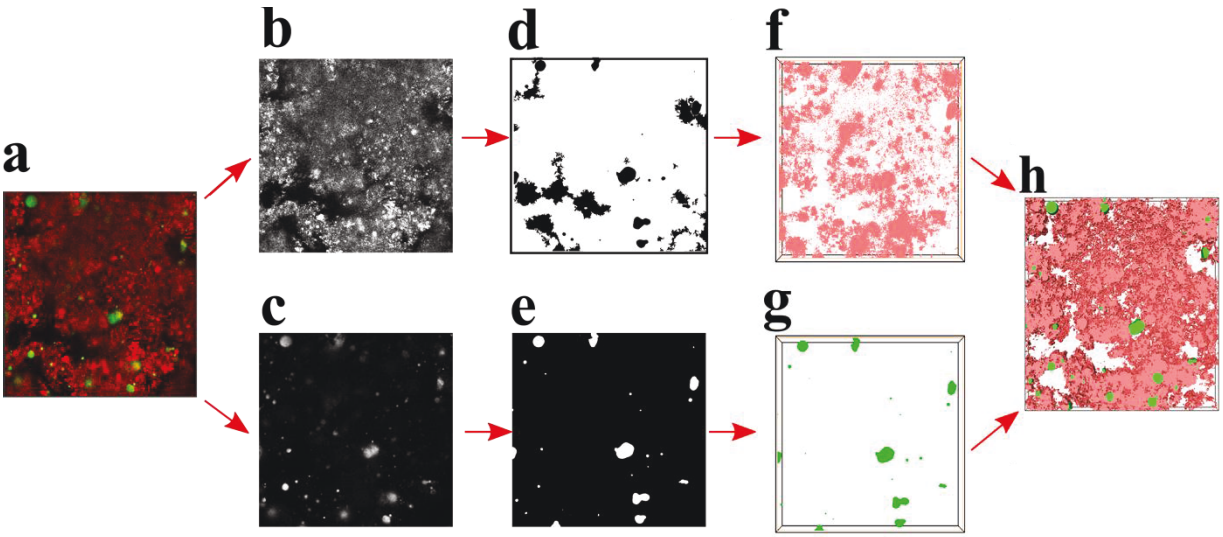

Figure 5-1: Schematic of the Protocol used to obtain the 3D image of the flocculated MFT sediments by confocal laser scanning microscope. a) Raw image of the sediments, b) Raw clay channel, c) Raw bitumen channel, d) Binary image of the clay channel by contrast enhancement, reconstruction and thresholding, e) Binary image of the bitumen channel by contrast enhancement, reconstruction and thresholding, f) Noise reduction, contrast enhancement, smoothening and thresholding of the raw clay channel once again to obtain an actual 3D representation of the flocculated sediments, g) Noise reduction, contrast enhancement, smoothening and thresholding of the raw bitumen channel once again to obtain an actual 3D representation of the flocculated sediments, h) Reconstruction using the stack of images to attain the 3D structure of the flocculated MFT sediments.

5.2.4 Shear Rheology

The rheological measurements were performed using Anton Paar MCR302 stress-controlled rheometer (Anton Paar, Canada). The viscosity curves of the polymer dispersions were determined by increasing the shear rate from 0.1 s^{-1} to 1000 s^{-1} in a ramp logarithmic manner using a parallel plate system (d=50 mm). The effect of aging on the strength of the flocculated MFT sediments was determined by performing stress sweep experiments on days 1, 7, 14, and 120 using a concentric cylinder measuring system. Oscillatory shear sweep experiments were executed by increasing the shear stress from 0.01 Pa to 1000 Pa at a frequency of 1 Hz. All measurements were performed thrice at room temperature to ensure their reproducibility.

5.3 Results and Discussion

5.3.1 Flocculant Characterization

To investigate the polymer dispersion and aggregation behaviour in water, confocal laser scanning microscopy (CLSM) is used. The individual polymer chains are well below the optical resolution limit, but the polymer chain aggregates can serve as a good indicator of how well the flocculant is dispersed in DI water.

Figure 5-2 shows how graft density affects the dispersibility of EPDM-*g*-HPMA and the viscosity of the corresponding EPDM-*g*-HPMA dispersions.

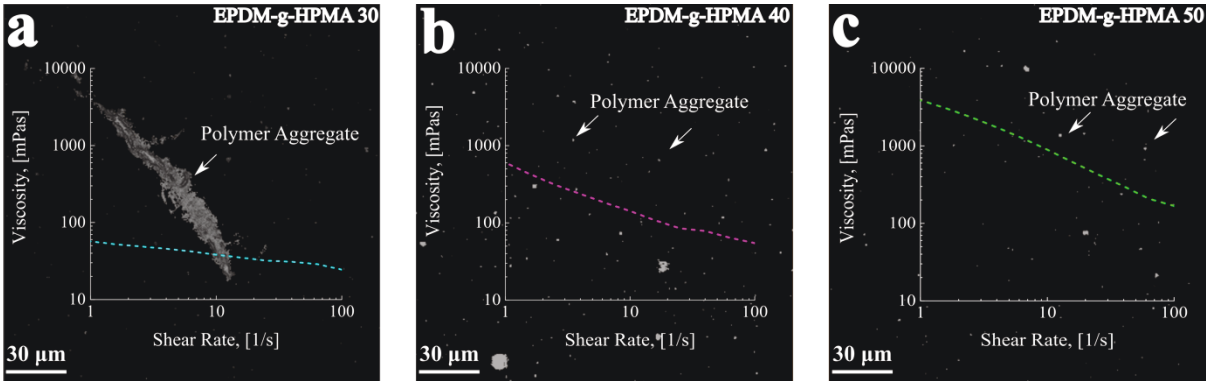

Figure 5-2: Microstructure and viscosity of different EPDM-*g*-HPMA in DI water, obtained by confocal laser scanning microscope and stress-controlled rheometer respectively. a) EPDM-*g*-HPMA 30 (Avg. size = ~35.08 μm), b) EPDM-*g*-HPMA 40 (Avg. size = ~10.29 μm), c) EPDM-*g*-HPMA 50 (Avg. size = ~4.79 μm)

These images show that EPDM-*g*-HPMA with higher graft density disperse more easily in water. The least grafted polymer, EPDM-*g*-HPMA 30 (Figure 5-2a) formed aggregates with an average characteristic size of 35.08 μm. This result suggested that 30 % graft density was not sufficient to efficiently disperse the polymer in water, which was also confirmed by the low viscosity of the EPDM-*g*-HPMA 30 dispersion. By increasing the graft density, the number and size of aggregates decreased (Figure 5-2b and Figure 5-2c), and the viscosity of the dispersions increased.

5.3.2 Characterization of the Polymer-Treated MFT

The flocculant must disperse well to bridge the suspended clay particles effectively. The solids content in the flocculated sediment varied from 18.89 wt% to 20.57 wt% by increasing the graft density of EPDM-*g*-HPMA. The solids contents of the sediments are in agreement with the confocal microscopy results, which indicate EPDM-*g*-HPMA with higher grafts density dispersed better, and consequently produced sediments with higher solids contents.

Changes in the 3D structure of the sediments and structural parameters (volume fraction and fractal dimension) were monitored for 120 days to quantify the efficiency of each flocculant, which is summarized in Figure 5-3.

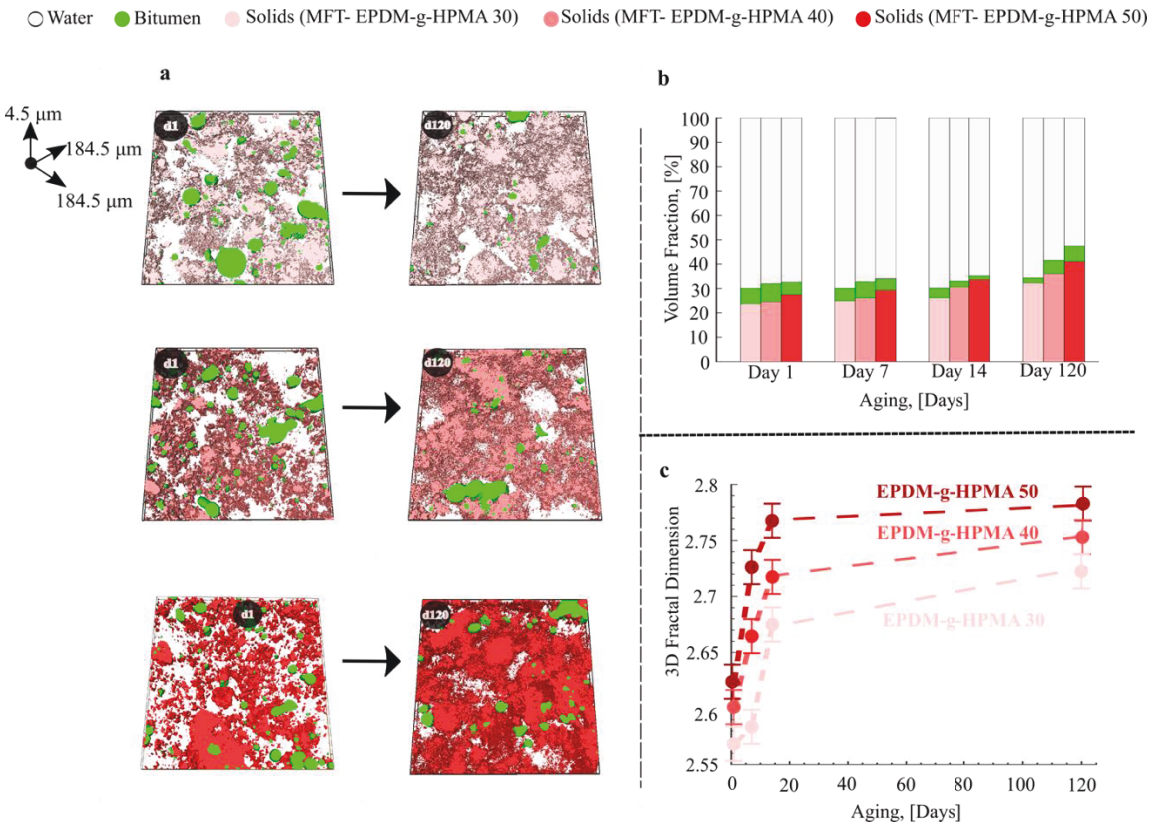

Figure 5-3**:** Microstructure of flocculated MFT treated with 2000 ppm of flocculant after 1 day and 120 days obtained from confocal laser scanning microscope. a) 3D structures of sediments (red: solids, white: water, and green: bitumen), b) volume fraction evolution, c) 3D fractal dimension evolution.

As shown in Figure 5-3a, wide water channels were formed between the flocs in all sediments immediately after flocculation. These channels narrowed as the solids compacted to different

extents for 120 days. During aging, the volume fraction of the solids in the sediments increased, while the volume fraction of water (in the channels between the flocs) decreased. The amounts of volume fractions for solids, bitumen and water is estimated from 3D images. For all samples, at least three aliquots were imaged and the averages of estimated values are reported in Figure 5-3b. Sediments flocculated with EPDM-*g*-HPMA with higher graft densities produced sediments with higher solid volume fractions at all times. While the volume fractions of clay and water follow clear trends, the volume fraction of bitumen does not. This behaviour is not unexpected because bitumen is heterogeneously distributed throughout the sediments, and the depth and size of the acquired images were not large enough to capture the actual trend of bitumen compaction.

Finally, the compaction of the sediments during aging changed their fractal dimensions (Figure 5-3c) according to two regimes: a fast linear increase over the first 14 days (high sediment compaction rate), followed by a second, slower compaction rate until the end of the aging period. Since consolidation takes place during the second regime, the slopes of the curves in this regime indicates the difference in the compaction rate of sediments based on the polymer grafting density. Figure 5-3c shows that EPDM-*g*-HPMA 30 had the steepest slope in the second regime and therefore, the highest compaction rate during the consolidation period. The least grafted EPDM-*g*-HPMA 30 has the highest hydrophobicity among the three polymers and its functionality becomes evident over a long term settling rather than the rapid initial results, thus justifying the steepest curve and its consolidation.

This phenomenon was further investigated by comparing the volume fractions estimated from the 3D image data and measured by Dean-Stark analysis (Figure 5-4). The weight fractions of water, bitumen and solids from Dean-Stark analysis were converted to volume fractions assuming the density values shown in Figure 5-4b. Depending on the variation of the solids packing in the sediment, we will have slight variation of density for each measurement. Averages of 3 different density measurements were calculated for each of the samples to arrive at a density value that is homogeneous to the entire bed of solid layers. The mass, volume and composition of the solids, bitumen and water in the MFT samples flocculated and aged for 120 days were determined by the Dean Stark experiment, which is calculated and tabulated in Table 5-1. For all the 3 polymer flocculated and aged MFT samples, the obtained range of solids volume fraction by Dean Stark analysis, followed a trend similar to the solids volume fraction obtained by confocal laser scanning

microscope; where the MFT sample flocculated with highest grafting density polymer has the highest solids content.

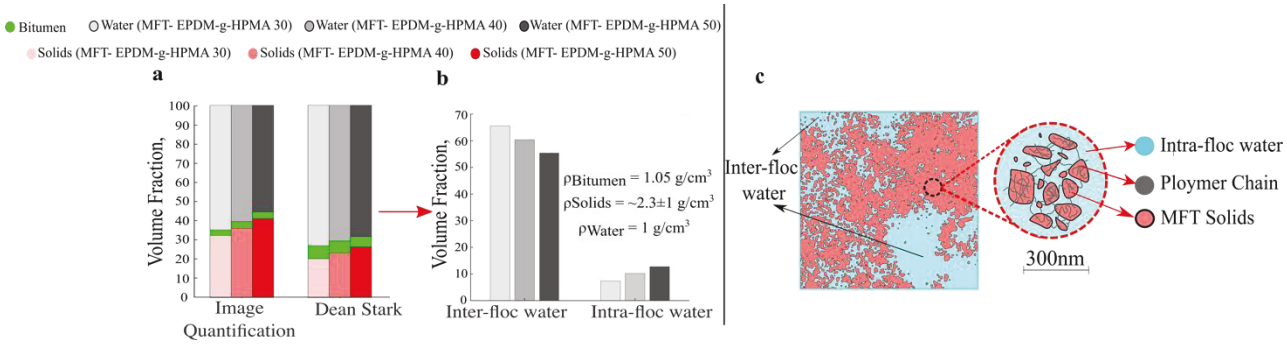

Figure 5-4: Volume fraction of solids, bitumen and water in sediments flocculated with different EPDM-*g*-HPMA after 120 days. a) Volume fractions estimated from the 3D image data and measured by Dean-Stark analysis. b) Volume fraction of *inter-floc* and *intra-floc* water calculated based on 3D image quantification results and Dean-Stark analysis. c) Schematic of typical polymer-flocculated MFT sediments showing intra-floc water, which is outside the resolution of confocal microscopy.

Figure 5-4a shows that similar compaction trends were captured by 3D image quantification and Dean-Stark analysis, but the fractions of solids estimated from the image data were higher. This difference comes from the resolution limitation of laser scanning confocal microscopy (LSCM) to detect water channels in the flocs. The resolution limit in LSCM is ~300 nm, thus the water channels in the flocs (*intra-floc* water) that were below the resolution limit would appear as clay in the reflectance channel. Figure 5-4c is a schematic of the 2D confocal image and a zoomed-in detail of the floc region, showing the unresolvable *intra-floc* water and polymer chains in the floc. As seen from the LSCM images in Figure 5-3, most of the water that we observe in the images are in channels between the flocs (*inter-floc* water). By assuming that all the water detected with LSCM was *inter-floc* water, the volume fraction of *inter-floc* water was estimated directly from the 3D images. The *intra-floc* water was calculated as the difference between the water volume fraction obtained by Dean Stark analysis and the 3D image data. Figure 5-4b compares the volume fractions of *inter-floc water* and *intra-floc water* for the sediments. These data are also tabulated in Table 5-1.

Table 5-1: The mass balance of the solids, bitumen and water in the MFT samples flocculated and aged for 120 days obtained from confocal imaging and Dean Stark, along with the volume fraction calculation based on the average densities for solids, water and bitumen.

	Confocal imaging data		Dean Stark data				
EPDM-*g*-HPMA 30		Vol %	ρ (g/cm^3)	Mass (g)	wt%	Vol (cm^3)	Vol%
	Solids	32.33	2.3	12.50	36.78	5.43	20.26
	Water	65.58	1	19.57	57.61	19.57	72.98
	Bitumen	2.09	1.05	1.91	5.61	1.82	6.77
	Total	100		33.98	100	26.82	100
	Intra-floc water		72.98 – 65.58 = 7.40 %				
EPDM-*g*-HPMA 40		Vol %	ρ (g/cm^3)	Mass (g)	wt%	Vol (cm^3)	Vol%
	Solids	36.03	2.3	23.04	40.11	10.01	23.13
	Water	60.39	1	30.56	53.21	30.56	70.59
	Bitumen	3.58	1.05	2.85	4.97	2.71	6.28
	Total	100		57.43	100	43.30	100
	Intra-floc water		70.59 – 60.39 = 10.20 %				
EPDM-*g*-HPMA 50		Vol %	ρ (g/cm^3)	Mass (g)	wt%	Vol (cm^3)	Vol%
	Solids	41.18	2.3	9.56	44.76	4.16	26.49
	Water	55.47	1	10.71	50.12	10.71	68.22
	Bitumen	3.35	1.05	0.87	4.08	0.83	5.28
	Total	100		21.37	100	15.70	100
	Intra-floc water		68.22 – 55.47 = 12.75 %				

This analysis allowed us to gain additional insights on how well the different flocculants performed. Figure 5-4b shows that the volume fraction of *intra-floc* water, which is harder to eliminate in the long term, is the highest for EPDM-*g*-HPMA 50 after 120 days of aging. This polymer contains the highest density of hydrophilic grafts, therefore the resulting flocs are expected to hold more water than those produced using polymers with lower graft densities. This result demonstrates the effect of grafting density on the floc water holding capacity, which can significantly influence the consolidation rate.

5.3.3 Rheological Characterization of the Flocculated MFT Sediments

To probe the effect of the graft density of EPDM-*g*-HPMA on the evolution of the flocculated sediments strength, we performed shear sweep experiments on days 1,7,14, and 120.

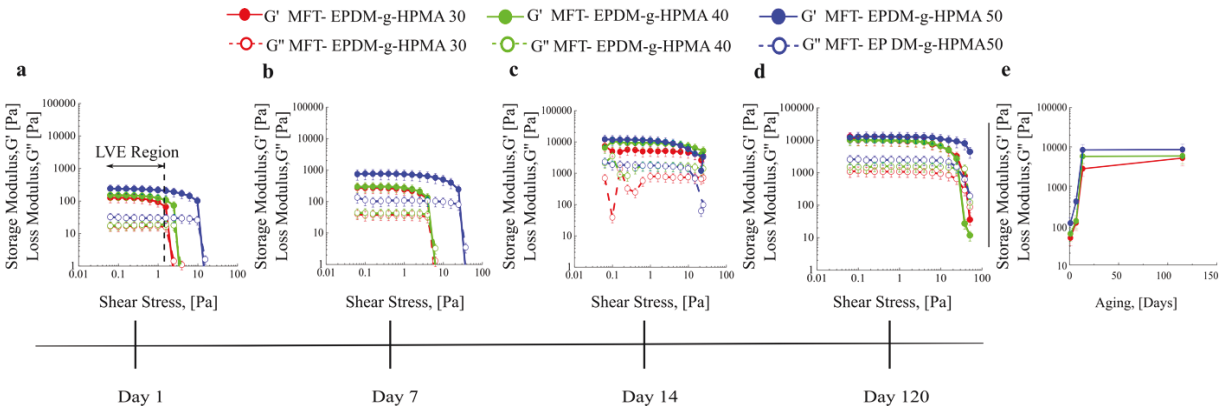

Figure 5-5: Shear sweep results for the flocculated MFT sediments flocculated with different EPDM-*g*-HPMA at 2000 ppm over 120 days. (a), (b), (c), (d) corresponds to stress sweep results from rheology after day 1, day 7, day 14 and day 120 respectively. (e) LVE storage modulus for flocculated MFT sediments at different aging times.

The linear viscoelastic response (LVE) of the sediments flocculated with EPDM-*g*-HPMA 50 is clearly the highest among the three tested samples at the beginning of the aging period. This was expected, due to the highest solids content of sediments flocculated with EPDM-*g*-HPMA 50. However, the difference between the three sediments is statistically insignificant after 120 days. Figure 5-5e shows similar trend as Figure 5-3c; demonstrating that there is a consistency between flocculated network strength and fractal dimension evolution during the aging of sediments. The trends agreed with our findings about the significance of the *intra-floc* water for the long-term dewatering. While the initial solids content in the sediment dictates its initial rheological signature, the evolution of the sediment sludge is governed by its water holding capacity, or more specifically, intra-floc water.

5.4 Conclusion

The results of this study provide microscopic insights into the effect of the graft density of EPDM-*g*-HPMA flocculant on how well it can be dispersed in water, how water is distributed in the flocculated sediments, and consequent dewatering over 120 days after flocculation. In this study, confocal laser scanning microscopy utilizedas to observe the dispersion and aggregation of EPDM-*g*-HPMA in water, along with stress-controlled rheometery to measure the viscosity of the corresponding polymer solutions. Microscopy observations and rheology measurements were in agreement that EPDM-*g*-HPMA with higher graft density disperse more easily in water and aggregate less, which produce solutions with higher viscosity. This better dispersibility of EPDM-*g*-HPMA with higher graft density leads to production of sediments with higher solids contents.

The spatial distribution of water within the flocculated sediments after 120 days of sedimentation were quantified. Volume fractions of water and solids in sediments obtained by the 3D microscope image data and Dean-Stark analysis were compared for this purpose. The *intra-floc* water was calculated as the difference between the water volume fraction obtained by Dean Stark analysis and the 3D image data. The results show that the volume fraction of *intra-floc* water, which is harder to eliminate in the long term, is higher for EPDM-*g*-HPMA with higher graft densities. Polymers with higher graft densities contains more hydrophilic grafts that hold more water as *intra-floc* water. Thus, the graft density governs the flocculation efficiency and long-term consolidation. In other word, the graft density of EPDM-*g*-HPMA controls how effectively the EPDM-*g*-HPMA flocculant repelled water and consequently affects the rate of dewatering and the sediment strength evolution.

References

[1] P.F. Luckham and S. Rossi, "Colloidal and rheological properties of bentonite suspensions", Adv.Colloid Interface Sci., vol. 82, pp. 43-92, 1999.

[2] C.E. Willis, V.L. St. Louis, J.L. Kirk, K.A. St. Pierre and C. Dodge, "Tailings ponds of the Athabasca Oil Sands Region, Alberta, Canada, are likely not significant sources of total mercury and methylmercury to nearby ground and surface waters", Sci.Total Environ., vol. 647, pp. 1604-1610, 2019.

[3] R.J. Mikula, K.L. Kasperski, R.D. Burns and M.D. MacKinnorr, "Nature and fate of oil sands fine tailings", Adv.Chem.Ser., vol. 251, pp. 718-723, 1996.

[4] W.F. Eckert, J.H. Masliyah, M.R. Gray and P.M. Fedorak, "Prediction of Sedimentation and Consolidation of Fine Tails", AIChE J., vol. 42, pp. 960-972, 1996.

[5] M.A. Kessick, "STRUCTURE AND PROPERTIES OF OIL SANDS CLAY TAILINGS", J can Pet Technol 18, pp. 49-52, 1979.

[6] F.L. Motta, R. Gaikwad, L. Botha and J.B.P. Soares, "Quantifying the effect of polyacrylamide dosage, Na+ and Ca2+ concentrations, and clay particle size on the flocculation of mature fine tailings with robust statistical methods", Chemosphere, vol. 208, pp. 263-272, 2018.

[7] Q. Lu, B. Yan, L. Xie, J. Huang, Y. Liu and H. Zeng, "A two-step flocculation process on oil sands tailings treatment using oppositely charged polymer flocculants", Sci.Total Environ., vol. 565, pp. 369-375, 2016.

[8] G.R. Younes, A.R. Proper, T.R. Rooney, R.A. Hutchinson, S.P. Gumfekar and J.B.P. Soares, "Structure Modifications of Hydrolytically-Degradable Polymer Flocculant for Improved Water Recovery from Mature Fine Tailings", Ind Eng Chem Res, vol. 57, pp. 10809-10822, 2018.

[9] J.B.P. Soares and F.L. Motta, "Using polymer reaction engineering principles to help the environment: The case of the Canadian oil sands tailings", J.Braz.Chem.Soc., vol. 30, pp. 826-835, 2019.

[10] H. Shang, J. Liu, Y. Zheng and L. Wang, "Synthesis, characterization, and flocculation properties of poly(acrylamide-methacryloxyethyltrimethyl ammonium chloride-methacryloxypropyltrimethoxy silane)", J Appl Polym Sci, vol. 111, pp. 1594-1599, 2009.

[11] J.H. Masliyah, Z. Xu, J.A. Czarnecki and M. Dabros, Handbook on theory and practice of bitumen recovery from Athabasca Oil Sands, Cochrane, Alberta: Kingsley Knowledge Pub., 2011.

[12] R.P. Singh, S. Pal, S. Krishnamoorthy, P. Adhikary and S.A. Ali, "High-technology materials based on modified polysaccharides", Pure Appl.Chem., vol. 81, pp. 525-547, 2009.

[13] S. Krishnamoorthi and R.P. Singh, "Synthesis, characterization, flocculation, and rheological characteristics of hydrolyzed and unhydrolyzed polyacrylamide-grafted poly(vinyl alcohol)", J Appl Polym Sci, vol. 101, pp. 2109-2122, 2006.

[14] R. Hogg, "Flocculation and dewatering", Int.J.Miner.Process., vol. 58, pp. 223-236, 2000.

[15] P. Mpofu, J. Addai-Mensah and J. Ralston, "Investigation of the effect of polymer structure type on flocculation, rheology and dewatering behaviour of kaolinite dispersions", Int.J.Miner.Process., vol. 71, pp. 247-268, 2003.

[16] S. Soleimani, P. Simms, A. Dunmola, G. Freeman, G.W. Wilson, "Desiccation and Consolidation in Thin-Lift Deposition of Polymer-Amended Mature Fine Tailings", in Proceedings of the 17th International Seminar on Paste and Thickened Tailings, Info Mine Inc., pp. 307−322, 2014.

[17] Z.L. Yang, B.Y. Gao, C.X. Li, Q.Y. Yue and B. Liu, "Synthesis and characterization of hydrophobically associating cationic polyacrylamide", Chem.Eng.J., vol. 161, pp. 27-33, 2010.

[18] D.A.Z. Wever, F. Picchioni and A.A. Broekhuis, "Polymers for enhanced oil recovery: A paradigm for structure-property relationship in aqueous solution", Prog Polym Sci (Oxford), vol. 36, pp. 1558-1628, 2011.

[19] Y. Li and J.C.T. Kwak, "Rheology of hydrophobically modified polyacrylamide-co-poly(acrylic acid) on addition of surfactant and variation of solution pH", Langmuir, vol. 20, pp. 4859-4866, 2004.

[20] H. Li, J. Zhou, R. Chow, A. Adegoroye and A.S. Najafi, "Enhancing treatment and geotechnical stability of oil sands fine tailings using thermo-sensitive poly(n-isopropyl acrylamide)",' Can.J.Chem.Eng., vol. 93, pp. 1780-1786, 2015.

[21] B. Bazoubandi and J.B.P. Soares, "Amylopectin-graft-polyacrylamide for the flocculation and dewatering of oil sands tailings", Minerals Eng, vol. 148, 2020.

[22] J. Li, S. Jiao, L. Zhong, J. Pan and Q. Ma, "Optimizing coagulation and flocculation process for kaolinite suspension with chitosan" Colloids Surf.A Physicochem.Eng.Asp., vol. 428, pp. 100-110, 2013.

[23] H. Zheng, Y. Sun, J. Guo, F. Li, W. Fan, Y. Liao and Q. Guan, "Characterization and evaluation of dewatering properties of PADB, a highly efficient cationic flocculant", Ind Eng Chem Res, vol. 53, pp. 2572-2582, 2014.

[24] M. Isik, A.M. Fernandes, K. Vijayakrishna, M. Paulis and D. Mecerreyes, "Preparation of poly(ionic liquid) nanoparticles and their novel application as flocculants for water purification", Polym.Chem., vol. 7, pp. 1668-1674, 2016.

[25] L.G. Reis, R.S. Oliveira, T.N. Palhares, L.S. Spinelli, E.F. Lucas, D.R.L. Vedoy, E. Asare and J.B.P. Soares, "Using acrylamide/propylene oxide copolymers to dewater and densify mature fine tailings", Minerals Eng, vol. 95, pp. 29-39, 2016.

[26] Y. Liao, H. Zheng, L. Qian, Y. Sun, L. Dai and W. Xue, "UV-initiated polymerization of hydrophobically associating cationic polyacrylamide modified by a surface-active monomer: A comparative study of synthesis, characterization, and sludge dewatering performance", Ind Eng Chem Res, vol. 53, pp. 11193-11203, 2014.

[27] H. Zheng, Y. Sun, C. Zhu, J. Guo, C. Zhao, Y. Liao and Q. Guan, "UV-initiated polymerization of hydrophobically associating cationic flocculants: Synthesis, characterization, and dewatering properties", Chem.Eng.J., vol. 234, pp. 318-326, 2013.

[28] Y. Deng, H. Xiao and R. Pelton, "Temperature-sensitive flocculants based on poly (N-isopropylacrylamide-co-diallyldimethylammonium chloride)", J.Colloid Interface Sci., vol. 179, pp. 188-193, 1996.

[29] J.P. O'Shea, G.G. Qiao and G.V. Franks, "Temperature responsive flocculation and solid-liquid separations with charged random copolymers of poly(N-isopropyl acrylamide)", J.Colloid Interface Sci., vol. 360, pp. 61-70, 2011.

[30] J. Pinaud, E. Kowal, M. Cunningham and P. Jessop, "2-(diethyl)aminoethyl methacrylate as a CO2-switchable comonomer for the preparation of readily coagulated and redispersed polymer latexes", ACS Macro Lett., vol. 1, pp. 1103-1107, 2012.

[31] S.P. Gumfekar, T.R. Rooney, R.A. Hutchinson and J.B.P. Soares, "Dewatering Oil Sands Tailings with Degradable Polymer Flocculants", ACS Appl.Mater.Interfaces, vol. 9, pp. 36290-36300, 2017.

[32] L. Botha, S. Davey, B. Nguyen, A.K. Swarnakar, E. Rivard and J.B.P. Soares, "Flocculation of oil sands tailings by hyperbranched functionalized polyethylenes (HBfPE)", Minerals Eng, vol. 108, pp. 71-82, 2017.

[33] A.D. Costine, V. Vajihinejad, L. Botha, P.D. Fawell and J.B.P. Soares, "Aggregate structures formed by hyperbranched functionalized polyethylene (HBfPE) treatment of oil sands tailings", Can.J.Chem.Eng., vol. 97, pp. 99-102, 2019.

[34] T.R. Rooney, S.P. Gumfekar, J.B.P. Soares and R.A. Hutchinson, "Cationic Hydrolytically Degradable Flocculants with Enhanced Water Recovery for Oil Sands Tailings Remediation", Macromol.Mater.Eng., vol. 301, pp. 1248-1254, 2016.

[35] R. Cong and R. Pelton, "The influence of PEO/poly(vinyl phenol-co-styrene sulfonate) aqueous complex structure on flocculation", J.Colloid Interface Sci., vol. 261, pp. 65-73, 2003.

[36] Z. Rostami Najafabadi and J.B.P. Soares, "Ethylene/Propylene/Diene (EPDM) Chains Grafted with Poly(methyl acrylate) by Reverse Atom Transfer Radical Polymerization", Macromol. Chem. Phys, vol. 222, article no. 2100189, 2021.

[37] Z. Rostami Najafabadi and J.B.P. Soares, "Flocculation and dewatering of oil sands tailings with a novel functionalized polyolefin flocculant", Separation and Purification Technology, vol. 274, pp. 119018, 2021.

[38] E.S. Kazak and A.V. Kazak, "A novel laboratory method for reliable water content determination of shale reservoir rocks", J Pet Sci Eng, vol. 183, 2019.

[39] E.W. Dean and D.D. Stark, "A convenient method for the determination of water in petroleum and other organic emulsions", Ind.Eng.Chem., vol. 12, pp. 486-490, 1920.

[40] E.J. Semler, J.S. Tjia and P.V. Moghe, "Analysis of surface microtopography of biodegradable polymer matrices using confocal reflection microscopy", Biotechnol.Prog., vol. 13, pp. 630-634, 1997.

[41] A. Govedarica, E.J. Molina Bacca and M. Trifkovic, "Structural investigation of tailings flocculation and consolidation via quantitative 3D dual fluorescence/reflectance confocal microscopy", J.Colloid Interface Sci., vol. 571, pp. 194-204, 2020.

[42] S.S. Shende, S. Pendharker, Z. Jacob and N. Nazemifard, "Total Internal Reflection Fluorescence Microscopy to Investigate the Distribution of Residual Bitumen in Oil Sands Tailings", Energy Fuels, vol. 30, pp. 5537-5546, 2016.

[43] V.A. Muñoz, K.L. Kasperski, O.E. Omotoso and R.J. Mikula, "The use of microscopic bitumen froth morphology for the identification of problem oil sand ores", Petrol Sci Technol, vol. 21, pp. 1509-1529, 2003.

[44] S. Bearsley, A. Forbes and R.G. Haverkamp, "Direct observation of the asphaltene structure in paving-grade bitumen using confocal laser-scanning microscopy", J.Microsc., vol. 215, pp. 149-155, 2004.

[45] R.J. Mikula and V.A. Munoz, "Characterization of emulsions and suspensions in the petroleum industry using cryo-SEM and CLSM", Colloids Surf.A Physicochem.Eng.Asp., vol. 174, pp. 23-36, 2000.

Chapter 6

6 Conclusion and Future Work

6.1 Conclusion

The main objective of this thesis was to synthesize novel hybrid flocculants by reverse ATRP combining a hydrophobic ethylene/propylene/diene copolymer backbone and hydrolyzed poly(methyl acrylate) grafts (EPDM-*g*-HPMA) and to quantify how the microstructure of the EPDM-*g*-HPMA affects its flocculation and dewatering performance of oil sands MFT.

To accomplish this objective, first, graft copolymers of poly(methyl acrylate) and EPDM, EPDM-*g*-PMAs, were synthesized by grafting PMA side chains onto EPDM backbones with various graft molecular weights and densities via reverse ATRP. The graft molecular weight and density were controlled by varying methyl acrylate concentration and conversion, and the ratio of initiator to EPDM backbone. Graft densities and molecular weights of the EPDM-*g*-PMA samples were estimated theoretically using ATRP kinetics and by ^{1}H NMR and GPC. Measurements and estimates for these properties agreed well, confirming that the EPDM-*g*-PMA samples were synthesised successfully with controllable graft lengths and densities.

In the next step, acrylate functional groups in EPDM-*g*-PMA were converted by base hydrolysis to acrylic acids to enable polymer dispersion in water. Then, a series of hydrolyzed poly(methyl acrylate) grafted onto ethylene-propylene-diene copolymer backbones (EPDM-*g*-HPMA) were used as flocculant to treat oil sands mature fine tailings. The impact of graft molecular weights (M_g) and graft densities (ρ_g) of a series of EPDM-*g*-HPMA polymers on the flocculation and dewatering of MFT were investigated through a systematic statistical approach. The results showed that the initial settling rate (ISR) for 5 wt. % MFT was lower for EPDM-*g*-HPMAs with higher M_g and low ρ_g. Flocculants with high M_g and low ρ_g performed even better for 10 and 20

wt. % MFT due to the fast formation of larger flocs that settled quickly. Based on the CST measurements, a balance between M_g and ρ_g of the EPDM-*g*-HPMAs is required for fast dewatering of the sediments. The turbidity was significantly decreased by increasing M_g and decreasing ρ_g for MFT samples of all concentrations. Sediments solids content measurements show that the highest solids content were achieved using EPDM-*g*-HPMAs with high M_g and low ρ_g.

Based on these results, high molecular weight poly(methyl acrylate) side chains with low graft density were added to two different EPDM backbones with different weight average molecular weights of 115 and 210 kDa to find out the effect of backbone length on the flocculation and dewatering of MFT in comparison with a reference HPAM. Initial settling rate, CST, turbidity, and solids content results for these two series of EPDM-*g*-HPMA showed that their flocculation properties depended significantly on their backbone lengths. Flocculants with shorter EPDM backbones seemed to disperse more effectively in water and, consequently, improve the settling rate of the suspended clay particles, decrease supernatant turbidity, and increase the solids content of sediments. On the other hand, the longer hydrophobic EPDM backbones expelled water from the flocs faster and generated more compact mudlines.

Although EPDM-*g*-HPMAs with lower M_b = 115 kDa enhanced the settling rate of the clay particles, but it is still lower than HPAM. The CST results show that both series of EPDM-*g*-HPMAs with high M_g (180 kDa) dewatered MFT faster than HPAM. Both series also produced supernatants with lower turbidity than HPAM, which shows the capability of these flocculants in capturing more fine particles.

Finally, we assessed the effect of the graft density of EPDM-*g*-HPMA flocculant on how well it can be dispersed in water, how water is distributed in the flocculated sediments, and consequent dewatering over 120 days after flocculation. The confocal laser scanning microscopy was used to observe the dispersion and aggregation of EPDM-*g*-HPMA in water, along with stress-controlled rheometery to measure the viscosity of the corresponding polymer solutions. Microscopy observations and rheology measurements showed that EPDM-*g*-HPMA with higher graft density disperse more easily in water and aggregate less, which produced solutions with higher viscosity. This better dispersity of EPDM-*g*-HPMA with higher graft density leads to production of sediments with higher solids contents.

In addition, the spatial distribution of water within the flocculated sediments after 120 days of sedimentation were quantified. Volume fractions of water and solids in sediments obtained by the 3D microscope image data and Dean-Stark analysis were compared for this purpose. The *intra-floc* water was calculated as the difference between the water volume fraction obtained by Dean Stark analysis and the 3D image data. The results show that the volume fraction of *intra-floc* water, which is harder to eliminate in the long term, is higher for EPDM-*g*-HPMA with higher graft densities. Polymers with higher graft densities contains more hydrophilic grafts that hold more water as *intra-floc* water. Thus the graft density governs the flocculation efficiency and long-term consolidation. In other word, the graft density of EPDM-*g*-HPMA controls how effectively the EPDM-*g*-HPMA flocculant repelled water and consequently affects the rate of dewatering and the sediment strength evolution.

Understanding and quantifying these dependencies is the starting point for the optimal design of these polymers not only for the treatment of the oil sands tailings, but also the treatment of other mineral and metal tailings.

6.2 Future Work

The findings of this thesis gave rise to several areas that need further investigation:

1. Different series of EPDM-*g*-HPMA flocculants were synthesized and used to flocculate diluted and undiluted MFT. The initial settling rate, turbidity, and sediments solids content measurements show that lower ISR and turbidity, and the highest solids content were achieved using EPDM-*g*-HPMAs with high M_g and low ρ_g. According to the surface responses plots in the current study, the optimal polymer flocculant could be achieved by synthesizing the EPDM-*g*-HPMA flocculants with grafts molecular weight higher than 179 kDa and low graft density (~15 %). It would be interesting to continue this optimal trend by increasing the grafts molecular weight while keeping the graft density constant, and investigate the flocculation behavior of these polymers. The challenge, however, would remain in obtaining side chains with high molecular weights (in the range of millions) with narrow distributions, because the typical molecular weight range achieved in this study by ATRP is maximum of a few 100,000 Da. It is necessary to investigate the potential of other

controlled polymerization methods to gain the desirable EPDM-*g*-HPMA having high M_g with narrow distribution and low ρ_g.

2. There are plenty of valuable investigations on polymer-induced flocculation and dewatering of MFT, which some of them was mentioned in the literature review of this study. In this research path, polymers properties was varied and their effect on a constant tailings composition was evaluated; consequently, applicability of different polymers in tailings treatment would be achieved. This is the pathway of our study in the first and second phase of the current research. However, the fundamental interactions between polymer and tailing components that are responsible in the flocculation process remain unclear. Thus, there is an absence for a systematic study on the adsorption behavior and interaction forces between polymer flocculants and the solid particles in MFT. Even though the general mechanisms of flocculation due to polymer-clay interactions for pure clay systems are studied, the properties of clays in oil sands tailings would be significantly altered due to the surface chemistry adjustments of clays in contact with organic material, which concludes to a wider range of polymer-clay interactions. In this regard, investigating the interaction forces between polymer and MFT components with Atomic Force Microscope (AFM) and Surface Force Apparatus (SFA) would be a good start to obtain some knowledge of polymer-clay interactions in oil sands MFT.

3. The microstructure of polymer flocculants and the resulted flocs are also rarely characterized in detail. Understanding the effects of polymer microstructure on bridging and trapping fine particles is important. This knowledge helps researchers to tailor polymers to be more effective in settling fine particles. In the current study, confocal scanning laser microscope provided an introduction to the microstructure of flocs and the spatial distribution of water between and in the flocs. This visual and analytical observation was a great assistance to realize the long-term dewatering behavior of sediments. This path needs to be continued with other microscopy techniques including cryo-SEM and TEM to provide better insight of the polymer structure and the resulted flocs.

Bibliography

A. Alamgir, D. Harbottle, J. Masliyah and Z. Xu, "Al-PAM assisted filtration system for abatement of mature fine tailings", Chem.Eng.Sci., vol. 80, pp. 91-99, 2012.

A. Govedarica, E.J. Molina Bacca and M. Trifkovic, "Structural investigation of tailings flocculation and consolidation via quantitative 3D dual fluorescence/reflectance confocal microscopy", J.Colloid Interface Sci., vol. 571, pp. 194-204, 2020.

A. Pourmohammadbagher and J.M. Shaw, "Probing the Role of Water Chemistry on the Behavior of Clays in Process and Natural Environments Using Solution Calorimetry", Energy Fuels, vol. 30, pp. 5964-5969, 2016.

A. Sworska, J.S. Laskowski and G. Cymerman, "Flocculation of the Syncrude fine tailings Part I. Effect of pH, polymer dosage and Mg2+ and Ca2+ cations", Int.J.Miner.Process., vol. 60, pp. 143-152, 2000.

A.D. Costine, V. Vajihinejad, L. Botha, P.D. Fawell and J.B.P. Soares, "Aggregate structures formed by hyperbranched functionalized polyethylene (HBfPE) treatment of oil sands tailings", Can.J.Chem.Eng., vol. 97, pp. 99-102, 2019.

A.M. Kasko, A.M. Heintz and C. Pugh, "The effect of molecular architecture on the thermotropic behavior of poly[11-(4′-cyanophenyl-4′-phenoxy)undecyl acrylate] and its relation to polydispersity", Macromolecules, vol. 31, pp. 256-271, 1998.

Alberta Energy Regulator, "State of Fluid Tailings Management for Mineable Oil Sands", Alberta Energy Regulator, 2019.

Anonymous "Government, Alberta Energy (2014), Oil sands Alberta, http://www.energy.alberta.ca/oilsands/791.asp".

B. Bazoubandi and J.B.P. Soares, "Amylopectin-graft-polyacrylamide for the flocculation and dewatering of oil sands tailings", Minerals Eng, vol. 148, 2020.

C. Wang, C. Han, Z. Lin, J. Masliyah, Q. Liu and Z. Xu, "Role of Preconditioning Cationic Zetag Flocculant in Enhancing Mature Fine Tailings Flocculation", Energy Fuels, vol. 30, pp. 5223-5231, 2016.

C.E. Willis, V.L. St. Louis, J.L. Kirk, K.A. St. Pierre and C. Dodge, "Tailings ponds of the Athabasca Oil Sands Region, Alberta, Canada, are likely not significant sources of total mercury and methylmercury to nearby ground and surface waters", Sci.Total Environ., vol. 647, pp. 1604-1610, 2019.

C.S. Popeney, D.H. Camacho and Z. Guan, "Efficient incorporation of polar comonomers in copolymerizations with ethylene using a cyclophane-based Pd(II) α-diimine catalyst", J.Am.Chem.Soc., vol. 129, pp. 10062-10063, 2007.

D. Zhang, T. Thundat and R. Narain, "Flocculation and dewatering of mature fine tailings using temperature-responsive cationic polymers", Langmuir, vol. 33, pp. 5900-5909, 2017.

D.A.Z. Wever, F. Picchioni and A.A. Broekhuis, "Polymers for enhanced oil recovery: A paradigm for structure-property relationship in aqueous solution", Prog Polym Sci (Oxford), vol. 36, pp. 1558-1628, 2011.

D.J. Haloi, K. Naskar and N.K. Singha, "Poly(meth)acrylate grafted EPDM via reverse atom transfer radical polymerization: A single pot process", Eur Polym J, vol. 49, pp. 4098-4107, 2013.

D.M. Clementz, "Interaction of petroleum heavy ends with montmorillonite", Clays Clay Miner., vol. 24, pp. 312-319, 1976.

D.M. Moore and R.C. Reynolds, X-ray diffraction and the identification and analysis of clay minerals, Oxford University Press, 1997.

D.R.L. Vedoy and J.B.P. Soares, "Water-soluble polymers for oil sands tailing treatment: A Review", Can.J.Chem.Eng., vol. 93, pp. 888-904, 2015.

E.J. Semler, J.S. Tjia and P.V. Moghe, "Analysis of surface microtopography of biodegradable polymer matrices using confocal reflection microscopy", Biotechnol.Prog., vol. 13, pp. 630-634, 1997.

E.S. Kazak and A.V. Kazak, "A novel laboratory method for reliable water content determination of shale reservoir rocks", J Pet Sci Eng, vol. 183, 2019.

E.W. Dean and D.D. Stark, "A convenient method for the determination of water in petroleum and other organic emulsions", Ind.Eng.Chem., vol. 12, pp. 486-490, 1920.

F. Bergaya, B.K.G. Theng and G. Lagaly, Handbook of clay science. [electronic resource], Elsevier, 2006.

F.L. Motta, R. Gaikwad, L. Botha and J.B.P. Soares, "Quantifying the effect of polyacrylamide dosage, Na+ and Ca2+ concentrations, and clay particle size on the flocculation of mature fine tailings with robust statistical methods", Chemosphere, vol. 208, pp. 263-272, 2018.

G. Chen, X.S. Ma and Z. Guan, "Synthesis of functional olefin copolymers with controllable topologies using a chain-walking catalyst", J.Am.Chem.Soc., vol. 125, pp. 6697-6704, 2003.

G. Coullerez, A. Carlmark, E. Malmström and M. Jonsson, "Understanding copper-based atom-transfer radical polymerization in aqueous media", J Phys Chem A, vol. 108, pp. 7129-7131, 2004.

G. Lligadas, J.S. Ladislaw, T. Guliashvili and V. Percec, "Functionally terminated poly(methyl acrylate) by SET-LRP initiated with CHBr3 and CHI3", J.Polym.Sci.Part A, vol. 46, pp. 278-288, 2008.

G.R. Younes, A.R. Proper, T.R. Rooney, R.A. Hutchinson, S.P. Gumfekar and J.B.P. Soares, "Structure Modifications of Hydrolytically-Degradable Polymer Flocculant for Improved Water Recovery from Mature Fine Tailings", Ind Eng Chem Res, vol. 57, pp. 10809-10822, 2018.

H. Kaneko, J. Saito, N. Kawahara, S. Matsuo, T. Matsugi and N. Kashiwa, "Polypropylene-graft-poly(methyl methacrylate) Graft Copolymers: Synthesis and Compatibilization of Polypropylene/Polylactide in Controlled/Living Radical Polymerization: Progress in ATRP", American Chemical Society, 2009, pp. 357-371.

H. Li, J. Long, Z. Xu and J.H. Masliyah, "Novel polymer aids for low-grade oil sand ore processing", Can.J.Chem.Eng., vol. 86, pp. 168-176, 2008.

H. Li, J. Long, Z. Xu and J.H. Masliyah, "Synergetic role of polymer flocculant in low-temperature bitumen extraction and tailings treatment", Energy Fuels, vol. 19, pp. 936-943, 2005.

H. Li, J. Zhou, R. Chow, A. Adegoroye and A.S. Najafi, "Enhancing treatment and geotechnical stability of oil sands fine tailings using thermo-sensitive poly(n-isopropyl acrylamide)", Can.J.Chem.Eng., vol. 93, pp. 1780-1786, 2015.

H. Lu, L. Xiang, X. Cui, J. Liu, Y. Wang, R. Narain and H. Zeng, "Molecular Weight Dependence of Synthetic Glycopolymers on Flocculation and Dewatering of Fine Particles", Langmuir, vol. 32, pp. 11615-11622, 2016.

H. Lu, Y. Wang, L. Li, Y. Kotsuchibashi, R. Narain and H. Zeng, "Temperature- and pH-Responsive Benzoboroxole-Based Polymers for Flocculation and Enhanced Dewatering of Fine Particle Suspensions", ACS Appl.Mater.Interfaces, vol. 7, pp. 27176-27187, 2015.

H. Shang, J. Liu, Y. Zheng and L. Wang, "Synthesis, characterization, and flocculation properties of poly(acrylamide-methacryloxyethyltrimethyl ammonium chloride-methacryloxypropyltrimethoxy silane)", J Appl Polym Sci, vol. 111, pp. 1594-1599, 2009.

H. Zheng, Y. Sun, C. Zhu, J. Guo, C. Zhao, Y. Liao and Q. Guan, "UV-initiated polymerization of hydrophobically associating cationic flocculants: Synthesis, characterization, and dewatering properties", Chem.Eng.J., vol. 234, pp. 318-326, 2013.

H. Zheng, Y. Sun, J. Guo, F. Li, W. Fan, Y. Liao and Q. Guan, "Characterization and evaluation of dewatering properties of PADB, a highly efficient cationic flocculant", Ind.Eng.Chem.Res., vol. 53, pp. 2572-2582, 2014.

H.A.W. Kaminsky, T.H. Etsell, D.G. Ivey and O. Omotoso, "Distribution of clay minerals in the process streams produced by the extraction of bitumen from athabasca oil sands", Can.J.Chem.Eng., vol. 87, pp. 85-93, 2009.

J. Li, S. Jiao, L. Zhong, J. Pan and Q. Ma, "Optimizing coagulation and flocculation process for kaolinite suspension with chitosan", Colloids Surf.A Physicochem.Eng.Asp., vol. 428, pp. 100-110, 2013.

J. Long, H. Li, Z. Xu and J.H. Masliyah, "Improving oil sands processability using a temperature-sensitive polymer", Energy Fuels, vol. 25, pp. 701-707, 2011.

J. Long, H. Li, Z. Xu and J.H. Masliyah, "Role of colloidal interactions in oil sand tailings treatment", AIChE J., vol. 52, pp. 371-383, 2006.

J. Masliyah, Z. Zhou, Z. Xu, J. Czarnecki and H. Hamza, "Understanding water-based bitumen extraction from athabasca oil sands", Can.J.Chem.Eng., vol. 82, pp. 628-654, 2004.

J. Neter, W. Wasserman and M.H. Kutner, Applied linear statistical models : regression, analysis of variance, and experimental designs. Published in Homewood, IL by Irwin, 1990; pp. 1181; ISBN:025608338X.

J. Pinaud, E. Kowal, M. Cunningham and P. Jessop, "2-(diethyl)aminoethyl methacrylate as a CO2-switchable comonomer for the preparation of readily coagulated and redispersed polymer latexes", ACS Macro Lett., vol. 1, pp. 1103-1107, 2012.

J. Xia and K. Matyjaszewski, "Controlled/living radical polymerization. Homogeneous reverse atom transfer radical polymerization using AIBN as the initiator", Macromolecules, vol. 30, pp. 7692-7696, 1997.

J.P. O'Shea, G.G. Qiao and G.V. Franks, "Temperature responsive flocculation and solid-liquid separations with charged random copolymers of poly(N-isopropyl acrylamide)", J.Colloid Interface Sci., vol. 360, pp. 61-70, 2011.

J.R. Riba Ruiz, T. Canals and R. Cantero, "Supervision of Ethylene Propylene Diene M-Class (EPDM) Rubber Vulcanization and Recovery Processes Using Attenuated Total Reflection Fourier Transform Infrared (ATR FT-IR) Spectroscopy and Multivariate Analysis", Appl.Spectrosc., vol. 71, pp. 141-151, 2017.

J.S. Wang and K. Matyjaszewski, "Controlled/living radical polymerization. Atom transfer radical polymerization in the presence of transition-metal complexes", J.Am.Chem.Soc., vol. 117, pp. 5614-5615, 1995.

J.B.P. Soares and F.L. Motta, "Using polymer reaction engineering principles to help the environment: The case of the Canadian oil sands tailings", J.Braz.Chem.Soc., vol. 30, pp. 826-835, 2019.

J.H. Masliyah, Z. Xu, J.A. Czarnecki and M. Dabros, Handbook on theory and practice of bitumen recovery from Athabasca Oil Sands, Cochrane, Alberta: Kingsley Knowledge Pub., 2013.

J.H. Masliyah, Z. Xu, J.A. Czarnecki and M. Dabros, Handbook on theory and practice of bitumen recovery from Athabasca Oil Sands. Published in Cochrane, Alberta by Kingsley Knowledge Pub., 2013; ISBN:9781926832036.

J.H. Masliyah, Z. Xu, J.A. Czarnecki and M. Dabros, Handbook on theory and practice of bitumen recovery from Athabasca Oil Sands, Cochrane, Alberta: Kingsley Knowledge Pub., 2011.

J.K. Haken and R.L. Werner, "Infrared spectrum of polymethyl acrylate", Brit.Poly.J., vol. 3, pp. 263-265, 1971.

K. Matyjaszewski and J. Xia, "Atom transfer radical polymerization", Chem.Rev., vol. 101, pp. 2921-2990, 2001.

K. Matyjaszewski and N.V. Tsarevsky, "Nanostructured functional materials prepared by atom transfer radical polymerization", Nat.Chem., vol. 1, pp. 276-288, 2009.

K. Matyjaszewski, "Atom transfer radical polymerization: From mechanisms to applications", Isr.J.Chem., vol. 52, pp. 206-220, 2012.

K. Matyjaszewski, T. Pintauer and S. Gaynor, "Removal of copper-based catalyst in atom transfer radical polymerization using ion exchange resins", Macromolecules, vol. 33, pp. 1476-1478, 2000.

K. Ute, R. Niimi, K. Hatada and A.C. Kolbertb, "Characterization of Ethylene—Propylene—Diene Terpolymers (EPDM) by 750 MHz On-line SEC-NMR", vol. 5, pp. 47-59, 1999.

K. Yamamoto, H. Tanaka, M. Sakaguchi and S. Shimada, "Well-defined poly(methyl methacrylate) grafted to polyethylene with reverse atom transfer radical polymerization initiated by peroxides", Polymer, vol. 44, pp. 7661-7669, 2003.

K.A. Davis and K. Matyjaszewski, Statistical, gradient block and graft copolymers by controlledliving radical polymerizations. Published in Berlin ;New York by Springer, 2002; pp. 191; ISBN:3540432442.

K.C. Lister, H. Kaminsky and R.A. Hutchinson, "Evaluation of a novel polymeric flocculant for enhanced water recovery of mature fine tailings", Process., vol. 8, pp. 1-14, 2020.

K.L. Kasperski and R.J. Mikula, "Waste streams of mined oil sands: Characteristics and remediation", Elements, vol. 7, pp. 387-392, 2011.

K.L. Konan, C. Peyratout, J.P. Bonnet, A. Smith, A. Jacquet, P. Magnoux and P. Ayrault, "Surface properties of kaolin and illite suspensions in concentrated calcium hydroxide medium", J.Colloid Interface Sci., vol. 307, pp. 101-108, 2007.

L. Besra, D.K. Sengupta, B.P. Singh and S. Bhattacharjee, "A novel method based on Capillary Suction Time (CST) for assessment of dispersion characteristics of suspensions", J Am Ceram Soc, vol. 88, pp. 109-113, 2005.

L. Botha and J.B.P. Soares, "The Influence of Tailings Composition on Flocculation", Can.J.Chem.Eng., vol. 93, pp. 1514-1523, 2015.

L. Botha, D. Vedoy and J. Soares, "Novel hyperbranched functionalized polyethylenes for the treatment of oil sands tailings", in 19th International Seminar on Paste and Thickened Tailings, 2016.

L. Botha, S. Davey, B. Nguyen, A.K. Swarnakar, E. Rivard and J.B.P. Soares, "Flocculation of oil sands tailings by hyperbranched functionalized polyethylenes (HBfPE)", Minerals Eng, vol. 108, pp. 71-82, 2017.

L. Botha, S. Davey, B. Nguyen, A.K. Swarnakar, E. Rivard and J.B.P. Soares, "Flocculation of oil sands tailings by hyperbranched functionalized polyethylenes (HBfPE)", Minerals Eng, vol. 108, pp. 71-82, 2017.

L. Gross, T.L. Joly and C. Westman, Extracting home in the oil sands : settler colonialism and environmental change in subarctic Canada. Published in Milton by Routledge, 2020; ISBN:1351127438.

L. Pennetta De Oliveira, S.P. Gumfekar, F. Lopes Motta and J.B.P. Soares, "Dewatering of Oil Sands Tailings with Novel Chitosan-Based Flocculants", Energy Fuels, vol. 32, pp. 5271-5278, 2018.

L.G. Reis, R.S. Oliveira, T.N. Palhares, L.S. Spinelli, E.F. Lucas, D.R.L. Vedoy, E. Asare and J.B.P. Soares, "Using acrylamide/propylene oxide copolymers to dewater and densify mature fine tailings", Minerals Eng, vol. 95, pp. 29-39, 2016.

L.K. Johnson, S. Mecking and M. Brookhart, "Copolymerization of ethylene and propylene with functionalized vinyl monomers by palladium(II) catalysts", J.Am.Chem.Soc., vol. 118, pp. 267-268, 1996.

M. Hollósi, Z.M. Shen, A. Perczel and G.D. Fasman, "Stable intrachain and interchain complexes of neurofilament peptides: A putative link between Al3+ and Alzheimer disease", Proc.Natl.Acad.Sci.U.S.A., vol. 91, pp. 4902-4906, 1994.

M. Isik, A.M. Fernandes, K. Vijayakrishna, M. Paulis and D. Mecerreyes, "Preparation of poly(ionic liquid) nanoparticles and their novel application as flocculants for water purification", Polym.Chem., vol. 7, pp. 1668-1674, 2016.

M. Kamigaito, T. Ando and M. Sawamoto, "Metal-catalyzed living radical polymerization", Chem.Rev., vol. 101, pp. 3689-3745, 2001.

M. Kato, M. Kamigaito, M. Sawamoto and T. Higashimura, "Polymerization of methyl methacrylate with the carbon tetrachloride/dichlorotris-(triphenylphosphine)ruthenium(II) /methylaluminum bis(2,6-di-tert-butylphenoxide) initiating system: possibility of living radical polymerization", Macromolecules, vol. 28, pp. 1721-1723, 1995.

M. Scholz, "Review of recent trends in Capillary Suction Time (CST) dewaterability testing research", Ind Eng Chem Res, vol. 44, pp. 8157-8163, 2005.

M.A. Kessick, "STRUCTURE AND PROPERTIES OF OIL SANDS CLAY TAILINGS.", J can Pet Technol 18, pp. 49-52, 1979.

O.E. Omotoso and R.J. Mikula, "High surface areas caused by smectitic interstratification of kaolinite and illite in Athabasca oil sands", Appl.Clay.Sci., vol. 25, pp. 37-47, 2004.

P. Mpofu, J. Addai-Mensah and J. Ralston, "Investigation of the effect of polymer structure type on flocculation, rheology and dewatering behaviour of kaolinite dispersions", Int.J.Miner.Process., vol. 71, pp. 247-268, 2003.

P.F. Luckham and S. Rossi, "Colloidal and rheological properties of bentonite suspensions", Adv.Colloid Interface Sci., vol. 82, pp. 43-92, 1999.

Q. Lu, B. Yan, L. Xie, J. Huang, Y. Liu and H. Zeng, "A two-step flocculation process on oil sands tailings treatment using oppositely charged polymer flocculants", Sci.Total Environ., vol. 565, pp. 369-375, 2016.

R. Cong and R. Pelton, "The influence of PEO/poly(vinyl phenol-co-styrene sulfonate) aqueous complex structure on flocculation", J.Colloid Interface Sci., vol. 261, pp. 65-73, 2003.

R. Hogg, "Flocculation and dewatering", Int.J.Miner.Process., vol. 58, pp. 223-236, 2000.

R. Ma, Z. Song, Y. Hou, Y. Liu, B. Xing, Z. Tan and F. Bao, "Synthesis of norbornene and methyl methacrylate graft copolymers with high norbornene content by using mixed catalytic system", J Macromol Sci Part A Pure Appl Chem, vol. 46, pp. 193-201, 2009.

R.J. Mikula and V.A. Munoz, "Characterization of emulsions and suspensions in the petroleum industry using cryo-SEM and CLSM", Colloids Surf.A Physicochem.Eng.Asp., vol. 174, pp. 23-36, 2000.

R.J. Mikula, K.L. Kasperski, R.D. Burns and M.D. MacKinnorr, "Nature and fate of oil sands fine tailings", Adv.Chem.Ser., vol. 251, pp. 718-723, 1996.

R.P. Singh, S. Pal, S. Krishnamoorthy, P. Adhikary and S.A. Ali, "High-technology materials based on modified polysaccharides", Pure Appl.Chem., vol. 81, pp. 525-547, 2009.

S. Bearsley, A. Forbes and R.G. Haverkamp, "Direct observation of the asphaltene structure in paving-grade bitumen using confocal laser-scanning microscopy", J.Microsc., vol. 215, pp. 149-155, 2004.

S. Krishnamoorthi and R.P. Singh, "Synthesis, characterization, flocculation, and rheological characteristics of hydrolyzed and unhydrolyzed polyacrylamide-grafted poly(vinyl alcohol)", J Appl Polym Sci, vol. 101, pp. 2109-2122, 2006.

S. Mecking, "Mechanistic studies of the palladium-catalyzed copolymerization of ethylene and a-olefins with methyl acrylate", J.Am.Chem.Soc., vol. 120, pp. 888-899, 1998.

S. Soleimani, P. Simms, A. Dunmola, G. Freeman, G.W. Wilson, "Desiccation and Consolidation in Thin-Lift Deposition of Polymer-Amended Mature Fine Tailings", in Proceedings of the 17th International Seminar on Paste and Thickened Tailings, Info Mine Inc., pp. 307−322, 2014.

S. Wang, L. Alagha and Z. Xu, "Adsorption of organic–inorganic hybrid polymers on kaolin from aqueous solutions", Colloids Surf.Physicochem.Eng.Aspects, vol. 453, pp. 13-20, 2014.

S. Wang, L. Zhang, B. Yan, H. Xu, Q. Liu and H. Zeng, "Molecular and surface interactions between polymer flocculant chitosan g polyacrylamide and kaolinite particles: Impact of salinity", J.Phys.Chem.C, vol. 119, pp. 7327-7339, 2015.

S.P. Gumfekar, T.R. Rooney, R.A. Hutchinson and J.B.P. Soares, "Dewatering Oil Sands Tailings with Degradable Polymer Flocculants", ACS Appl.Mater.Interfaces, vol. 9, pp. 36290-36300, 2017.

S.S. Shende, S. Pendharker, Z. Jacob and N. Nazemifard, "Total Internal Reflection Fluorescence Microscopy to Investigate the Distribution of Residual Bitumen in Oil Sands Tailings", Energy Fuels, vol. 30, pp. 5537-5546, 2016.

T.C. Chung, "Synthesis of functional polyolefin copolymers with graft and block structures", Prog.Polym.Sci. (Oxford), vol. 27, pp. 39-85, 2002.

T.C. Chung, Functionalization of polyolefins. Published in San Diego by Academic Press, 2002; ISBN:9780080477930.

T.C. Chung, W. Janvikul, R. Bernard and G.J. Jiang, "Synthesis of ethylene-propylene rubber graft copolymers by borane approach", Macromolecules, vol. 27, pp. 26-31, 1994.

T.C. Chung, W. Janvikul, R. Bernard, R. Hu, C.L. Li, S.L. Liu and G.J. Jiang, "Butyl rubber graft copolymers: synthesis and characterization", Polymer, vol. 36, pp. 3565-3574, 1995.

T.R. Rooney, S.P. Gumfekar, J.B.P. Soares and R.A. Hutchinson, "Cationic Hydrolytically Degradable Flocculants with Enhanced Water Recovery for Oil Sands Tailings Remediation", Macromol.Mater.Eng., vol. 301, pp. 1248-1254, 2016.

V. Coessens, T. Pintauer and K. Matyjaszewski, "Functional polymers by atom transfer radical polymerization", Progress in Polymer Science, vol. 26, pp. 337-377, 2001.

V. Theodorou, K. Skobridis, A.G. Tzakos and V. Ragoussis, "A simple method for the alkaline hydrolysis of esters", Tetrahedron Lett., vol. 48, pp. 8230-8233, 2007.

V.A. Muñoz, K.L. Kasperski, O.E. Omotoso and R.J. Mikula, "The use of microscopic bitumen froth morphology for the identification of problem oil sand ores", Petrol Sci Technol, vol. 21, pp. 1509-1529, 2003.

V.M.C. Coessens and K. Matyjaszewski, "Fundamentals of atom transfer radical polymerization", J.Chem.Educ., vol. 87, pp. 916-919, 2010.

W. Tang and K. Matyjaszewski, "Kinetic Modeling of Normal ATRP, Normal ATRP with [CuII]0, Reverse ATRP and SR&NI ATRP", Macromol.Theory Simul., vol. 17, pp. 359-375, 2008.

W.F. Eckert, J.H. Masliyah, M.R. Gray and P.M. Fedorak, "Prediction of Sedimentation and Consolidation of Fine Tails", AIChE J., vol. 42, pp. 960-972, 1996.

W.J. Wang, L. Pingwei, B.G. Li and Z. Shiping, "One-step synthesis of hyperbranched polyethylene macroinitiator and its block copolymers with methyl methacrylate or styrene via ATRP", J.Polym.Sci.Part A, vol. 48, pp. 3024-3032, 2010.

X.S. Wang, N. Luo and S.K. Ying, "Synthesis of EPDM-g-PMMA through atom transfer radical polymerization", Polymer, vol. 40, pp. 4515-4520, 1999.

X.W. Wang, X. Feng, Z. Xu and J.H. Masliyah, "Polymer aids for settling and filtration of oil sands tailings", Can.J.Chem.Eng., vol. 88, pp. 403-410, 2010.

Y. Deng, H. Xiao and R. Pelton, "Temperature-sensitive flocculants based on poly (N-isopropylacrylamide-co-diallyldimethylammonium chloride)", J.Colloid Interface Sci., vol. 179, pp. 188-193, 1996.

Y. Inoue, T. Matsugi, N. Kashiwa and K. Matyjaszewski, "Graft copolymers from linear polyethylene via atom transfer radical polymerization", Macromolecules, vol. 37, pp. 3651-3658, 2004.

Y. Liao, H. Zheng, L. Qian, Y. Sun, L. Dai and W. Xue, "UV-initiated polymerization of hydrophobically associating cationic polyacrylamide modified by a surface-active monomer: A comparative study of synthesis, characterization, and sludge dewatering performance", Ind Eng Chem Res, vol. 53, pp. 11193-11203, 2014.

Y. Wang, Y. Kotsuchibashi, Y. Liu and R. Narain, "Temperature-responsive hyperbranched amine-based polymers for solid-liquid separation", Langmuir, vol. 30, pp. 2360-2368, 2014.

Z. Dong and Z. Ye, "Hyperbranched polyethylenes by chain walking polymerization: Synthesis, properties, functionalization, and applications", Polym.Chem., vol. 3, pp. 286-301, 2012.

Z. Rostami Najafabadi and J.B.P. Soares, "Ethylene/Propylene/Diene Terpolymers Grafted with Poly(methyl acrylate) via Reverse Atom Transfer Radical Polymerization", Macromol. Chem. Phys, vol. 222, article no. 2100189, 2021.

Z. Rostami Najafabadi and J.B.P. Soares, "Flocculation and dewatering of oil sands tailings with a novel functionalized polyolefin flocculant", Separation and Purification Technology, vol. 274, pp. 119018, 2021.

Z. Ye and S. Li, "Hyperbranched polyethylenes and functionalized polymers by chain walking polymerization with PD-diimine catalysis", Macromol.React.Eng., vol. 4, pp. 319-332, 2010.

Z.L. Yang, B.Y. Gao, C.X. Li, Q.Y. Yue and B. Liu, "Synthesis and characterization of hydrophobically associating cationic polyacrylamide", Chem.Eng.J., vol. 161, pp. 27-33, 2010.

Appendix A

1 Supplementary Information for Chapter 4

Table A 1: ANOVA table for CST for 5 wt.% MFT.

Source of Variation	Sum of Squares	Degrees of Freedom	Mean Squares	F	P	Comments
1) M_g (L: linear)	0.2044	1	0.2044	41.9919	0.0029	significant
M_g (Q: quadratic)	0.0063	1	0.0063	1.2861	0.3201	
2) ρ_g (L)	0.0056	1	0.0056	1.1457	0.3447	significant
ρ_g (Q)	0.0104	1	0.0104	2.1415	0.2172	significant
1L by 2L	0.0035	1	0.0035	0.7231	0.4430	
Error	0.0195	4	0.0049			
Total SS	0.2455	9				

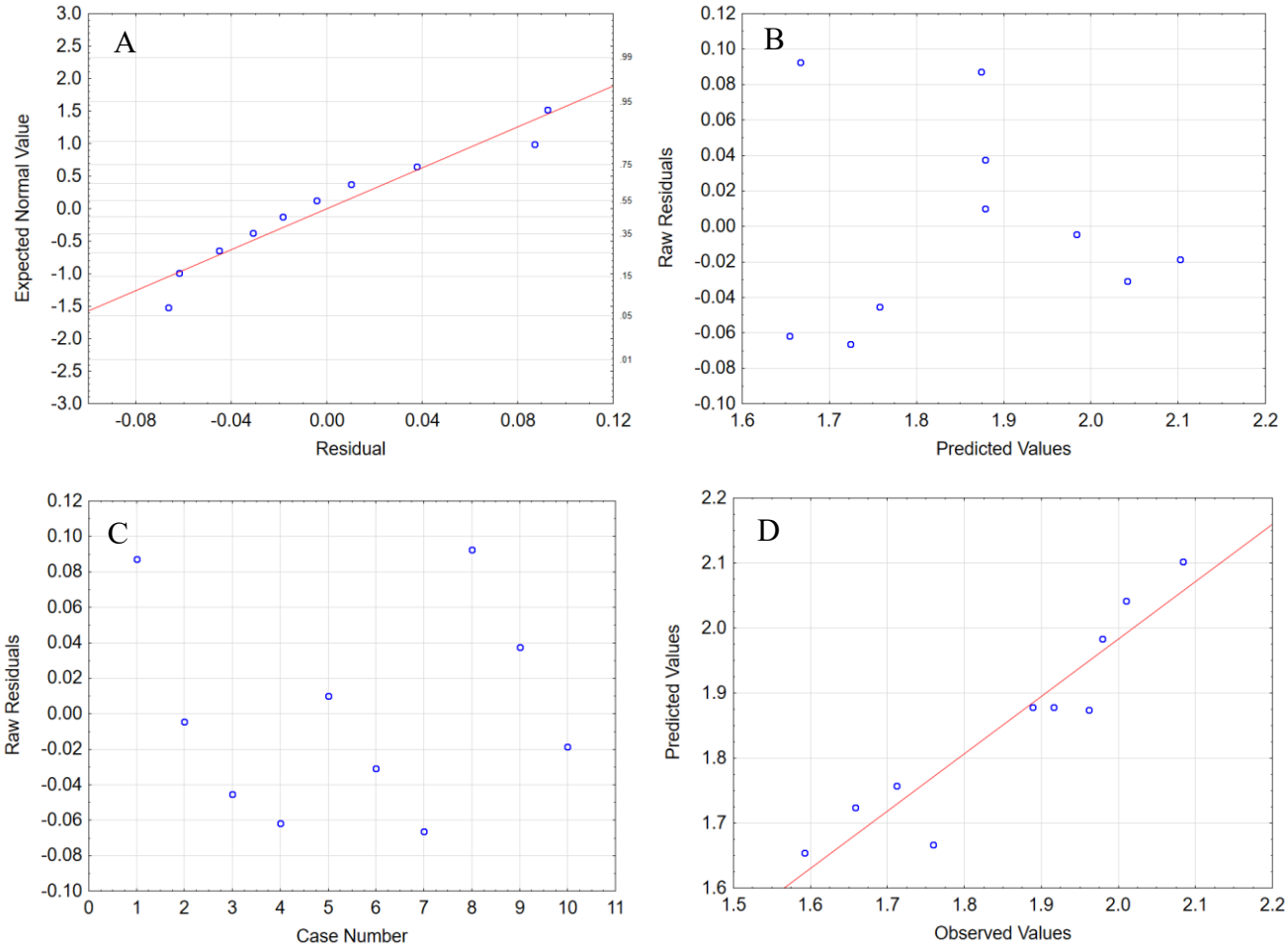

Figure A 1: CST model plots for 5 wt.% MFT: a) normal plot, b) scatterplot of the standardized residuals as a function of the standardized predicted values, c) residuals versus run number, d) predicted versus observed values.

Table A 2: ANOVA table for CST for 10 wt.% MFT.

Source of Variation	Sum of Squares	Degrees of Freedom	Mean Squares	F	P	Comments
1) M_g (L: linear)	0.0702	1	0.0702	38.6223	0.0034	significant
M_g (Q: quadratic)	0.000002	1	0.000002	0.0011	0.9755	
2) ρ_g (L)	0.0045	1	0.0045	2.4855	0.1900	significant
ρ_g (Q)	0.0013	1	0.0013	0.7236	0.4429	significant
1L by 2L	0.0001	1	0.0001	0.0608	0.8174	
Error	0.0073	4	0.0018			
Total SS	0.0857	9				

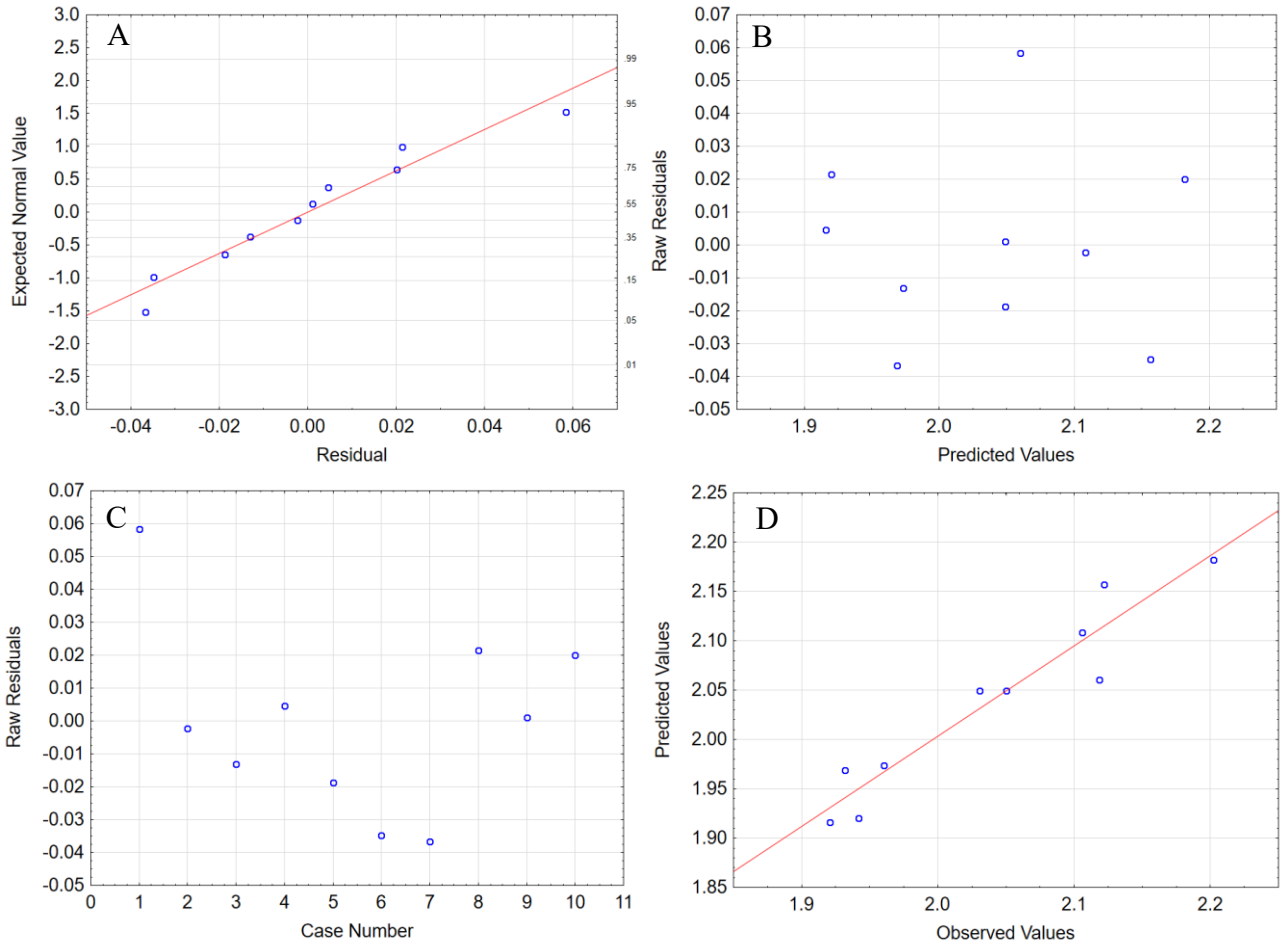

Figure A 2: CST model plots for 10 wt.% MFT: a) normal plot, b) scatterplot of the standardized residuals as a function of the standardized predicted values, c) residuals versus run number, d) predicted versus observed values.

Table A 3: ANOVA table for CST for 20 wt.% MFT.

Source of Variation	Sum of Squares	Degrees of Freedom	Mean Squares	F	P	Comments
1) M_g (L: linear)	0.1461	1	0.1461	286.4833	0.0007	significant
M_g (Q: quadratic)	0.0128	1	0.0128	25.1644	0.0074	
2) ρ_g (L)	0.02235	1	0.02235	43.7984	0.0027	significant
ρ_g (Q)	0.000007	1	0.000007	0.0129	0.9151	significant
1L by 2L	0.0086	1	0.0086	16.8931	0.0147	
Error	0.0020	4	0.0005			
Total SS	0.1902	9				

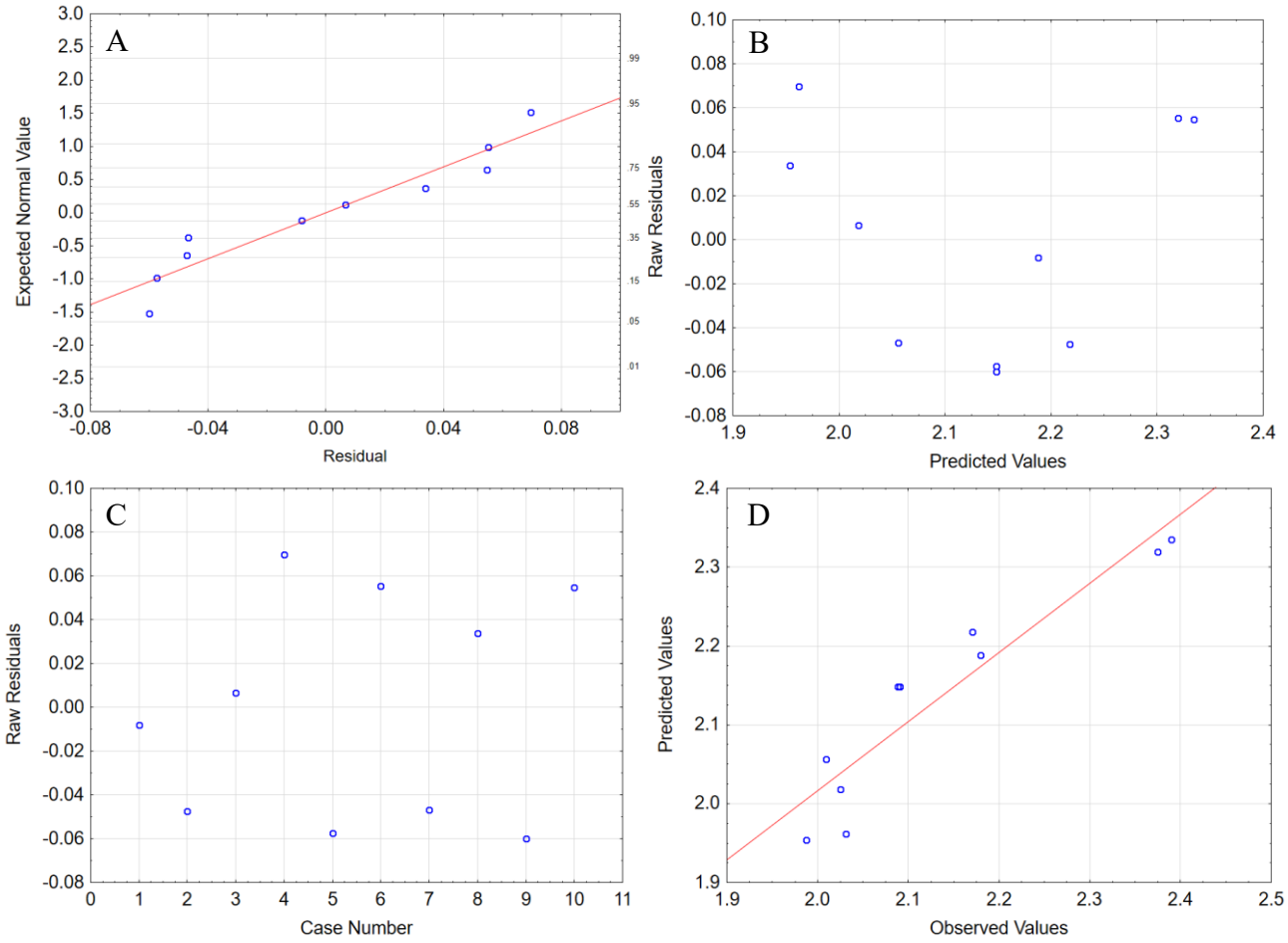

Figure A 3: CST model plots for 20 wt.% MFT: a) normal plot, b) scatterplot of the standardized residuals as a function of the standardized predicted values, c) residuals versus run number, d) predicted versus observed values.

Table A 4: ANOVA table for turbidity for 5 wt.% MFT.

Source of Variation	Sum of Squares	Degrees of Freedom	Mean Squares	F	P	Comments
1) M_g (L: linear)	0.4652	1	0.4652	26.5019	0.0068	significant
M_g (Q: quadratic)	0.0439	1	0.0439	2.5009	0.1889	
2) ρ_g (L)	0.1885	1	0.1885	10.7360	0.0306	significant
ρ_g (Q)	0.0014	1	0.0014	0.0771	0.7950	
1L by 2L	0.0496	1	0.0496	2.8235	0.1682	significant
Error	0.0702	4	0.0176			
Total SS	0.8003	9				

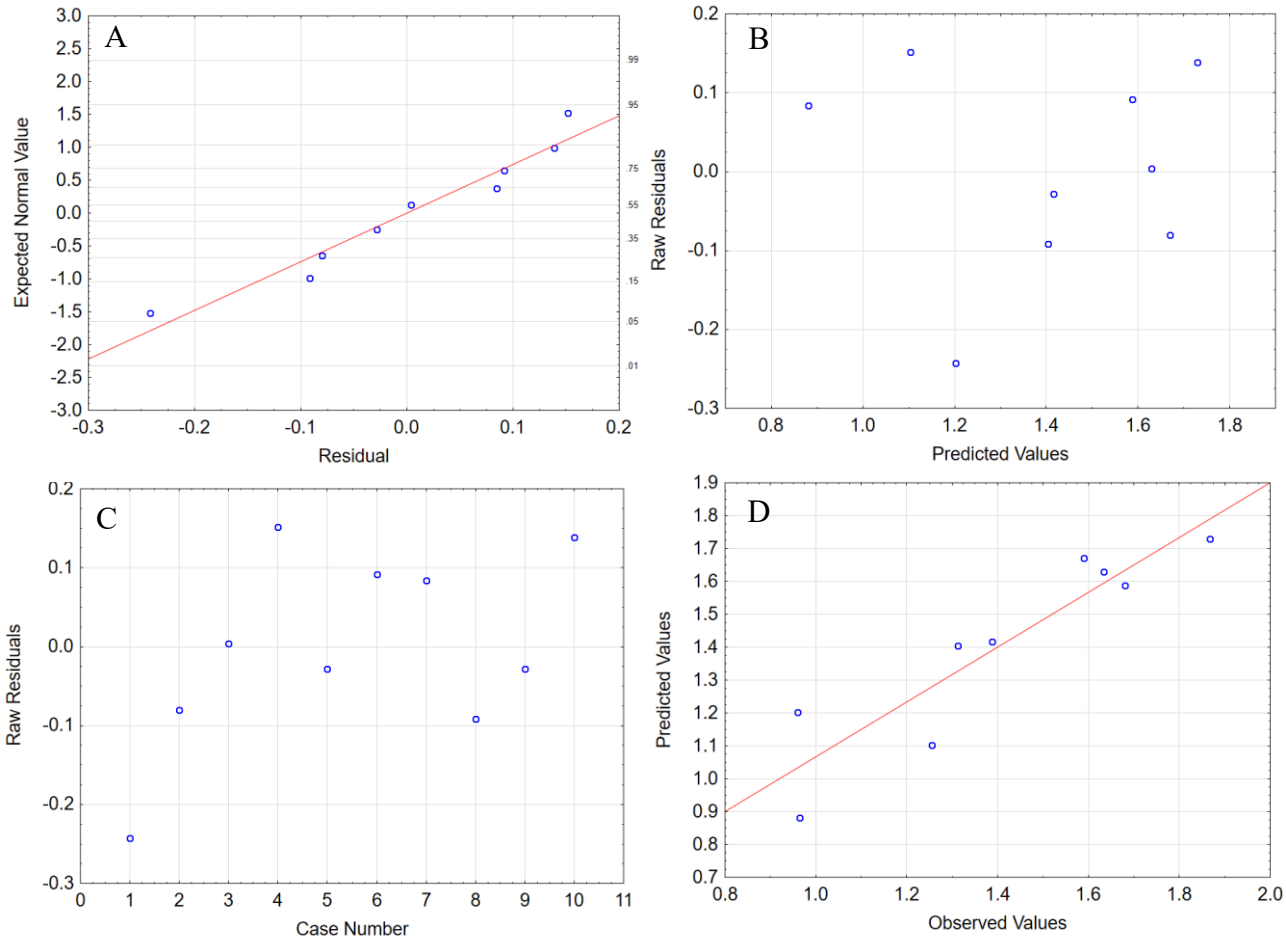

Figure A 4: Turbidity model plots for 5 wt.% MFT: a) normal plot, b) scatterplot of the standardized residuals as a function of the standardized predicted values, c) residuals versus run number, d) predicted versus observed values.

Table A 5: ANOVA table for turbidity for 10 wt.% MFT.

Source of Variation	Sum of Squares	Degrees of Freedom	Mean Squares	F	P	Comments
1) M_g (L: linear)	0.0838	1	0.0838	60.3852	0.0014	significant
M_g (Q: quadratic)	0.0022	1	0.0022	1.5584	0.2800	
2) ρ_g (L)	0.0113	1	0.0113	8.1314	0.0463	significant
ρ_g (Q)	0.00001	1	0.00001	0.0097	0.9264	
1L by 2L	0.0193	1	0.0193	13.9142	0.0203	significant
Error	0.0056	4	0.0014			
Total SS	0.1137	9				

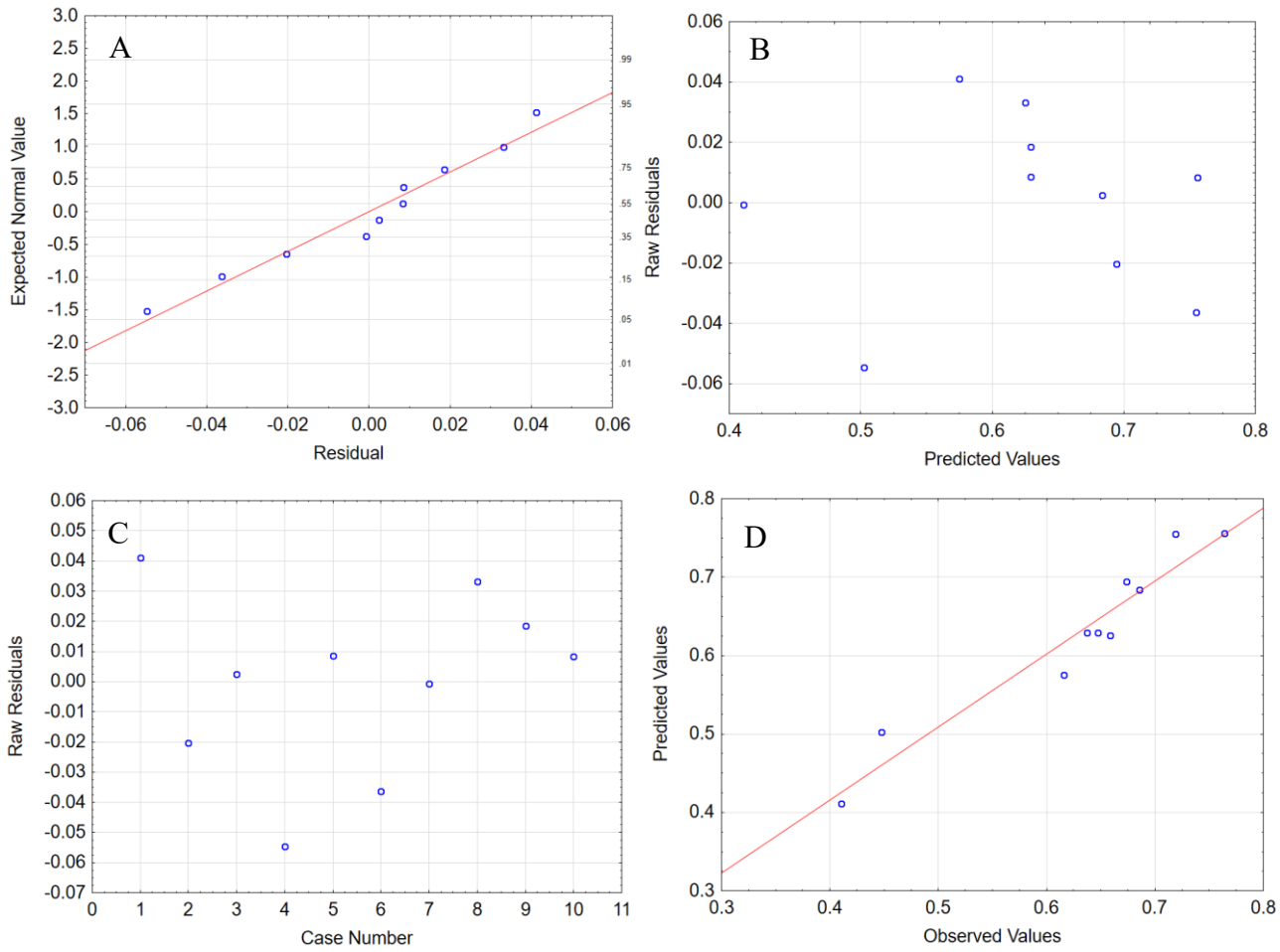

Figure A 5: Turbidity model plots for 10 wt.% MFT: a) normal plot, b) scatterplot of the standardized residuals as a function of the standardized predicted values, c) residuals versus run number, d) predicted versus observed values.

Table A 6: ANOVA table for turbidity for 20 wt.% MFT.

Source of Variation	Sum of Squares	Degrees of Freedom	Mean Squares	F	P	Comments
1) M_g (L: linear)	0.0361	1	0.0361	47.5570	0.0023	significant
M_g (Q: quadratic)	0.0003	1	0.0003	0.3588	0.5814	
2) ρ_g (L)	0.0040	1	0.0040	5.3205	0.0823	significant
ρ_g (Q)	0.0001	1	0.0001	0.1504	0.7179	
1L by 2L	0.0103	1	0.0103	13.5625	0.0212	significant
Error	0.0031	4	0.0008			
Total SS	0.0501	9				

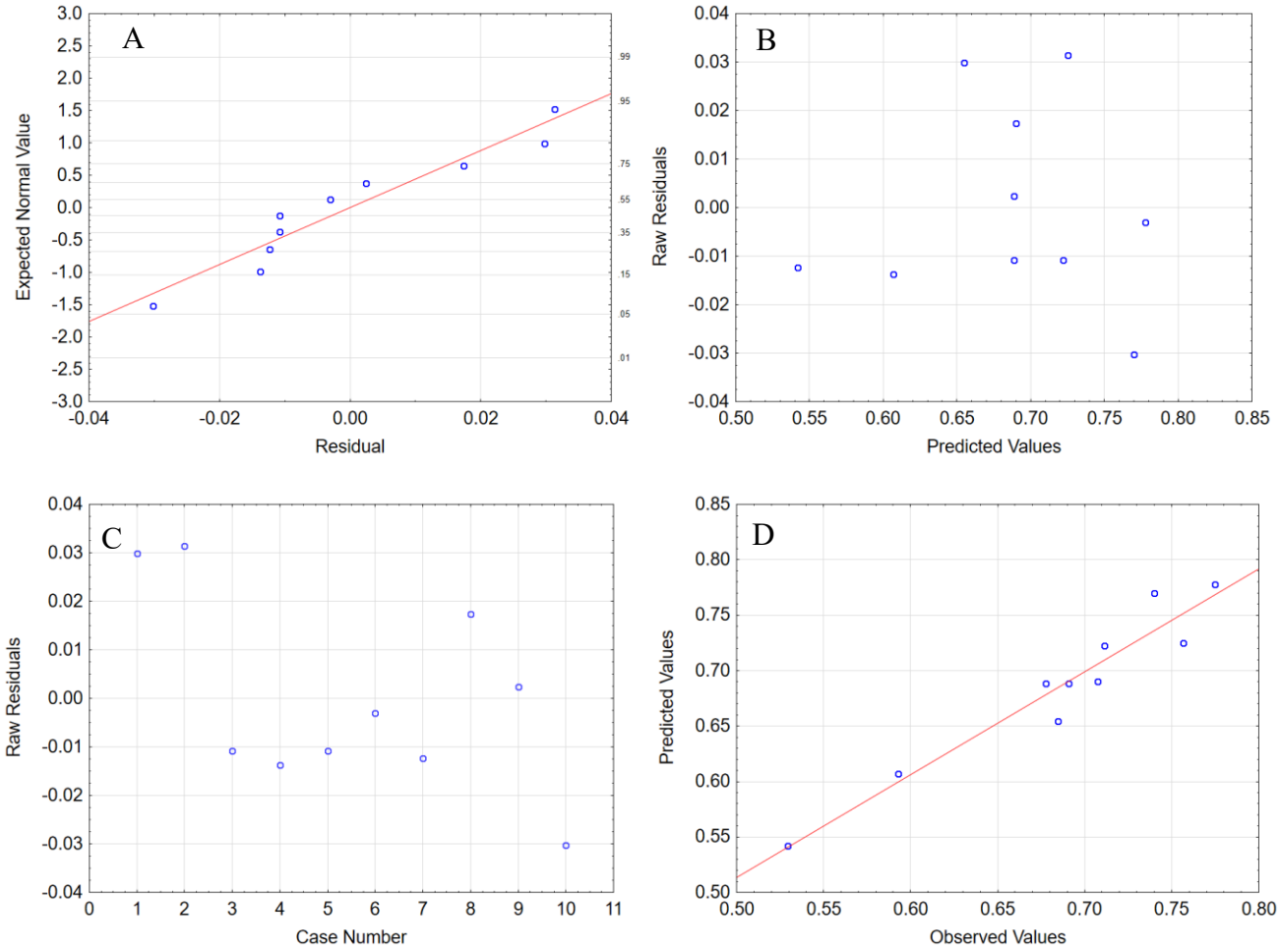

Figure A 6: Turbidity model plots for 20 wt.% MFT: a) normal plot, b) scatterplot of the standardized residuals as a function of the standardized predicted values, c) residuals versus run number, d) predicted versus observed values.

Table A 7: ANOVA table for solid content for 5 wt.% MFT.

Source of Variation	Sum of Squares	Degrees of Freedom	Mean Squares	F	P	Comments
1) M_g (L: linear)	46.1684	1	46.1684	47.1053	0.0024	significant
M_g (Q: quadratic)	5.2824	1	5.2824	5.3896	0.0810	significant
2) ρ_g (L)	11.7178	1	11.7178	11.9556	0.0259	significant
ρ_g (Q)	0.6547	1	0.6547	0.6679	0.4597	
1L by 2L	5.6796	1	5.6796	5.7948	0.0738	significant
Error	3.9204	4	0.9801			
Total SS	70.7242	9				

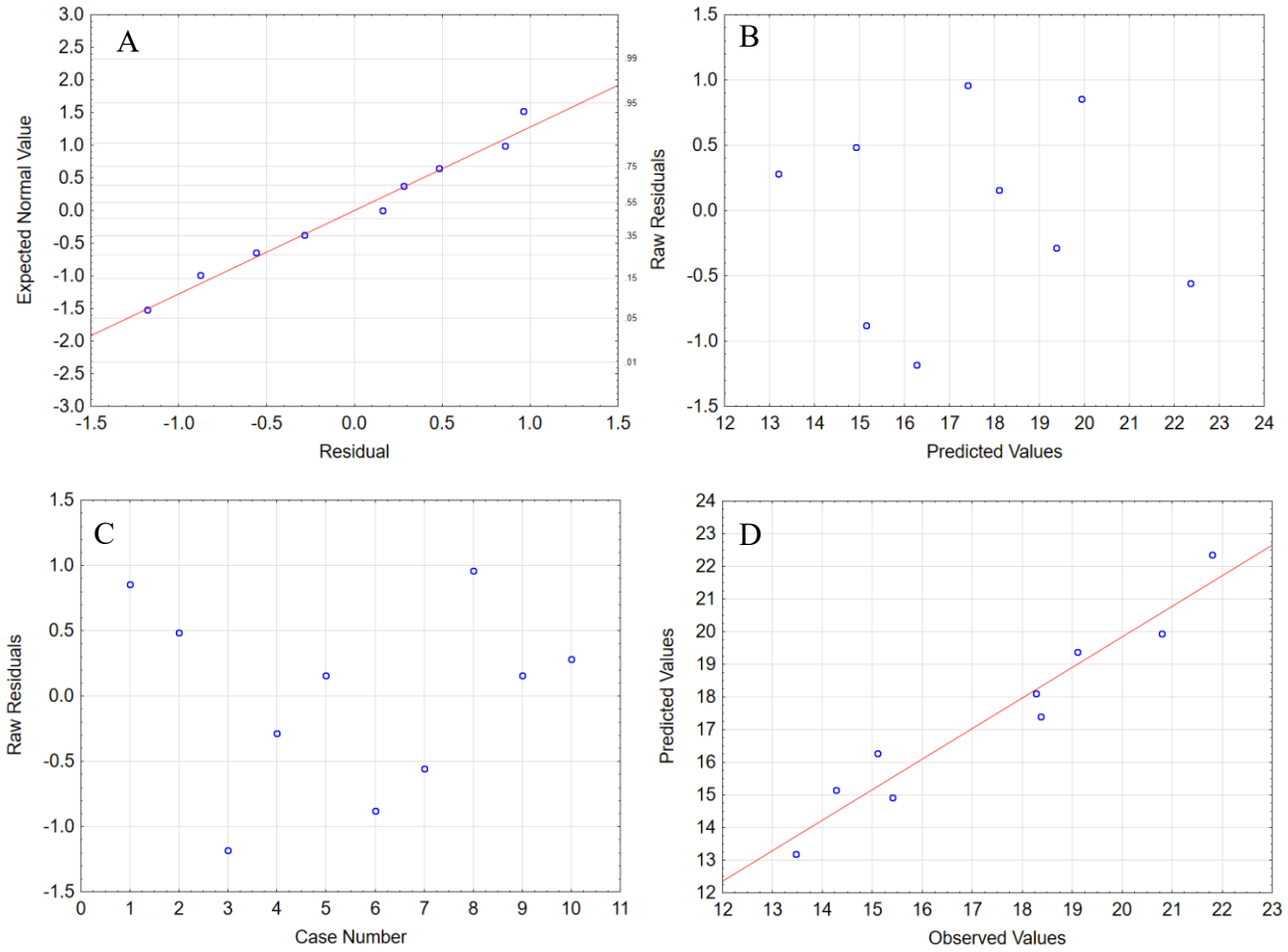

Figure A 7: Solid content model plots for 5 wt.% MFT: a) normal plot, b) scatterplot of the standardized residuals as a function of the standardized predicted values, c) residuals versus run number, d) predicted versus observed values.

Table A 8: ANOVA table for solid content for 10 wt.% MFT.

Source of Variation	Sum of Squares	Degrees of Freedom	Mean Squares	F	P	Comments
1) M_g (L: linear)	66.2256	1	66.2256	286.1520	0.00007	significant
M_g (Q: quadratic)	1.5770	1	1.5770	6.8141	0.0594	significant
2) ρ_g (L)	18.2054	1	18.2054	78.6630	0.0009	significant
ρ_g (Q)	0.1889	1	0.1889	0.8163	0.4173	
1L by 2L	3.8941	1	3.8941	16.8257	0.0148	significant
Error	0.9257	4	0.2314			
Total SS	88.5250	9				

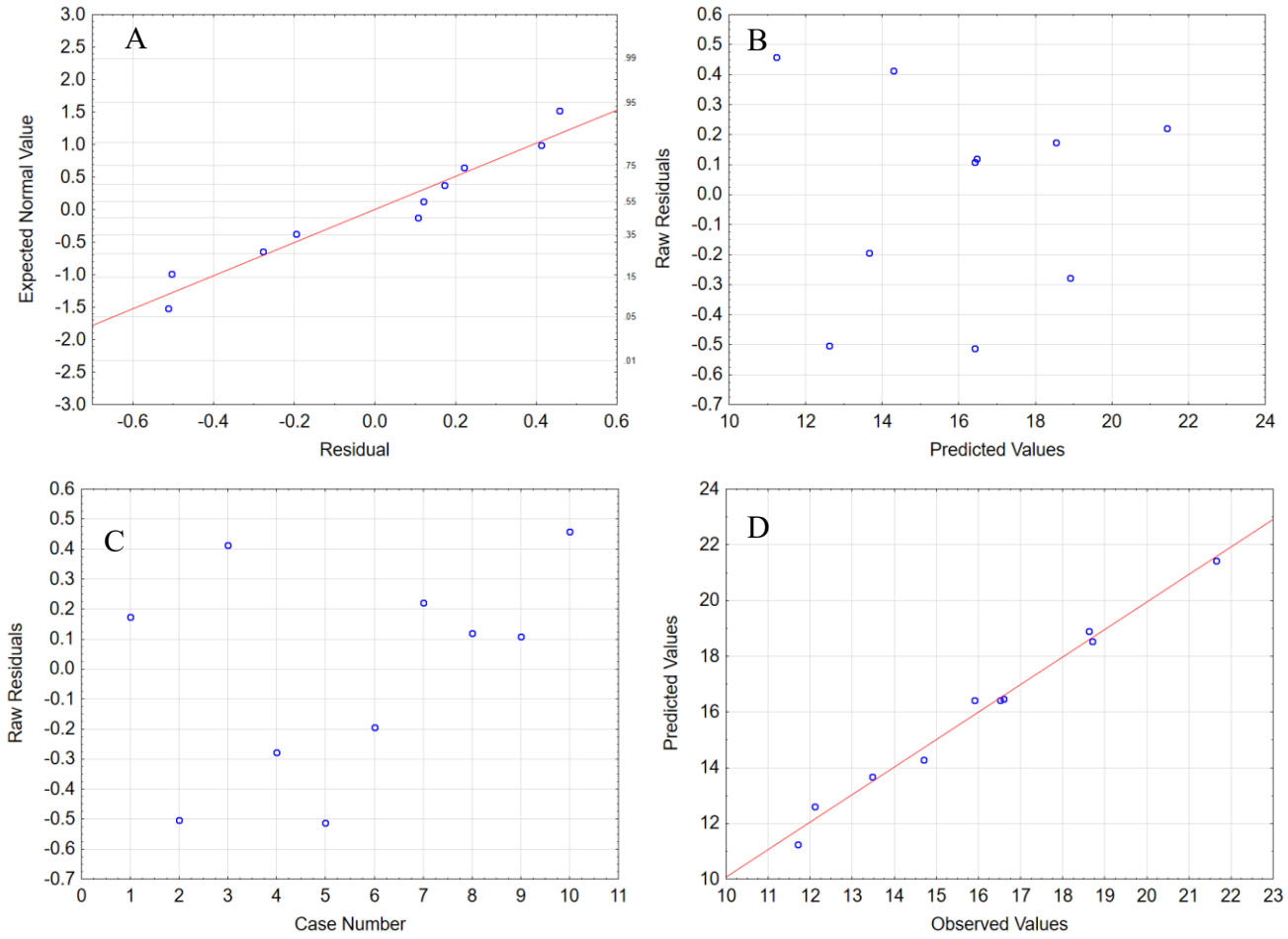

Figure A 8: Solid content model plots for 10 wt.% MFT: a) normal plot, b) scatterplot of the standardized residuals as a function of the standardized predicted values, c) residuals versus run number, d) predicted versus observed values.

Table A 9: ANOVA table for solid content for 20 wt.% MFT.

Source of Variation	Sum of Squares	Degrees of Freedom	Mean Squares	F	P	Comments
1) M_g (L: linear)	80.2160	1	80.2160	83.6080	0.0008	significant
M_g (Q: quadratic)	0.8865	1	0.8865	0.9240	0.3909	
2) ρ_g (L)	0.3978	1	0.3978	0.4146	0.5547	
ρ_g (Q)	1.6578	1	1.6578	1.7279	0.2590	significant
1L by 2L	4.1415	1	4.1415	4.3167	0.1063	significant
Error	3.8377	4	0.9594			
Total SS	89.9431	9				

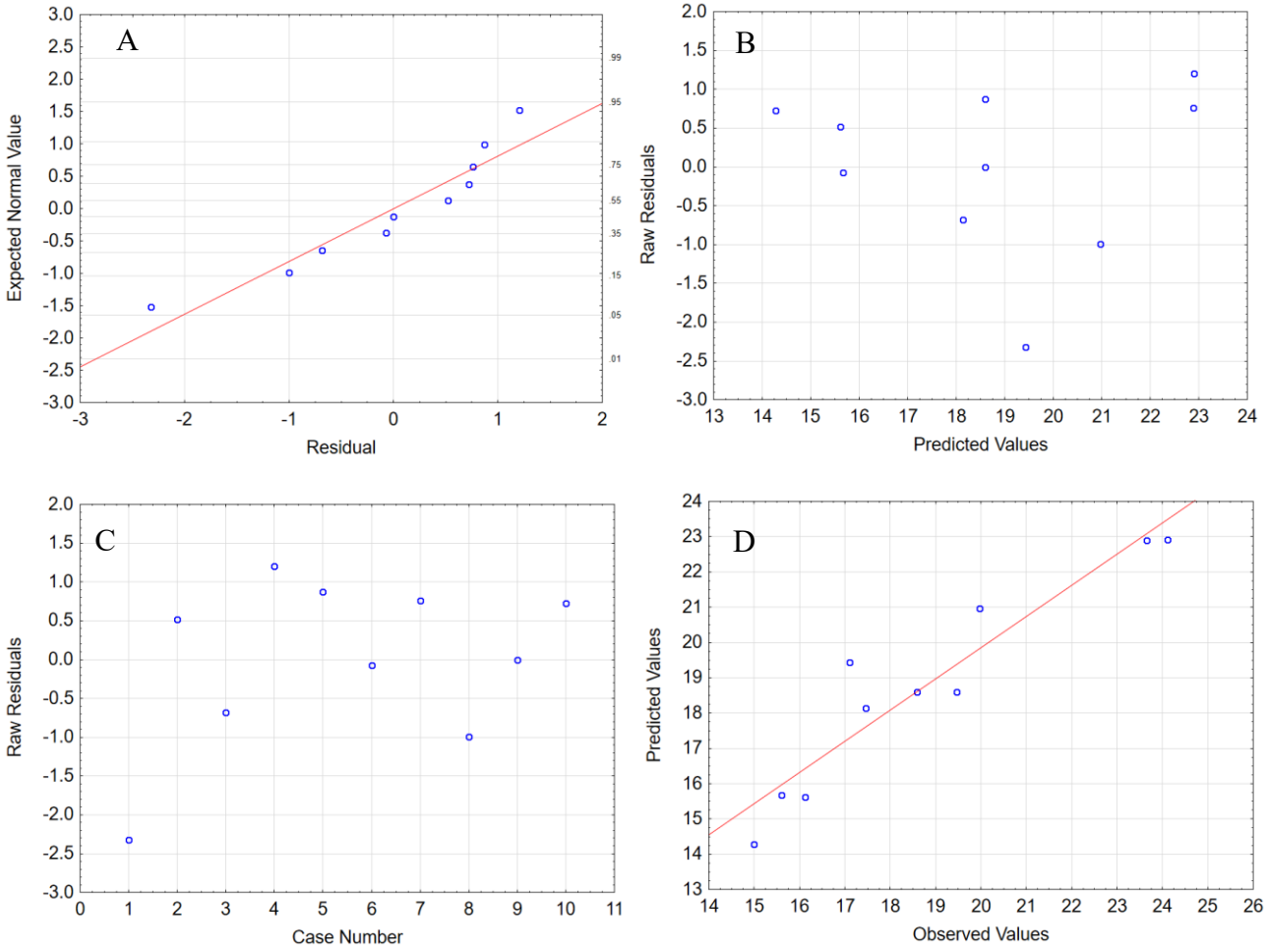

Figure A 9: Solid content model plots for 20 wt.% MFT: a) normal plot, b) scatterplot of the standardized residuals as a function of the standardized predicted values, c) residuals versus run number, d) predicted versus observed values.